NMR Spectroscopic Studies of Organocopper Compounds and Zintl Anions

Dissertation

zur Erlangung des Doktorgrades der Naturwissenschaften

(Dr. rer. nat.)

an der Fakultät für Chemie und Pharmazie

der Universität Regensburg

vorgelegt von

Maria Neumeier

aus Kelheim

September 2012

This PhD-thesis was carried out under the supervision of Prof. Dr. Ruth M. Gschwind between November 2008 and September 2012 at the Institute of Organic Chemistry at the University of Regensburg.

The PhD – thesis was submitted on: 07.09.2012

Board of Examiners:	Prof. Dr. Frank-Michael Matysik	Chairman
	Prof. Dr. R. M. Gschwind	1st Referee
	Prof. Dr. K. Zeitler	2nd Referee
	Prof. Dr. N. Korber	Examiner

Für

meine Familie.

„In der Wissenschaft gleichen wir alle nur den Kindern, die am Rande des Wissens hier und da einen Kiesel aufheben, während sich der weite Ozean des Unbekannten vor unseren Augen erstreckt“

Isaac Newton

An dieser Stelle möchte ich mich bei allen bedanken, die zum Gelingen dieser Arbeit beigetragen haben. Meiner Doktormutter Frau Prof. Dr. Ruth M. Gschwind danke ich für die interessante und anspruchsvolle Themenstellung, sowie für die Freiheit und das Vertrauen bei der Bearbeitung der Themen. Außerdem möchte ich mich bei den Professoren Dr. Kirsten Zeitler, Dr. Nikolaus Korber und Dr. Frank-Michael Matysik für die Ausübung des Amtes als Prüfer bzw. als Vorsitzender recht herzlich bedanken. Des Weiteren bedanke ich mich bei Prof, Dr. Nikolaus Korber und Prof. Dr. Manfred Scheer für die Ermöglichung der Kooperationen.

Ferner bedanke ich mich herzlich bei meinen Kooperationspartnern Dr. Stefanie Gärtner, Franziska Fendt, Ute Friedrich und Christoph Schwarzmaier für die produktive Zusammenarbeit und die interessanten Diskussionen, die zum Gelingen von Teilen dieser Arbeit beigetragen haben.

Großer Dank gebührt auch den Mitarbeitern des Arbeitskreises, die mit einer netten und respektvollen Umgangsweise für eine tolle Arbeitsatmosphäre gesorgt haben. Meinem thematischen Vorgänger Dr. Tobias Gärtner danke ich für die zahlreichen interessanten fachlichen Diskussionen. Meiner thematischen Nachfolgerin auf dem Gebiet der Zintl Anionen Carina Koch danke ich für das große Interesse und ihr Engagement und wünsche ihr, sowie ihren Kooperationspartnerinnen viel Erfolg bei der weiteren Bearbeitung dieses spannenden Themas. Mein Dank gilt auch Dr. Guido Federwisch, Dr. Roland Kleinmaier, Dr. Markus Schmid, Dr. Matthias Fleischmann, Dr. Katrin Schober, meinen beiden Mitstreiterinnen Diana Drettwan und Evelyn Hartmann, sowie allen neu hinzugekommenen Kollegen Nils Sorgenfrei, Felicitas von Rekowski, Christian Feldmeier, Michael Haindl, Michael Hammer und Hanna Bartling.

Des Weiteren bedanke ich mich bei Ulrike Weck und Nikola Kastner-Pustet für die tatkräftige Unterstützung bei bürokratischen und technischen Fragen. Besonderer Dank gilt auch den Mitarbeitern der NMR-Abteilung Dr. Thomas Burgemeister, Dr. Ilya Shenderovich, Fritz Kastner, Annette Schramm und Georgine Stühler, die für messtechnische Fragen und Probleme stehts ein offenes Ohr hatten.

Ganz besonderer Dank gilt meinen Eltern, die mich mit ihrem Vertrauen unterstützt und damit zum Erfolg meines Studiums und dieser Arbeit entscheidend beigetragen haben. Meinen Geschwistern und meiner baldigen Schwägerin, sowie meinen Freunden sei für die nötige Ablenkung in Krisensituationen gedankt.

Meinem Partner Alexander danke ich ganz besonders für seine liebevolle und verständnisvolle Unterstützung.

In liebevoller Erinnerung an meinen Vater (✝ 04.09.2012)

Table of Contents

1. Introduction and Outline

1.1 Organocuprates and their Intermediates in Cross Coupling Reactions

Organocuprates are valuable transition metal reagents for the C-C bond formation in 1,4-addition and cross coupling reactions. Since their discovery by Gilman in 1952, organocuprates experienced a breath-taking development to the most frequently applied organocopper compounds. Therefore, a lot of effort was spent on the characterization of these free reagents and their π- and σ-intermediate structures in particular reactions. Especially, methylcuprates developed into the most important mechanistic and structural model system for these reactions and (trimethylsilyl)methylcuprates show equal core structures as these methylcuprates. The combination of synthetical, theoretical and mechanistic studies gained insights into the relation between structure and reactivity of organocuprates and identified a square-planar Cu(III) complex as the key-intermediate for their reactions. Various spectroscopic studies on their structures were published by our and other research groups. Furthermore, targeted reactions with copper(III) complexes were performed, which illustrates the equivalence of Cu(I) and Cu(III) cuprate reactivity. Moreover, stabilizing effects on these copper(III) intermediates were investigated. Despite these elaborate studies, ligand exchange reactions in the copper(III) intermediate have not been investigated. In addition, subsequently formed copper(I) complexes, which can be caused by the change of stoichiometry during the course of organocuprate reactions and their potential influence on yields and selectivity have not been considered until now.

Therefore, section 2 describes combined NMR and DFT studies on ligand exchange processes in Cu(III) intermediates of cross coupling reactions. NMR studies of $^{12}C/^{13}C$ isotopic patterns of these Cu(III) complexes and reaction products as well as DFT calculations of possible reaction pathways indicate an intermolecular S_N2-like substitution mechanism for ligand exchange reactions in square-planar Cu(III) complexes.

Section 3 is about the investigations on copper(I) complexes, occurring throughout the course of cross coupling reactions, caused by a changed stoichiometry. Copper rich iodocomplexes were synthesized and structurally characterized by NMR methods. Their

appearance in cross coupling reactions can be now correlated to declining yields. By applying an excess of alkyl lithium compound, these copper rich iodocomplexes can be reconverted into the reactive cuprate. Equal investigations were performed with a cyanocuprate to clarify a potential special reactivity. The lack of additional copper rich complexes besides the heteroleptic cuprate provides an explanation for the long-standing myths about special cyanocuprate reactivity.

1.2 The Chemistry of Zintl Anions in Liquid Ammonia

The reactions of alkali metals or alkaline earth metals with metals or metalloids of group 13 to 16 lead to binary alloys, named Zintl phases. For these compounds intermetallic structures with heteropolar element-element-bound parts are characteristic. By now, a versatile number of crystal structures of homo- and heteroatomic polyanions from the elements of group 14 and 15 are known, ranging from oxidatively coupled to endo- and exohedral and even to intermetalloide clusters. Some of these materials have good prospects in the application of cluster-assembled nanomaterials and, in principle, the electrochemical deposition of appropriate materials on surfaces is possible. However, a targeted material research is hampered by the limited knowledge about the stabilities of such Zintl anions in solution. NMR spectroscopy presented itself as a powerful method in the studies of Zintl anions of group 15, but for naked Zintl anions of group 14 hardly any NMR signal is known. Therefore, the second part of this work is about NMR investigations on the properties and stabilizing effects on group 14 polyanions in liquid ammonia.

In section 4 the first NMR detection of the long-time elusive tetrahedranides Si_4^{4-} and Sn_4^{4-} is presented. Amazingly high signal intensities and stabilities were observed by utilizing the stabilizing effect of [2.2.2]-cryptand. Furthermore, by observing the generation of NH_2^- the first experimental evidence for the long-standing assumption of solvent molecules as oxidizing agent for Zintl anions is given and in case of silicides, SiH_3^- was detected as degradation product.

Section 5 deals with the stabilization of distinct tin polyanions and possible targeted reactions with transition metal complexes. Under different conditions, the binary phase Rb_4Sn_4 yielded varying anions in solution, which then are accessible for conversions with transition metal complexes. Hence, the result of these reactions is decisively influenced by the conditions in solution and provides the possibility for controllable syntheses.

Section 6 deals with the ^{75}As NMR spectroscopic detection of As_4, the molecular modification of arsenic, either prepared classically via a high temperature route or far less costly from a new storage source, which is light and X-ray stable and can be used for the in-situ generation of molecular yellow arsenic in chemical reactions.

2. Ligand Exchange Reactions in Cu(III) complexes: Mechanistic Insights by Combined NMR and DFT Studies

The structural investigations on the Cu(III) intermediate and the identification of ligand exchange reactions were performed by Tobias Gärtner, who also contributed to the DFT calculations on possible ligand exchange mechanisms. My contribution was an additional NMR study of the S_N2-like ligand exchange.

Tobias Gärtner, Naohiko Yoshikai, Maria Neumeier, Eiichi Nakamura, Ruth M. Gschwind

Chem. Commun. **2010**, *46*, 4625–4626

http://pubs.rsc.org/en/content/articlelanding/2010/cc/c0cc00360c

2.1 Abstract

NMR studies of $^{12}C/^{13}C$ isotopic patterns in Cu(III) intermediates and reaction products together with DFT calculations of possible reaction pathways indicate an intermolecular S_N2-like substitution mechanism for ligand exchange reactions in square-planar Cu(III) complexes, which is proposed to be slow compared to reductive elimination at synthetic conditions.

2.2 Discussion

In the past two years, high-resolution NMR studies revealed the elusive experimental evidence for Cu(III) intermediates in conjugate addition reactions[1] as well as S_N2'- and S_N2-type cross coupling reactions[2–4] of organocuprates, which had been proposed for years in theoretical studies.[5] In these NMR investigations not only the mechanistically expected Cu(III) intermediates but also tetra-alkyl Cu(III)-species ($[Me_4Cu]^-$ and $[Me_3EtCu]^-$) were detected[3,4] and prepared,[6] and for $[Me_3EtCu]^-$ and $[Me_4Cu]^-$ unexpected temperature stabilities were reported.[3,6] Furthermore, the formation of several tri-alkyl Cu(III)-complexes with different electron donating hetero-ligands was demonstrated.[7] These additional Cu(III) complexes hint at ligand exchange reactions in square-planar Cu(III) complexes. Therefore, in this contribution possible intra- and intermolecular ligand exchange processes in Cu(III) intermediates are investigated by NMR and DFT calculations. As a model, the S_N2 reaction of dimethyl cuprate (derived from CuCN and MeLi) with methyl iodide in diethyl ether was selected. In order to make the isotope distribution and thus possible ligand exchange processes in $[Me_3CuCN]^-$ (**I**) detectable, the methyl groups in the cuprate were 100 % ^{13}C-labeled and MeI was used at natural abundance (see Scheme 1).

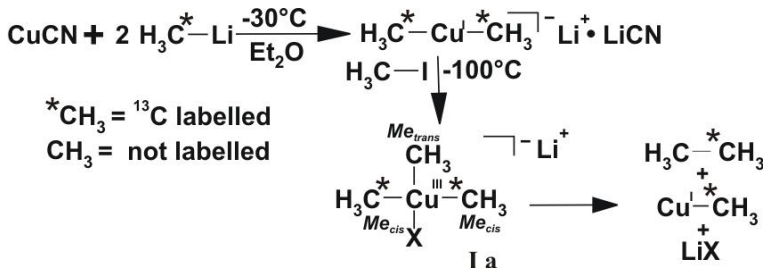

Scheme 1: Isotopic pattern of the model reaction expected according to the previously proposed mechanisms of Bertz, Ogle, and Nakamura.[3,8]

According to the previously proposed reaction mechanisms,[3,8] the unlabeled methyl group of MeI should be incorporated trans to the heteroligand X. As a result exclusively the isotopomer **Ia** should be formed as intermediate and $H_3{}^{12}C\text{-}{}^{13}CH_3$ as product (see Scheme 1). However, in the experimental spectrum of the model reaction (see Figure 1) the patterns of both isotopomers are detected in considerable amounts. In addition to the $^{1}H,^{13}C$ HMBC pattern of **Ia** a central peak ($^{1}H\text{-}^{12}C$) for Me_{cis}, and a doublet splitting ($^{1}H\text{-}^{13}C$) in the cross peak between Me_{trans} and Me_{cis} are detected, which are both indicative for the existence of isotopomer **Ib**.

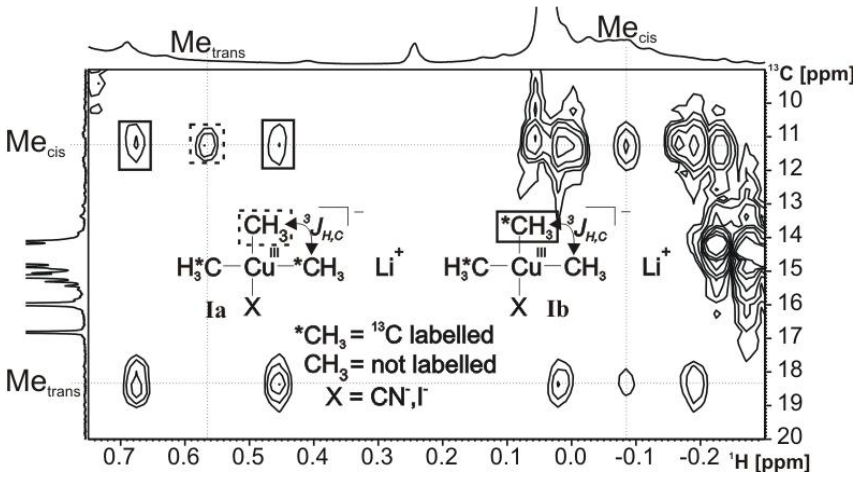

Figure 1: Section of a $^{1}H,^{13}C$ HMBC at -100 °C in diethyl ether which shows the cross peak patterns of both isotopomers **Ia** and **Ib** as highlighted on the cross peak between Me_{trans} and Me_{cis}.

The mixture of **Ia** and **Ib** detected at –100 °C indicates ligand exchange processes in **I** at this low temperature or a reaction mechanism differing from the proposed trans-addition.[3] To distinguish between these two possibilities, the isotopic pattern of the reaction product ethane was investigated, which is formed at temperatures above –90 °C (see Figure 2). Surprisingly, a comparison with simulated spectra showed mainly the formation of $H_3{}^{12}C\text{-}{}^{13}CH_3$, and only about 3 % ± 2 of $H_3{}^{13}C\text{-}{}^{13}CH_3$ were detected (see Figure 2). This isotope pattern of the product ethane is in agreement with the postulated syn-elimination from the "direct" Cu(III) intermediate **Ia** and the formation of only traces of Cu(III) intermediates, and hints at ligand exchange processes being slow compared to elimination at temperatures commonly applied in synthesis.

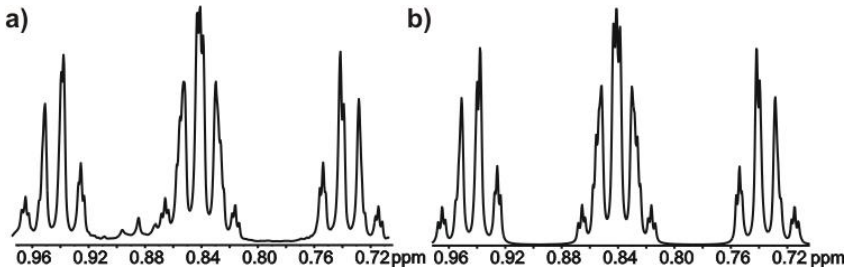

Figure 2: ^{1}H spectra of $H_3{}^{12}C\text{-}{}^{13}CH_3$ a) experimental and b) simulated.

Therefore, intermolecular exchange processes were considered as possible reaction pathways for **Ib**. The model reaction (Scheme 1) was applied using an excess of ^{13}C-labeled MeLi (3 and 4 equiv. of MeLi) and indeed, the resulting ^{1}H and $^{1}H,^{13}C$ HMBC spectra revealed a considerably increased amount of Me_4Cu^- ($\delta^{1}H$ = -0.31 ppm; $\delta^{13}C$ = 14.2 ppm;[6] for spectra see SI) indicating interligand exchange reactions of **I** and MeLi.

Therefore, DFT calculations (B3LYP) were performed to gain further insight into the mechanism of the ligand exchange reactions in Cu(III) complexes (see SI for method details). First, stabilization energies by coordination of several anionic ligands to trimethylcopper(III) were calculated (see Scheme 2). In agreement with previously reported results about the special stability of tetra-alkyl Cu(III) complexes,[3] coordination of a methyl anion to give tetramethylcuprate(III) **2** provides much larger stabilization (~25-50 kcal/mol) than that of other anions such as halides, thiolate, and cyanide (**1** or **3**-**5**). This is reasonable, because the methyl anion is the strongest σ-donor among those examined. Considering the large stabilization energies to form the complexes **1**-**5**, dissociative ligand exchange processes via trimethylcopper(III) are improbable.

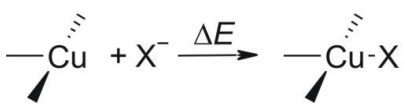

ΔE (kcal/mol)	**1** (X = I)	-20.8
	2 (X = Me)	-69.4
	3 (X = SMe)	-42.3
	4 (X = Cl)	-30.7
	5 (X = CN)	-44.0

Scheme 2: Stabilization of Me_3Cu(III) by anionic ligands as studied by DFT calculations.

The square-planar geometry and the d^8 electron configuration of the Cu(III) complexes resemble those for the well known Pt(II) and Au(III) complexes, for which both pseudorotation and S_N2 substitution are accepted models for isomerization processes.[9–11] Therefore, various complex geometries as possible intermediates were calculated on the basis of the pseudorotational processes reported for Pt(II) and Au(III) complexes. However, all the attempts to locate intermediates or transition states of cis/trans isomerization lead to reductive

elimination of the Cu(III) species to give ethane (see SI for details), presumably due to much lower kinetic stability of the Cu(III) complexes than of the corresponding Au(III) complexes.[12] Next, an intermolecular S_N2-like substitution mechanism was calculated with **4** and $MeLi\cdot(OMe_2)_3$ as reaction partners (see Scheme 3). As first step in the pathway, **4** and $MeLi\cdot(OMe_2)_3$ forms a complex **CP1** by Li-Cl electrostatic interaction with concomitant liberation of one Me_2O molecule, which is modestly exothermic (ΔE = –5.7 kcal/mol). The following substitution reaction through a pentacoordinated Cu(III) transition state **TS2** requires a surprisingly small activation energy of only 6.3 kcal/mol.

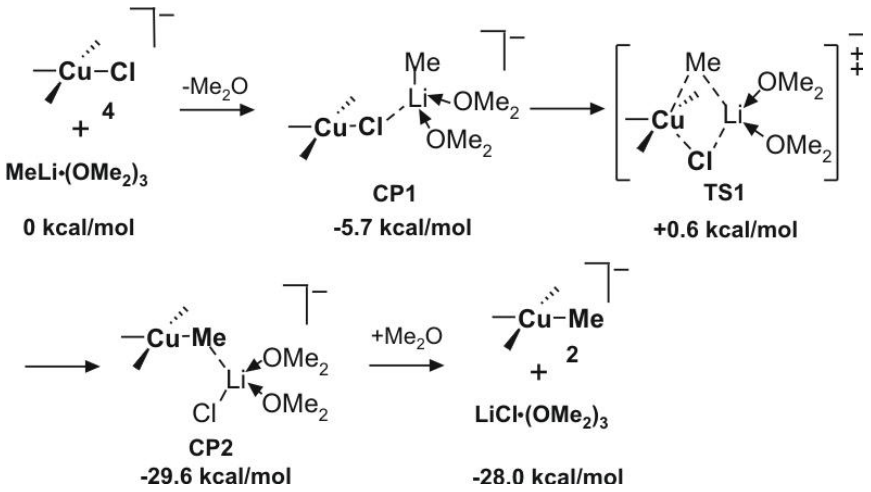

Scheme 3: Reaction pathway and energetics of substitution of $[Me_3CuCl]^-$ (**4**) with $MeLi\cdot(OMe_2)_3$ to form $[Me_4Cu]^-$ (**2**).

The substitution process (**CP1** to **CP2**) is largely exothermic (ΔE = –23.9 kcal/mol), presumably due to the strong coordination of the methyl anion to Cu(III) as well as the formation of the stable salt, i.e., LiCl. Dissociation of the copper and the lithium moieties of **CP2** (by coordination of Me_2O to Li) is almost thermoneutral. This reaction pathway reveals that intermolecular ligand exchanges in Cu(III) complexes should be possible, in case MeLi or other appropriate reaction partners are present in solution. Notably, the activation energy for the ligand exchange (6.3 kcal/mol) is much smaller than that of the reductive elimination of the Cu(III) complex **4** (ca. 18 kcal/mol),[8] while the former, intermolecular process should have much greater contribution of the entropy factor ($-T\Delta S$) to the activation free energy than the latter intramolecular process. In light of the entropy factor, we speculate that, at sufficiently low temperatures, such exchange processes may become more feasible than the reductive elimination.

In this combined NMR and DFT study, for the first time mechanistic insights into ligand exchange processes in square-planar Cu(III) complexes are presented. Specific ^{13}C labeling and the resulting isotopomeric pattern reveal that ligand exchange processes occur in Cu(III) complexes, but are slow compared to elimination under usual synthetic cross coupling conditions. Related theoretical calculations reveal an intermolecular S_N2 substitution mechanism and the low energy of the transition state suggests that also other ligand exchange reactions should be possible on Cu(III) intermediates, which allow for targeted chemical reactions. In fact, such reactions have appeared in this journal while our paper was in press.[11]

2.3 References

(1) Bertz, S. H.; Cope, S.; Murphy, M.; Ogle, C.; Taylor, B. J. *J. Am. Chem. Soc.* **2007**, *129*, 7208-7209.

(2) Bartholomew, E. R.; Bertz, S. H.; Cope, S.; Murphy, M.; Ogle, C. A. *J. Am. Chem. Soc.* **2008**, *130*, 11244-11245.

(3) Bertz, S. H.; Cope, S.; Dorton, D.; Murphy, M.; Ogle, C. A. *Angew. Chem. Int. Ed. Engl.* **2007**, *46*, 7082-7085.

(4) Gärtner, T.; Henze, W.; Gschwind, R. M. *J. Am. Chem. Soc.* **2007**, *129*, 11362-11363.

(5) Nakamura, E.; Mori, S. *Angew. Chem. Int. Ed.* **2000**, *39*, 3750-3771.

(6) Bartholomew, E. R.; Bertz, S. H.; Cope, S. K.; Murphy, M. D.; Ogle, C. A.; Thomas, A. A. *Chem. Commun.* **2010**, *46*, 1253-1254.

(7) Bartholomew, E. R.; Bertz, S. H.; Cope, S.; Dorton, D. C.; Murphy, M.; Ogle, C. A. *Chem. Commun.* **2008**, 1176-1177.

(8) Nakamura, E.; Mori, S.; Morokuma, K. *J. Am. Chem. Soc.* **2000**, *122*, 7294-7307.

(9) Chval, Z.; Sip, M.; Burda, J. V. *Journal of Computational Chemistry* **2008**, *29*, 2370-2381.

(10) Cooper, J.; Ziegler, T. *Inorganic Chemistry* **2002**, *41*, 6614-6622.

(11) Louw, W. J. *Inorganic Chemistry* **1977**, *16*, 2147-2160.

(12) Nakanishi, W.; Yamanaka, M.; Nakamura, E. *J. Am. Chem. Soc.* **2005**, *127*, 1446-1453.

2.4 Supporting Information

2.4.1. Experimental Section

All cuprate samples were prepared by a method described by John et al.[1] The synthesis of the cuprate was directly done in Et_2O-d_{10} to exclude protonated Et_2O. The protonated Et_2O from the ^{13}C-labeled MeLi solution was removed as much as possible before the addition to the Cu-salt suspension. Having the cuprate in hand it was cooled down to 170 K and a solution MeI in Et_2O-d_{10} was added depending on the synthesis. The amount of MeI was adjusted to the synthesis of the cuprate solution.

1. John, M.; Auel, C.; Behrens, C.; Marsch, M.; Harms, K.; Bosold, F.; Gschwind, R. M.; Rajamohanan, P. R.; Boche, G. *Chem. Eur. J.* **2000**, *6*, 3060-3068.

2.4.2. NMR Data Collecting and Processing

The NMR spectra were recorded on a Bruker Avance 600 spectrometer equipped with a 5 mm broadband triple resonance Z-gradient probe. ^{1}H,^{13}C HMBC measurements were carried out with a standard Bruker pulse program using 32 number of scans, 16 dummy scans, TD(F2) = 16k and TD(F1) = 400 with a relaxation delay of 2 s. The processing parameters were TD(F1) = 1k and TD(F2) = 1k. The temperatures for all measurements were controlled by a Bruker BVTE 3900 temperature unit.

2.4.3. Increased Formation of Me_4Cu^- Applying an Excess of MeLi

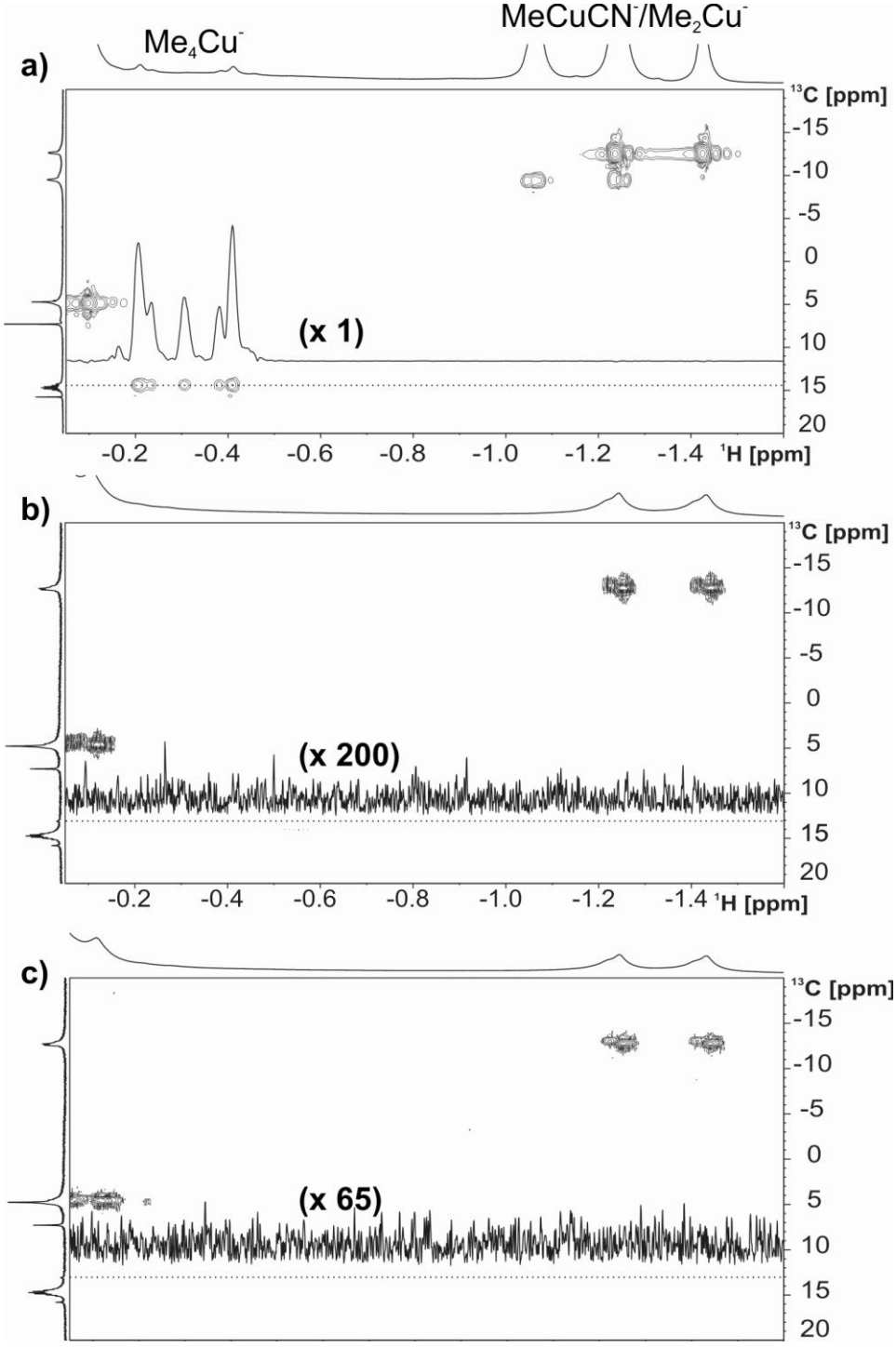

SI Figure 1: Sections of $^1H,^{13}C$ HMBC spectra at –63 °C in diethyl ether showing the signals of Me_4Cu^-, $MeCuCN^-$ and Me_2Cu^-. To visualize the increased concentration of Me_4Cu^- in the sample with excess of MeLi, in addition, the row of the HMBC spectrum showing Me_4Cu^- is presented as insert with their scaling factors given in brackets.
a) $Cu^{13}CN + 3\ ^{13}CH_3Li + CH_3I$
b) $Cu^{13}CN + 2\ ^{13}CH_3Li + CH_3I$ (number of scans identical to a)
c) $Cu^{13}CN + 2\ ^{13}CH_3Li + CH_3I$ (number of scans three times higher than in a)

2.4.4. Analysis of the Isotopic Pattern of Ethane in the Reaction of ^{13}C-Labeled Cyanocuprate Converted with MeI and an Excess of ^{13}C-Labeled MeLi

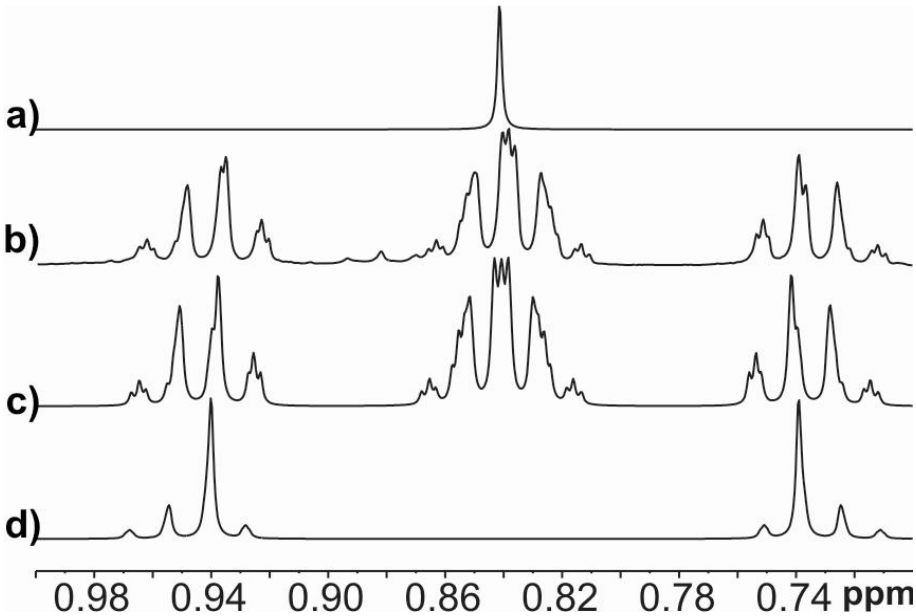

SI Figure 2: Simulated ^{1}H spectra of a) $H_3C\text{-}CH_3$, c) $H_3C\text{-}^{13}CH_3$ and d) $H_3{}^{13}C\text{-}^{13}CH_3$ in comparison with b) the experimental spectrum of the resulting products of ^{13}C-labeled cyanocuprate converted with MeI and an excess of ^{13}C-labeled MeLi.

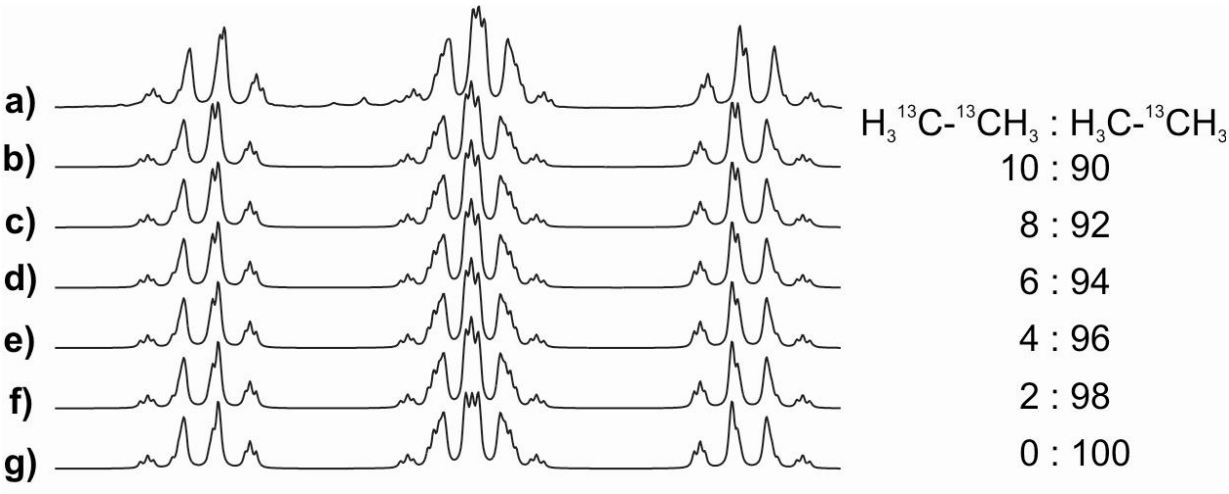

SI Figure 3: a) Experimental spectrum of the resulting products of the ^{13}C-labeled cyanocuprate converted with MeI and an excess of ^{13}C-labeled MeLi in comparison with b-g) the simulated ^{1}H spectra of different mixtures of $H_3{}^{13}C\text{-}CH_3$ and $H_3{}^{13}C\text{-}^{13}CH_3$ (ratios given aside).

2.4.5. DFT Functional Calculations

All calculations were done using the GAUSSIAN 03 package.[2] All geometry optimizations were performed with the DFT-method and the B3LYP hybrid functional, using SDD for copper, iodine and gold and 6-31+G(d) for all other atoms. Local minima have zero and transition states (TS) have one and only one imaginary frequency. The intrinsic reaction coordinate (IRC) analysis[3-5] was carried out to confirm that stationary points are smoothly connected to each other. All energies used throughout are zero-point corrected and calculated for the gas-phase.

2. Gaussian 03, R. C.; Frisch, M. J.; Trucks, G. W.; Schlegel, H. B.; Scuseria, G. E.; Robb, M. A.; Cheeseman, J. R.; Montgomery, J. A.; Jr., T. V.; Kudin, K. N.; Burant, J. C.; Millam, J. M.; Iyengar, S. S.; Tomasi, J.; Barone, V.; Mennucci, B.; Cossi, M.; Scalmani, G.; Rega, N.; Petersson, G. A.; Nakatsuji, H.; Hada, M.; Ehara, M.; Toyota, K.; Fukuda, R.; Hasegawa, J.; Ishida, M.; Nakajima, T.; Honda, Y.; Kitao, O.; Nakai, H.; Klene, M.; Li, X.; Knox, J. E.; Hratchian, H. P.; Cross, J. B.; Adamo, C.; Jaramillo, J.; Gomperts, R.; Stratmann, R. E.; Yazyev, O.; Austin, A. J.; Cammi, R.; Pomelli, C.; Ochterski, J. W.; Ayala, P. Y.; Morokuma, K.; Voth, G. A.; Salvador, P.; Dannenberg, J. J.; Zakrzewski, V. G.; Dapprich, S.; Daniels, A. D.; Strain, M. C.; Farkas, O.; Malick, D. K.; Rabuck, A. D.; Raghavachari, K.; Foresman, J. B.; Ortiz, J. V.; Cui, Q.; Baboul, A. G.; Clifford, S.; Cioslowski, J.; Stefanov, B. B.; Liu, G.; Liashenko, A.; Piskorz, P.; Komaromi, I.; Martin, R. L.; Fox, D. J.; Keith, T.; Al-Laham, M. A.; Peng, C. Y.; Nanayakkara, A.; Challacombe, M.; Gill, P. M. W.; Johnson, B.; Chen, W.; Wong, M. W.; Gonzalez, C.; Pople, a. J. A.; Gaussian, I., Wallingford CT, 2004.
3. Fukui, K. *Acc. Chem. Res.* **1981**, *14*, 363-368.
4. Gonzalez, C.; Schlegel, H. B. J. *Chem. Phys.* **1989**, *90*, 2154-2161.
5. Gonzalez, C.; Schlegel, H. B. J. *Phys. Chem.* **1990**, *94*, 5523-5527.

2.4.6. Energies and Cartesians Coordinates of Stationary Points

$MeLi{\cdot}(OMe_2)_3$

SCF Done: E(RB+HF-LYP) = -512.564881634 A.U. after 6 cycles

Center Number	Atomic Number	Atomic Type	Coordinates (Angstroms) X	Y	Z
1	1	0	-0.788842	1.055813	2.975777
2	6	0	-0.013699	0.350495	2.609524
3	1	0	0.940869	0.768948	2.991726
4	1	0	-0.172692	-0.571035	3.208609
5	3	0	-0.009230	0.090102	0.544882
6	8	0	-1.754444	-0.669118	-0.217108
7	8	0	1.527804	-1.051062	-0.164216
8	8	0	0.247165	1.786007	-0.598593
9	6	0	-2.644681	-1.140739	0.796707
10	1	0	-2.287121	-0.718958	1.736989
11	1	0	-2.621108	-2.239059	0.846667
12	1	0	-3.671606	-0.808215	0.585589
13	6	0	-2.062628	-1.170125	-1.507584
14	1	0	-1.352353	-0.725630	-2.209189
15	1	0	-3.085236	-0.891173	-1.802781
16	1	0	-1.970413	-2.266303	-1.537504
17	6	0	1.457705	2.433948	-0.208502
18	1	0	2.261919	1.704748	-0.322852

19	1	0	1.404413	2.750317	0.841118
20	1	0	1.650163	3.303090	-0.854469
21	6	0	-0.882101	2.649506	-0.482113
22	1	0	-0.763319	3.524916	-1.137201
23	1	0	-1.010923	2.978334	0.557745
24	1	0	-1.757457	2.074620	-0.790040
25	6	0	2.178410	-1.839037	0.833273
26	1	0	1.781452	-1.505683	1.793466
27	1	0	3.266060	-1.680660	0.795223
28	1	0	1.961940	-2.906709	0.681156
29	6	0	1.951469	-1.349209	-1.484145
30	1	0	1.423643	-0.667368	-2.155326
31	1	0	1.711429	-2.389572	-1.751174
32	1	0	3.035824	-1.196367	-1.591802

Me_2O

SCF Done: E(RB+HF-LYP) = -155.033688970 A.U. after 7 cycles

Center Number	Atomic Number	Atomic Type	Coordinates (Angstroms) X	Y	Z
1	8	0	0.000000	0.587561	0.000000
2	6	0	1.177331	-0.195661	0.000000
3	1	0	1.233901	-0.836130	-0.895388
4	1	0	1.233901	-0.836130	0.895389
5	1	0	2.023631	0.495986	0.000000
6	6	0	-1.177331	-0.195661	0.000000
7	1	0	-1.233901	-0.836130	-0.895388
8	1	0	-2.023631	0.495986	0.000000
9	1	0	-1.233901	-0.836130	0.895388

CP1

SCF Done: E(RB+HF-LYP) = -1134.88630484 A.U. after 8 cycles

Center Number	Atomic Number	Atomic Type	Coordinates (Angstroms) X	Y	Z
1	1	0	4.804038	0.179295	1.367932
2	6	0	3.861348	-0.076711	1.900031
3	1	0	4.040145	-1.076201	2.349273
4	1	0	3.807466	0.618673	2.763107
5	3	0	2.140180	-0.013532	0.679157
6	8	0	2.253065	1.574693	-0.648369
7	8	0	2.163424	-1.506307	-0.781244
8	6	0	2.673173	2.745822	0.039471
9	1	0	3.440099	2.427722	0.748458
10	1	0	1.832539	3.199665	0.584433
11	1	0	3.084852	3.481973	-0.670728
12	6	0	1.190705	1.813862	-1.562785
13	1	0	0.945336	0.852695	-2.018886
14	1	0	1.509790	2.526635	-2.341129
15	1	0	0.305325	2.199400	-1.043299
16	6	0	1.468618	-2.699367	-0.437519

17	1	0	0.474605	-2.402625	-0.101082
18	1	0	1.988569	-3.229919	0.374176
19	1	0	1.390381	-3.363111	-1.313538
20	6	0	3.503564	-1.744417	-1.187599
21	1	0	3.522905	-2.380305	-2.088552
22	1	0	4.077385	-2.220937	-0.381417
23	1	0	3.947594	-0.771813	-1.407129
24	17	0	-0.316098	0.088658	1.246509
25	29	0	-2.387269	-0.021244	0.152812
26	6	0	-2.508414	1.964525	-0.057417
27	1	0	-1.789172	2.432486	0.623350
28	1	0	-3.522166	2.326396	0.160911
29	1	0	-2.262529	2.227156	-1.096873
30	6	0	-2.481839	-2.012453	0.325698
31	1	0	-1.846155	-2.316040	1.164632
32	1	0	-2.099545	-2.454791	-0.606288
33	1	0	-3.508225	-2.367893	0.485033
34	6	0	-4.066097	-0.129793	-0.825925
35	1	0	-4.183786	0.735022	-1.483608
36	1	0	-4.848816	-0.128469	-0.058978
37	1	0	-4.104950	-1.061446	-1.396312

TS1

SCF Done: E(RB+HF-LYP) = -1134.87649990 A.U. after 9 cycles

Center Number	Atomic Number	Atomic Type	Coordinates (Angstroms) X	Y	Z
1	29	0	-1.912119	-0.048872	-0.047769
2	6	0	-1.875615	-2.042889	-0.159832
3	1	0	-0.941936	-2.345570	-0.647468
4	1	0	-2.726301	-2.415848	-0.747854
5	1	0	-1.922060	-2.459657	0.854523
6	6	0	-2.158205	1.928632	0.084088
7	1	0	-1.259554	2.411292	-0.316338
8	1	0	-2.306623	2.217012	1.133128
9	1	0	-3.030315	2.245546	-0.505372
10	6	0	-3.775963	-0.220590	0.529497
11	1	0	-4.355299	-0.240631	-0.400306
12	1	0	-4.063061	0.639134	1.139330
13	1	0	-3.907913	-1.154621	1.080633
14	17	0	-0.068324	0.211577	-1.821935
15	6	0	-0.031477	-0.174374	2.131064
16	1	0	-0.169284	-1.235320	2.411374
17	1	0	0.822378	0.200244	2.741371
18	1	0	-0.919784	0.362316	2.500417
19	3	0	0.941240	0.016402	0.267890
20	8	0	2.299951	1.605023	0.345222
21	8	0	2.427689	-1.458728	0.054122
22	6	0	3.051572	1.828003	-0.838512
23	1	0	3.835665	2.582995	-0.660363
24	1	0	2.398039	2.153094	-1.658983
25	1	0	3.511733	0.873836	-1.104183
26	6	0	1.638600	2.777157	0.809858
27	1	0	1.027127	2.475066	1.661554
28	1	0	0.987090	3.191083	0.028820

29	1	0	2.377817	3.535829	1.115808
30	6	0	2.135350	-2.517163	-0.851370
31	1	0	1.683806	-2.058502	-1.732706
32	1	0	1.418529	-3.222045	-0.407168
33	1	0	3.059337	-3.054904	-1.120974
34	6	0	2.908128	-1.917325	1.309093
35	1	0	2.164077	-2.557792	1.802151
36	1	0	3.079818	-1.034785	1.928178
37	1	0	3.850499	-2.475571	1.180891

CP2

SCF Done: E(RB+HF-LYP) = -1134.92455705 A.U. after 9 cycles

Center Number	Atomic Number	Atomic Type	Coordinates (Angstroms) X	Y	Z
1	29	0	-2.718215	-0.044376	0.157558
2	6	0	-4.677411	-0.045688	-0.156602
3	1	0	-4.844226	-0.426396	-1.175666
4	1	0	-5.123333	0.953938	-0.070361
5	1	0	-5.168481	-0.729386	0.549349
6	6	0	-2.718315	1.946924	-0.015239
7	1	0	-3.311718	2.255555	-0.888098
8	1	0	-1.709918	2.378315	-0.094234
9	1	0	-3.202419	2.355873	0.885130
10	6	0	-2.767937	-2.037366	0.284900
11	1	0	-2.690778	-2.296255	1.352180
12	1	0	-1.905392	-2.480806	-0.235088
13	1	0	-3.691370	-2.473378	-0.119113
14	6	0	-0.736513	-0.079921	0.479057
15	1	0	-0.313808	-0.099494	-0.537655
16	1	0	-0.433371	-0.976384	1.036543
17	1	0	-0.410818	0.825336	1.008716
18	3	0	1.686165	-0.070277	0.402464
19	17	0	3.239728	-0.487828	1.972954
20	8	0	2.115479	1.718699	-0.472935
21	8	0	2.101195	-1.363654	-1.144514
22	6	0	2.737187	2.689557	0.366741
23	1	0	3.413413	3.325056	-0.225844
24	1	0	3.296894	2.131749	1.120392
25	1	0	1.978617	3.320754	0.852146
26	6	0	1.308124	2.293236	-1.493808
27	1	0	0.900334	1.470561	-2.084252
28	1	0	1.916669	2.946669	-2.138216
29	1	0	0.478740	2.869577	-1.062714
30	6	0	1.656211	-2.690734	-0.866438
31	1	0	0.592698	-2.630116	-0.628754
32	1	0	2.204408	-3.107413	-0.010688
33	1	0	1.800669	-3.331003	-1.749929
34	6	0	3.481741	-1.319105	-1.497634
35	1	0	4.103299	-1.675446	-0.666863
36	1	0	3.722816	-0.273486	-1.699925
37	1	0	3.659525	-1.924788	-2.400136

$LiCl{\cdot}(OMe_2)_3$

SCF Done: E(RB+HF-LYP) = -932.976896813 A.U. after 12 cycles

Center Number	Atomic Number	Atomic Type	Coordinates (Angstroms) X	Y	Z
1	17	0	0.003482	0.882891	2.259162
2	8	0	-1.647813	-0.998481	-0.201492
3	8	0	1.644403	-1.003460	-0.202886
4	8	0	0.002712	1.588489	-1.130556
5	6	0	-2.451683	-1.403286	0.912393
6	1	0	-2.062692	-0.872869	1.783543
7	1	0	-2.375413	-2.489781	1.060491
8	1	0	-3.501979	-1.131109	0.737709
9	6	0	-2.039008	-1.604305	-1.424306
10	1	0	-3.086056	-1.364672	-1.660325
11	1	0	-1.925119	-2.697254	-1.375177
12	1	0	-1.393211	-1.204210	-2.209961
13	6	0	2.445779	-1.414073	0.910691
14	1	0	2.060479	-0.881330	1.782054
15	1	0	3.497806	-1.148794	0.735870
16	1	0	2.362289	-2.500090	1.058429
17	6	0	2.030754	-1.611779	-1.426034
18	1	0	1.388735	-1.205392	-2.211564
19	1	0	1.907302	-2.703723	-1.377776
20	1	0	3.079919	-1.381067	-1.661447
21	6	0	-1.180235	2.377438	-0.968739
22	1	0	-1.203114	3.181427	-1.717796
23	1	0	-1.221711	2.798075	0.043600
24	1	0	-2.031639	1.710886	-1.120218
25	6	0	1.188673	2.373200	-0.969820
26	1	0	1.214233	3.176377	-1.719654
27	1	0	2.037528	1.703306	-1.120875
28	1	0	1.232061	2.794529	0.042131
29	3	0	0.000437	0.070331	0.199855

2.4.7. Attempted Study of Intramolecular Isomerization of Organocopper(III) Complex

In order to probe the possibility of the pseudorotation mechanism for the isomerization of organocopper(III) complexes, geometry optimization of dianionic Cu(III) complex $[Me_3CuCl_2]^{2-}$ was carried out starting from a series of possible pentacoordinate (i.e., trigonal bipyramidal (TBP) and square-pyramidal (SPL)) structures as shown below. However, none of such structures was located as a stationary point, and all the attempts uniformly led to dissociation into a square-planar $[Me_3CuCl]^-$ complex and a chloride anion (closest distance > 10 Å). In addition, inclusion of a lithium cation into the below computational model did not give a pentacoordinate Cu(III) complex as well. Thus, geometry optimization led to the formation of a complex between $[Me_3CuCl]^-$ and LiCl, where the Cl atom of the former and

T. Gärtner, N. Yoshikai, M. Neumeier, E. Nakamura, R. M. Gschwind, *Chem. Commun.* **2010**, *46*, 4625-4626.

the Li atom of the latter electrostatically interact with each other (i.e., the Cl atom of LiCl does not interact with the Cu atom). Note also that attempts to locate a pentacoordinate Cu(III) complex of $[Me_4CuCl]^-$ led to dissociation into square-planar $[Me_4Cu]^-$ and a chloride anion. Because none of pentacoordinate Cu(III) complexes existed as a local minimum, we concluded that the classical pseudorotation mechanism is unlikely to operate in the organocopper(III) reactions.

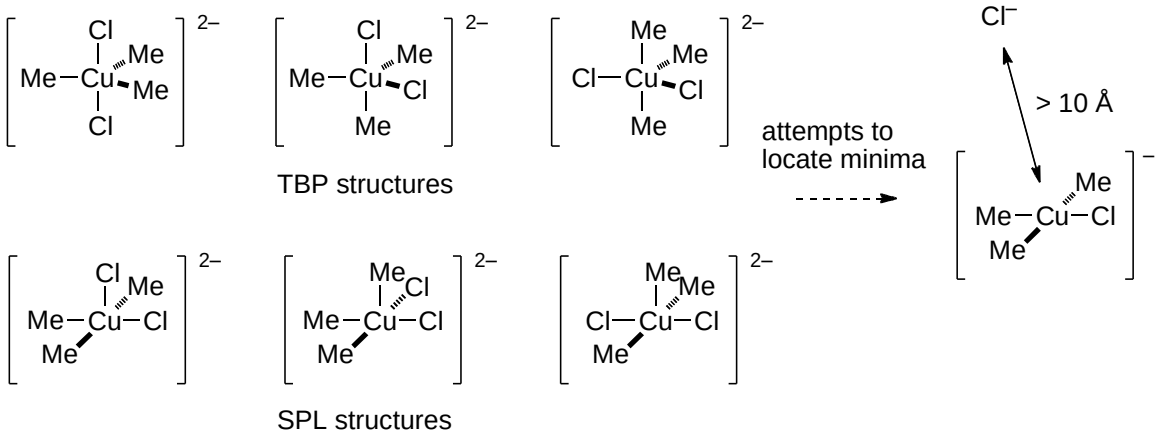

We also examined the possibility of unimolecular isomerization of a tetracoordinate Cu(III) complex. Thus, trigonal pyramidal (TP) and tetrahedral (Th) structures of $[Me_3CuCl]^-$ were calculated assuming that they are either intermediates or transition states for the cis/trans isomerization of the square-planar structure. However, the attempts to locate them as local minima and as TSs uniformly led to the square-planar structure and the TS for reductive elimination of ethane, respectively.

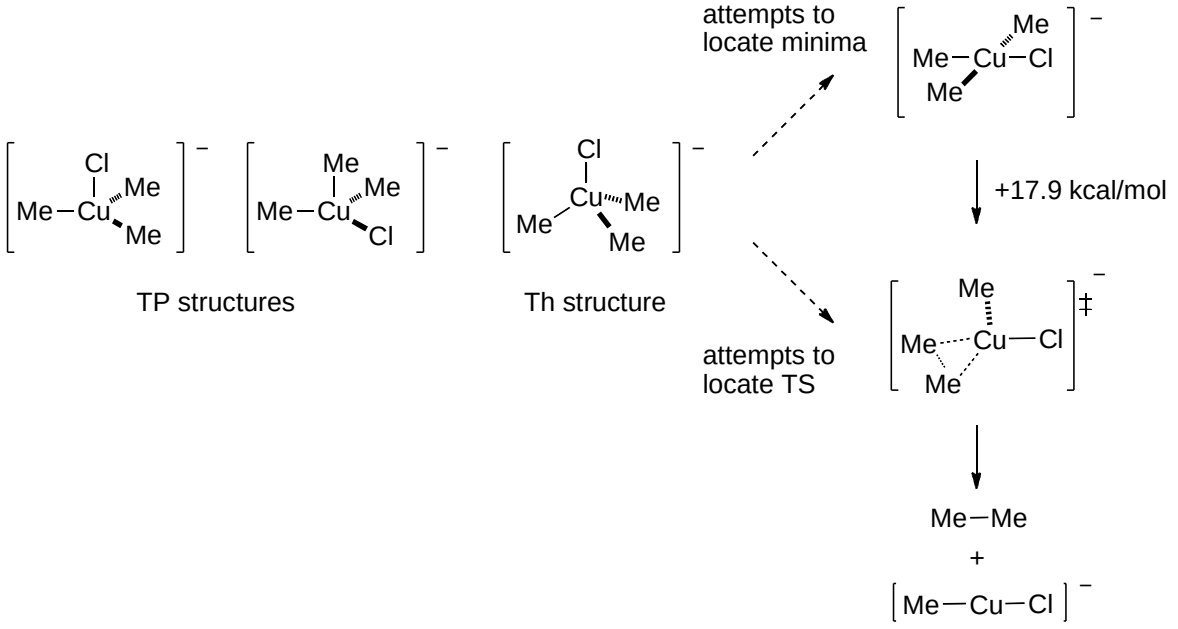

3. NMR Spectroscopic Investigations on Organocopper(I) Complexes and their Reactivity in Cross Coupling Reactions with Alkyl Halides

Maria Neumeier, Ruth M. Gschwind

to be published

3.1 Abstract

Organocuprates are one of the most frequently applied transition metal reagents in C-C bond formation reactions and the mechanistic and structural model system for organocopper reactions in general. A lot of effort was made to elucidate the structure-reactivity correlation of organocuprates including their Cu(I) and Cu(III) intermediates. But beside different oligomerization trends no significant structural differences between iodo- and cyanocuprates were found to explain the widespread synthetic myths about a special reactivity of cyanocuprates. However, the effect of subsequently formed copper(I) complexes, which are caused by the change of stoichiometry during the course of the reaction and their potential influence on yields and selectivity have not been considered until now. Therefore, a variety of highly soluble copper rich complexes $R_{1\text{-}4}Cu_{1\text{-}3}Li_{0,1}X_{0,1}$ ($R = Me_3SiCH_2$; X = I, ^{13}CN) were synthesized and their molecular formulas, the position of the equilibriums, their monomers and their aggregation trends were investigated by NMR spectroscopic methods. In addition, the effect of these subsequently formed copper rich complexes on the yields and selectivity of cross coupling reactions with alkyl halides was tested. In the case of iodocuprates, the formation of such copper rich complexes can be correlated to a loss of reactivity and diminished yields. Their formation can be avoided by adding an excess of alkyl lithium compound to the reaction mixture, which is able to regenerate the reactive organocuprate from these less reactive copper rich complexes, but also promotes side-reactions via metal-halogen exchange. In contrast, in the case of cyanocuprates, only the heteroleptic cuprate is formed during the course of the reaction, which does not affect the yields. With this study we provide an alternative explanation for the old controversial myths about a special reactivity of cyanocuprates.

3.2 Introduction

Regio- and diasteroselective C-C bond formation is one of the most important tools in organic synthesis.[1] Therefore, organocopper reagents are frequently used in cross coupling reactions with alkyl halides or addition reactions with Michael acceptors.[1–3] A detailed knowledge about the Cu(I) structures and their equilibriums in solution is vital for the successful use of these copper complexes.

In the solid state, uncharged homoleptic organocopper compounds R_nCu_n often exist as highly aggregated species, and therefore are insoluble in common organic solvents

(e.g. R = Me).[3,4] Disaggregation can be achieved by applying bidentate ligands (e.g. R = $CuC_6H_4CH_2NMe_2$-2-Me-5)[5], bulky substituents (e.g. R = mesityl, Me_3SiCH_2)[6–8] or coordinating solvents (e.g. dimethyl sulfide, tetrahydrothiophene).[6,7,9] The use of donor molecules (e.g. phosphines[10] and amines[11]) further reduces aggregation and results in separated RCu molecules (for overview see Figure 1). The common binding feature is the bridging character of the organic moieties via electron deficient two-electron three-center bonds and results in an almost linear coordination of copper, which can be converted to a T-shaped coordination by introducing bidentate ligands. In these Cu(I) complexes the organic moieties can also be substituted by other anionic ligands, such as halides, which increases the diversity of these complexes.[5]

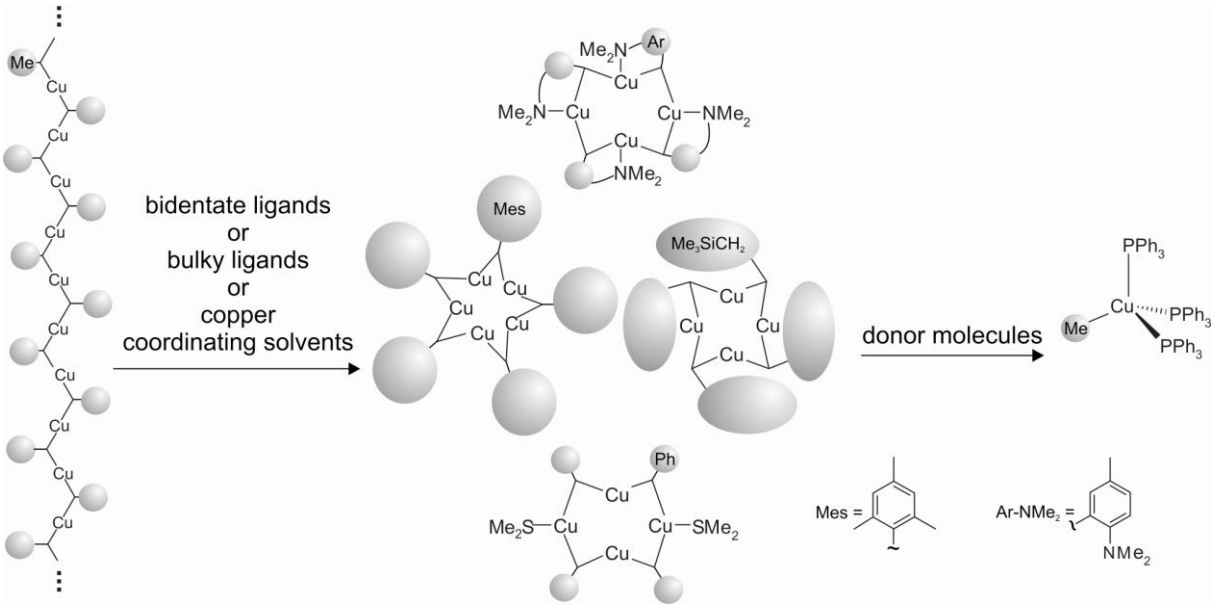

Figure 1: Schematic structures of organocopper compounds in the solid state illustrate the influence of ligands, solvents and donor molecules on the form and size of the aggregates, which crystallize preferentially from these solutions.

Conversions of copper(I) complexes with organolithium or Grignard reagents yield the organocuprates R_2CuM (M = Li, Mg).[3,4] Since the discovery by Gilman in 1952,[12] they developed rapidly to the most frequently applied organocopper compounds.[13–16] X-ray crystallography demonstrated a strong convergence of organocopper and organocuprate compounds. From solvents with little donor qualities, such as dimethyl sulfide (DMS) or diethyl ether (Et_2O), organocuprates crystallize aggregated, e.g. $[R_4Cu_2Li_2(DMS)_2]_n$[17] or $[R_4Cu_2Li_2(Et_2O)_3]$[18] (R = Me_3SiCH_2). The core structures are dimeric contact ion pairs (CIPs) of a cyclic $R_4Cu_2Li_2$ structure with alternating Cu and Li atoms and an almost linear $[R\text{-}Cu\text{-}R]^-$ moiety. These dimeric core structures can optionally be interlinked by solvent

molecules to higher aggregates. The size of aggregates can be reduced by strong Li^+ coordinating solvents or ligands, such as THF[19] or [12]-crown-4[20] (for overview see Figure 2). Also two homoleptic higher-order structures, characterized by the existence of $[R_3Cu]^{2-}$ anionic moieties, were observed, but remain exceptions.[9,21]

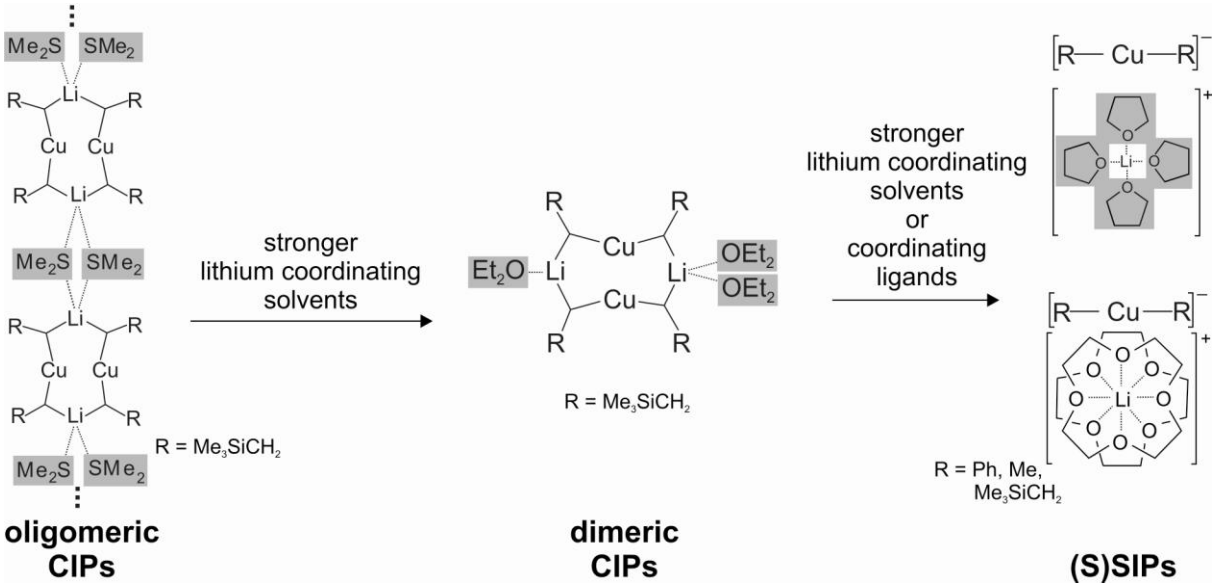

Figure 2: Schematic structures of organocuprates in the solid state illustrate the influence of lithium coordinating solvents and ligands on the size of aggregates, which crystallize from these solutions. Substances with strong Li^+ affinity lead preferentially to (solvent) separated ion pairs [(S)SIPs] instead of contact ion pairs [CIPs].

Since House published a higher reactivity of $Ph_2CuLi{\cdot}PhLi$ than Ph_2CuLi in coupling reactions with aryl bromide and Lipshutz introduced cyanocuprates formed from CuCN and two equivalents of RLi as special oragnocuprate reagents in 1981 and reported a special and enhanced reactivity of these cyanocuprates in substitution reactions of secondary alkyl halides,[22–25] a long standing vivid scientific discussion about the structural reason and later about the validity of the special reactivity of higher order and cyanocuprates started.[26] Thus, Liphutz initially reported yields between 82 to 100 % in reactions of $(n\text{-Bu})_2CuLi{\cdot}LiCN$ with unactiviated secondary alkyl halides in THF, while previous reports of reactions with $(n\text{-Bu})_2CuLi$ and Me_2CuLi led only to yields between 12 and 21%[3,27,28] and also later on better stereoselectivities using cyano- instead of iodocuprates were published.[29] Interestingly, the reactivity differences reported were dependent on the size of the cuprate substituent, while for $Me_2CuLi{\cdot}LiX$ (X = I, SCN) similar yields were found, significantly improved yields were reported for $(n\text{-Bu})_2CuLi{\cdot}LiSCN$ and $(n\text{-Pr})_2CuLi{\cdot}LiSCN$.[30] Furthermore, primary alkyl iodides were observed to react readily with $R_2CuLi{\cdot}LiCN$ and for substitution reactions with poorer leaving groups (Br, Cl) extremely mild reaction conditions could be applied,

i.e. applying lower temperatures than required for R_2CuLi.[31] In addition, despite its higher toxicity CuCN was claimed to be ideal for cuprate reactions due to several reasons, e.g. the lower costs, the reduced hygroscopic properties and the better light and thermal stability of CuCN itself and its cuprates.[22] The higher reactivity of these cyanocuprates were initially explained by a higher-order bisanionic structure $[R_2(CN)Cu]^{2-}$ of these cyanocuprates, in which both alkyl substituents and the cyanide ligand are all three directly bound to the copper center. This structural proposal was based on a previous low temperature ^1H NMR study of various ratios of MeLi to MeCu in Me_2O at 137 K by Ashby *et al.*[32] In this study, besides MeLi and the well known Gilman cuprate Me_2CuLi also copper rich Me_3Cu_2Li dimers (see Figure 3A) and two signals of a complex with the nominal stoichiometry Me_3CuLi_2 were detected, for which a higher-order structure was proposed based on an intensity ratio of 1:2 (see Figure 3B). This raised the famous discussion whether cyanocuprates exist as higher-order species or as cyano-Gilman cuprates in their thermodynamically most stable form.

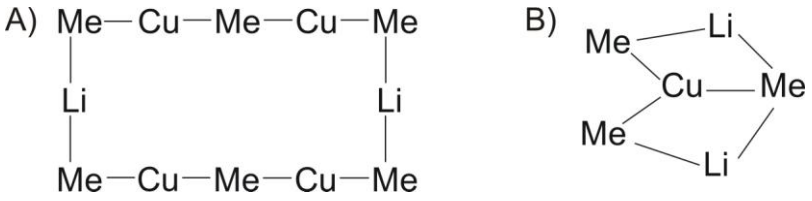

Figure 3: (A) Proposed structure of the $[Me_3Cu_2Li]_2$ dimer and (B) the higher order cuprate Me_3CuLi_2.[32]

Bertz *et al.* reported very similar ^{13}C chemical shifts for the organic moieties of $R_2CuLi{\cdot}LiI$ and $R_2CuLi{\cdot}LiCN$ (R = Ph, Et, Me) in THF.[33] In addition, they observed almost equal chemical shifts for the cyanide ligands of all homoleptic cuprates $R_2CuLi{\cdot}LiCN$ (R = Ph, Et, Me), which contrasted their observations for the corresponding heteroleptic cyanocuprates RCu(CN)Li (R = Ph, Et, Me). From the missing inductive effect on the ^{13}C chemical shift of the organic group and the independence of the CN chemical shift of the σ-donor properties of the organic moiety, they concluded cyano-Gilman structures. Though Lipshutz *et al.* reported similar ^{13}C chemical shifts for $Me_2CuLi{\cdot}LiI$ and $Me_2CuLi{\cdot}LiCN$ in THF, however they observed different chemical shifts in Me_2S and therefore concluded higher-order structures.[34] Later on Bertz and Berger *et al.* corroborated the cyano-Gilman structure by the missing coupling between the organic moieties and the cyanide ligand in $R_2CuLi{\cdot}LiCN$ (R = Ph, Et, Me), which was observable for the corresponding heteroleptic cyanocuprates RCuCN (R = Ph, Et, Me).[35,36] In contrast, Lipshutz *et al.* explained the missing coupling between the cyanide ligand and the organic moieties by π-bonding of CN to the

copper center.[37] Despite, ^{15}N-, ^{6}Li- and ^{13}C-NMR spectroscopic investigations on BuCu(CN)Li und $Bu_2CuLi{\cdot}LiCN$ evidenced the Gilman type structure.[38] Also other methods like EXAFS, XANES[39,40] and ab initio calculations[41–43] point toward Gilman type reagents, in which cyanide is bound to lithium. Finally, two independent X-ray structures $[Ar_2Cu(CN)Li_2(THF)_4]_\infty$ (Ar = $[C_6H_4CH_2NMe_2\text{-}2]^-$)[44] and [tBuCutBu{Li(THF)(PMTEDA)$_2$ CN}] (PMTEDA = pentamethyldiethylenetriamine)[45] solved the controversy in favor of the cyano-Gilman cuprate. Further ^{1}H,^{6}Li HOESY studies of $Me_2CuLi{\cdot}LiCN$ revealed an equilibrium of dimeric contact ion pairs (CIPs) and solvent separated ion pairs (SSIPs) in solution, depending on the lithium affinity of the solvent.[46] In addition, the same homodimeric core structure for $Me_2CuLi{\cdot}LiCN$ as for $Me_2CuLi{\cdot}LiI$ was shown to exist as main species in solution.[47] Finally, the correlation of these structural information to low reactivity rates of organocuprates with Michael acceptors in THF[48,49] or in the presence of lithium complexing crown ethers,[50] identified CIPs as the reactive species.[18,49] Diffusion ordered spectroscopy (DOSY) on highly concentrated solutions of $R_2CuLi{\cdot}LiX$ (R = Me, Me_3SiCH_2; X = I, CN) in Et_2O enabled the transfer of solid state structures into refined supramolecular models of higher aggregated organocuprates in solution.[51] There, the only difference found for the structures of cyano- and iodocuprates in solution was the trend of cyanocuprates to form higher aggregates than iodocuprates. Furthermore, the use of the bulky substituent Me_3SiCH_2 instead of Me resulted in a significant reduction of the aggregate size. In addition, disaggregation to dimeric CIPs was shown for lower concentrations of organocuprates in Et_2O[51] or by gradual addition of Li^+ coordinating THF[52] and, the reactivity of organocuprates could be correlated to these supramolecular structures.[52] In order to understand the selectivity of organocuprate reactions, the mechanisms were investigated by theoretical calculations and a dimeric CIP was found to be the minimal reactive cluster size.[53] Using this minimal cluster size various differently structured CIPs, Cu(I) π-intermediates, Cu(III) intermediates and transition states were proposed for conjugate addition and cross coupling reactions.[2] Later on the solution structures of central Cu(I) π-intermediates and square planar Cu(III) intermediates were elucidated by 2D NMR methods[54–59] and confirmed experimentally the main steps of the theoretical proposals. Aspects like Cu(III) stabilization by classical additives (amines, phosphines),[60] targeted reactions with copper(III) complexes[61] and ligand exchange reactions in Cu(III) intermediates[62] corroborated the identical reactivity of organocuprates and Cu(III) intermediates. Similarly to the Cu(I) clusters and intermediates in all of these studies the structures of cyanide- and iodide-containing Cu(III) intermediates were found to be

structurally equal. Hence, the special reactivity of cyanocuprates neither can be explained by structural differences of the organocuprates $R_2CuLi{\cdot}LiCN$ and $R_2CuLi{\cdot}LiI$ nor by structural variances of the Cu(I) or Cu(III) species. However, since the thermodynamically most stable form often is not the kinetically most active one, a fast equilibrium between the cyano-Gilman cuprate and a small concentration of other structures in solution cannot be excluded from these experimental investigations. Exemplary theoretical calculations on methylcuprates by Nakamura *et al.* revealed two further possible reactive species for the cyanocuprate, which possibly could explain a special reactivity for these reagents.[63,64] There, lower activation energies were calculated for the substitution reaction of MeBr with a heterodimeric core structure of $Me_2CuLi{\cdot}LiCN$ (bridged by LiCN) as well as heteroleptic species $MeCu(CN)Li{\cdot}MeLi$ (bridged by MeLi). A general problem in the discussion about higher reactivities of cyanocuprates is the direct comparability of reactivity data of cyano- and iodocuprates due to variations in the experimental conditions. Despite the widespread acceptance and belief in the higher reactivity of cyanocuprates in the synthetic community, Bertz showed in a direct comparison of reactivity profiles for $R_2CuLi{\cdot}LiI$ and $R_2CuLi{\cdot}LiCN$ (R = Me, Bu) in Michael addition reactions similar or even reduced reactivity of cyanocuprates.[43,49] Also our own previous investigations on this reaction type, revealed only a small difference in the reactivity of $Me_2CuLi{\cdot}LiI$ and $Me_2CuLi{\cdot}LiCN$, which is modulated by the aggregate size of the different reagents.[52] However, in the substitution reaction of $R_2CuLi{\cdot}LiX$ (X = I ,CN) with cyclohexyl iodide, the reaction which initialized the higher order discussion, Bertz and Oagle initially reported higher reactivities for the cyano-Gilman cuprate compared to the iodo-Gilman cuprate,[49] which were later on brought into line by several renormalization procedures taking side reactions into account.[65] Although the controversy of higher-order cuprates had been resolved in favor of the cyano-Gilman reagent[26] and dimeric CIPs had been identified as reactive species in organocuprate reactions,[18,49] the myths about a special reactivity of cyanocuprates still remain by certain published[66] and unpublished reactions that show a better performance with cyanocuprates $R_2CuLi{\cdot}LiCN$ than with classical Gilman reagents $R_2CuLi{\cdot}LiX$ (X = Br, I).

In contrast to the elaborated investigations on the organocuprate structure and the corresponding intermediates, the appearance of subsequently formed copper(I) complexes, which might arise due to a changed stoichiometry during the course of organocuprate reactions, have not been addressed in any study. Despite the fact that Me_3Cu_2Li had been detected in reactions of methyl copper with less than one equivalent of methyl lithium in

Me_2O or THF,[32] the influence of such copper rich complexes on organocuprate reactions have not been considered. It is proven fact that during the product formation of cross coupling or Michael addition reactions, alkyl copper compounds (RCu) are formed as by-products (see Scheme 1A, B).[3,67] Potentially, RCu is available for subsequent conversions with organocuprates and might yield copper rich complexes R_3Cu_2Li (see Scheme 1C). Since methyl copper is not soluble in Et_2O because of extended aggregates,[3,4] the formation of such copper rich complexes is expected to play a minor role in this case. However, by applying coordinating solvents,[6,7,9] e.g. THF or bulky substituents,[6–8] the alkyl copper structures become disaggregated, which provides sufficient solubility for subsequent conversions. Then, the formation of copper rich complexes similar to Me_3Cu_2Li is highly probable, and might influence the selectivity and yields of C-C bond formation reactions. During our NMR spectroscopic investigations on Cu(III) intermediates in cross coupling reactions[58,62] we noticed that such copper rich complexes are not spectroscopically resolved at temperatures typically applied in organocuprate reactions and only a shift of the organocuprate signal during the reaction is observed.

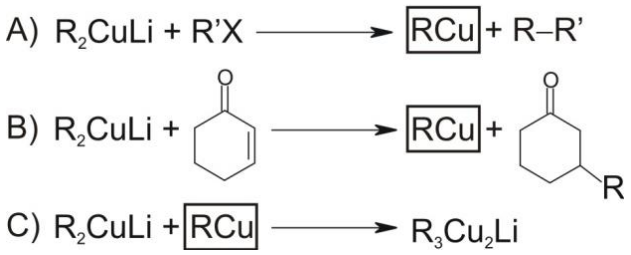

Scheme 1: Formation of alkyl copper compounds (RCu; black rectangle) in (A) cross coupling or (B) Michael addition reactions of organocuprates R_2CuLi and (C) a subsequent reaction pathway for RCu.

In order to clarify the long-standing myths about a special reactivity of cyanocuprates, we synthesized a variety of highly soluble copper rich complexes $R_{1\text{-}4}Cu_{1\text{-}3}Li_{0,1}X_{0,1}$ ($R = Me_3SiCH_2$; X = I, ^{13}CN) and investigated their structures and reactivity in cross coupling reactions with methyl iodide.

3.3 Results and Discussion

3.3.1. Model System

To test the influence of subsequently formed copper rich complexes on the reactivities and selectivity of organocuprate reactions, copper rich complexes $R_{1\text{-}4}Cu_{1\text{-}3}Li_{0,1}X_{0,1}$ ($R = Me_3SiCH_2$; X = I, ^{13}CN) **3a-f** were synthesized. Despite the lower solubility of copper

rich complexes in Et_2O, this solvent was chosen to be able to apply our over years developed approach for the structure elucidation of organocuprates in Et_2O. To compensate the extremely low solubility, e.g. of MeCu, in Et_2O, the extended and therefore highly soluble substituents R = Me_3SiCH_2 were chosen. As test system to reveal the influence of copper rich complexes on the selectivity and reactivity of organocuprate reactions, cross coupling reactions between the organocuprates $R_2CuLi{\cdot}LiX$ **3a•LiX** (R = Me_3SiCH_2; X = I, ^{13}CN) and methyl iodide **4a** were chosen, because reactivity differences between cyano- and iodocuprates were reported mainly in substitution reactions with sterically hindered alkyl halides and highly reactive organocuprates. A small alkyl halide and a large relatively unreactive cuprate substituent, which is usually used as dummy ligand,[63] were chosen to mimic a sterically hindered substitution reaction with a critical reactivity and sufficient solubility of copper rich complexes. In addition, all NMR spectroscopic measurements were performed at low temperatures between 170 and 185 K, to resolve the different complex species **3a-f**, since only broad or averaged signals are observed at temperatures typically applied for synthetic conditions (195-273 K),[32] (for details see SI).

3.3.2. Formation of Iodocopper(I) Complexes in Diethyl Ether

In order to study the formation of copper rich iodocomplexes, seven different stoichiometries of Me_3SiCH_2Li **1a** and CuI **2a** were investigated in Et_2O at 170 K. These mixtures yielded the copper(I) complexes $R_{1\text{-}4}Cu_{1\text{-}3}Li_{0,1}I_{0,1}$ (R = Me_3SiCH_2) **3a•LiI-3e** (see Scheme 2). The complex composition depending on the stoichiometric ratio of **1a** to **2a** was investigated by integral analysis of ^1H NMR spectra (for details see SI), the monomeric structures were determined with $^1H,^{13}C$ HMBC spectra and aggregation trends were studied with DOSY measurements.

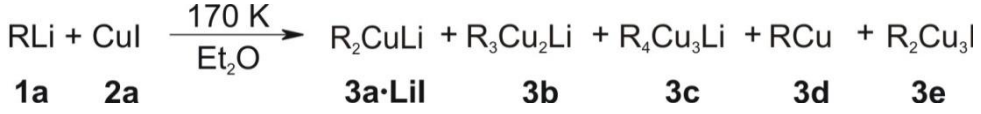

Scheme 2: Formation of the copper(I) complexes $R_{1\text{-}4}Cu_{1\text{-}3}Li_{0,1}I_{0,1}$ (R = Me_3SiCH_2) **3a•LiI-3e** in reactions of Me_3SiCH_2Li **1a** with CuI **2a** at 170 K in Et_2O.

By adding different amounts of **1a** to an ethereal suspension of **2a** at 170 K, the formation of the respective soluble copper(I) complexes started immediately. This could be followed in the corresponding proton spectra (see Figure 4) and was visible due to a specific color change (vide infra). The signals of **1a** and **3a•LiI** were assigned based on previous investigations[51]

and molecular formulas were determined by integral analysis of the copper rich complexes **3b-e**, which were observed downfield from **3a•LiI** (for details see SI).

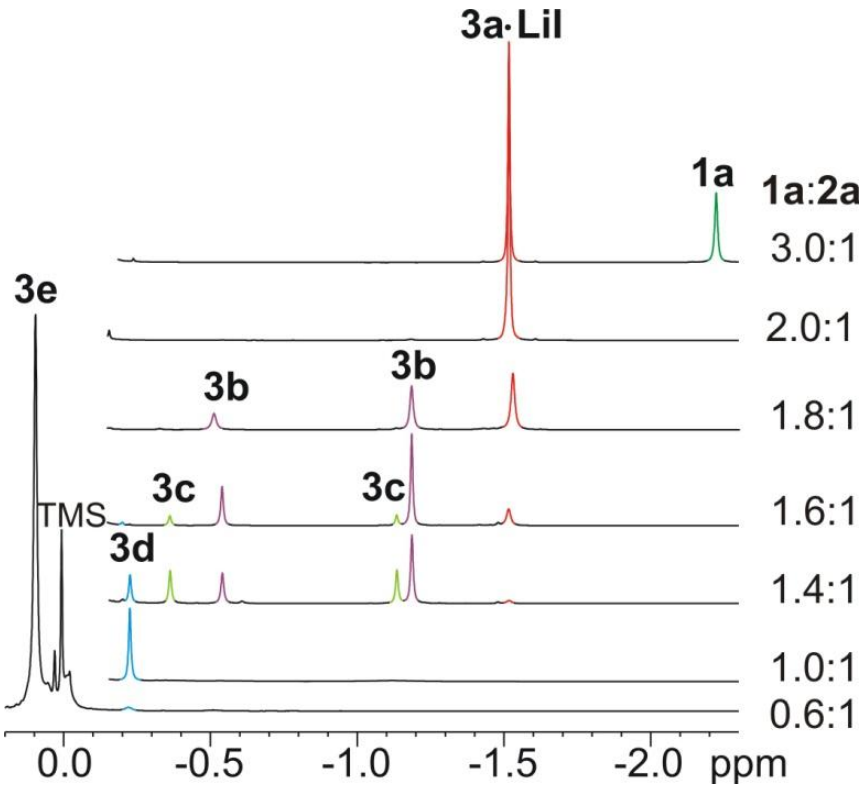

Figure 4: Cu(I)-sections of the ^{1}H spectra of Me_3SiCH_2Li **1a** and the different Cu(I) complexes **3a•LiI-3e** in diethyl ether at 170 K with accompanying ratios of **1a** to CuI **2a**. The CH_2-signals of the different components are depicted in green **1a**, red **3a•LiI**, purple **3b**, light green **3c** and blue **3d**. The uncolored signal on the left side includes all protons of **3e**. For clarity, the corresponding Me_3Si-signals are omitted from second spectrum.

The ^{1}H spectra of the clear and colorless sample with **1a**:**2a** = 3.0:1 revealed the formation of **3a•LiI** (red in Figure 4), leaving the over-stoichiometric amount of **1a** (green in Figure 4) unreacted in solution (deviating from Ashby's results[32] the integrals of **1a** and **3a•LiI** show exactly the expected 2:1 ratio). In the colorless sample with **1a**:**2a** = 2.0:1 exclusively **3a•LiI** and no more excess **1a** was detected. In the clear and pale brown solution with **1a**:**2a** = 1.8:1, besides **3a•LiI**, complex **3b** (purple in Figure 4) with two chemically non-equivalent organic moieties in a 1:2 ratio was observed, for which the molecular formula R_3Cu_2Li ($R = Me_3SiCH_2$) was determined. The clear and yellow sample with **1a**:**2a** = 1.6:1 indicated the formation of **3b** and additionally R_4Cu_3Li ($R = Me_3SiCH_2$) **3c** (light green in Figure 4) with two chemically non-equivalent organic moieties in a 1:1 ratio. Besides, small amounts of the alkyl copper compound RCu ($R = Me_3SiCH_2$) **3d** were detected (blue in Figure 4). From the ratio **1a**:**2a** = 1.4:1 onwards, only negligible amounts of **3a•LiI** were detected and exclusively the copper richer complexes **3b-d** were observed and at

1a:**2a** = 1.0:1 exclusively **3d** was detected. Below a 1:1 ratio (**1a**:**2a** = 0.6:1), the solution was still clear and yellow, but **2a** partly remained at the bottom of the NMR tube and complex **3e** (uncolored in Figure 4) was observed. According to a X-ray structure reported by van Koten *et al.*,[68] for **3e** the complex composition of R_2Cu_3I is expected and fits the observed spectra very well. However, an independent exact determination of the stoichiometry of **3e** is obscured by severe spectral overlap. In summary, in seven different mixtures of **1a** and **2a**, a variety of different Cu(I) complexes **3a•LiI**-**3e** with the general molecular formula $R_{1\text{-}4}Cu_{1\text{-}3}Li_{0,1}I_{0,1}$ were observed. At ratios of **1a** to **2a** larger than 2:1, exclusively, **3a•LiI** (R_2CuLi; R = Me_3SiCH_2) was present. By reducing the content of **1a**, the position of the equilibrium was shifted towards copper richer complexes, which appeared in the proton spectra downfield from **3a•LiI**, indicating a reduced polarization for **3b-e** with respect to **3a•LiI**.

3.3.3. Structures of Iodocopper(I) Complexes in Diethyl Ether

Next, the structures of complexes **3a•LiI**-**3e** were addressed. From various NMR spectroscopic investigations on organocuprates,[35,36] π-complexes[69] as well as Cu(III) complexes[58,62] and in agreement with theoretical calculations[41,70–72] it is known that the partly covalent copper-alkyl bond allows for a magnetization transfer via scalar coupling, e.g. observable in $^1H,^{13}C$ HMBC spectra, whereas the predominantly electrostatic lithium-alkyl interaction acts as a spin system barrier. In addition, DOSY measurements can be used to elucidate the hydrodynamic ratios of organocuprate aggregates including salt- and solvent-coordination.[51] Therefore, for the structure elucidation of complexes **3b-d**[a] mixtures of **1a** and **2a** were prepared and investigated by $^1H,^{13}C$ HMBC and DOSY measurements at 185 and 170 K, respectively. In order to avoid extended supramolecular aggregates, low concentrated samples were used (c = 0.07-0.13 mol/L).

For **3b**, two possible monomeric structures are conceivable (see Figure 5A) based on the common binding feature of linear copper coordination for all Cu(I) complexes (see Figures 1-2) and our proton NMR measurements, which indicated two chemically non-equivalent CH_2 groups in a 1:2 ratio. Structure **3b i** can be considered as the simple adduct of an organocuprate with an alkyl copper unit bridged by a lithium ion and one equivalent of

[a] Structure determination for **3e** was not possible because of spectral overlap.

lithium iodide. Hence, because for this connectivity, no cross signals between the chemically non-equivalent CH_2 groups are expected. In contrast, in **3b ii** all organic moieties are bridged by Cu atoms, which enable magnetization transfers between the chemically non-equivalent CH_2 groups. In the $^{1}H,^{13}C$ HMBC spectrum of **3b** (see Figure 5B), a cross signal between the chemically non-equivalent CH_2 groups (see black square in Figure 5B), a cross signals to their corresponding Me_3Si moieties and no cross signal between the two chemically equivalent CH_2 groups were detected.

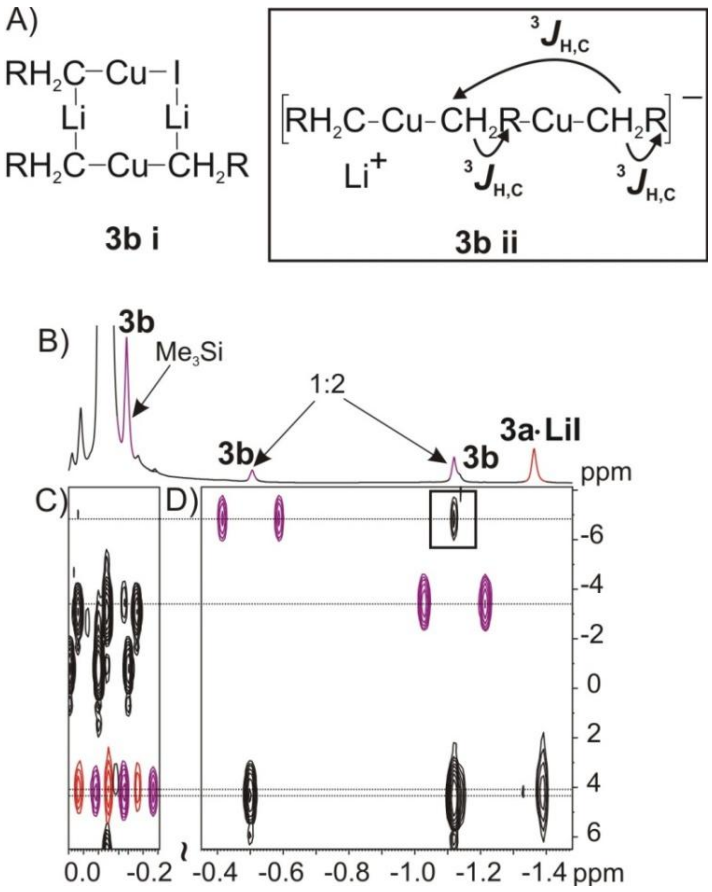

Figure 5: Identification of the monomeric structure of **3b** as **3b ii**: (A) Possible structures **3b i** and **3b ii** (R = Me_3Si) on the basis of (B) the ^{1}H NMR spectrum. (C,D) High-field sections of the $^{1}H,^{13}C$ HMBC spectrum at 185 K in Et_2O (Me_3Si region (C) scaled down for better resolution). The signals of the Cu(I) complexes **3a·LiI** and **3b** are depicted in red and purple, respectively. The decisive cross signal, which allows for the unambiguous identification of **3b** as **3b ii** is indicated by a black square. The observed couplings are indicated by arrows in structure **3b ii**.

Therefore, the $^{1}H,^{13}C$ HMBC coupling pattern is only consistent with the monomeric structure **3b ii**, in which the chemically non-equivalent CH_2 moieties share a $^{3}J_{H,C}$ coupling, which was observed and the chemically equivalent CH_2 moieties share a $^{5}J_{H,C}$ coupling, which was not detectable here. Accordingly, complex **3c** was investigated (for details see SI) and a similar structure was determined, which is elongated by one more RCu moiety. Since, **3d** is

the homoleptic organocopper(I) complex R_nCu_n, the monomeric structure is evidently RCu. The structures **3b** and **3c** derive from **3a•LiI** by gradual elongation of the homocuprate by one and two RCu units, respectively, and may be considered as charged organocuprate analogue structures, whereas **3d** is an uncharged alkyl copper structure.

Next, the aggregation level of **3b**-**3d** was determined by DOSY investigations. This was done in comparison with our previous DOSY studies of **3a•LiI** in Et_2O.[51] There, in highly concentrated samples (0.6 mol/L) homodimeric core structures had been observed to form oligomers via salt and solvent bridges. For the salt-containing dimer $[R_2CuLi]_2(Et_2O)_6(LiI)_2$, the average number of solvent units per dimer had been determined. In lower concentrated samples disaggregation to dimeric CIPs had been observed, which can be rationalized by the detachment and solvation of salt units and correlates with decreased aggregation tendencies for salt-free organocuprates.[51] Accordingly, in our studies, the experimental diffusion coefficients (D_{exp}) for **3a•LiI-3d** (c = 0.07-0.13 mol/L) were determined from DOSY experiments and compared to theoretically calculated diffusion coefficients D_{calc} for the respective monomers, dimers and higher aggregates. For all monomers and dimers of the organocuprate **3a•LiI** and the cuprate analogue structures **3b** and **3c** in a first approximation a spherical shape was assumed (hereafter named model free approach) and their diffusion coefficients were calculated using hard-sphere increments[73] and the Stokes-Einstein theory[74]. For the salt and solvent coordinated dimers **3a•LiI-3c**, the full salt content produced during their formation (see SI Scheme 1) was included into the structure and, according to the known structure of the organocuprate **3a•LiI**,[51] the salt to solvent ratio was set to 1:3. For the organocopper compound **3d** the model free approach was used for the monomer and tetramer, for which a schematic structure is shown in Figure 1. Additionally, a theoretical diffusion coefficient for a higher linear aggregate had been calculated including a shape factor for cylindrical geometry (for details see SI).[75] In Table 1 the experimental and calculated diffusion coefficients for **3a•LiI-3d** are listed.

Table 1: Experimental diffusion coefficients (D_{exp}) compared to calculated diffusion coefficients (D_{calc}) for monomers, dimers and higher aggregates of 0.07-0.13 mol/L **3a•LiI-3d** (R = Me_3SiCH_2) in Et_2O, obtained by a model free approach including hard-sphere increments[73] and the Stokes-Einstein theory.[74]

compound		D_{exp} [10^{-8} m^2 s^{-1}]	D_{calc} [10^{-8} m^2 s^{-1}]
3a	$[R_2CuLi]$		9.7
	$[R_2CuLi]_2$		7.7
	$[R_2CuLi]_2$•$2LiI$•$6Et_2O$		5.9
	$\{[R_2CuLi]_2$•$2LiI$•$6Et_2O\}_{1.3}$	5.8±0.5	5.8*
3b	$[R_3Cu_2Li]$		8.5
	$[R_3Cu_2Li]_2$	5.1±0.4	6.7
	$[R_3Cu_2Li]_2$•$4LiI$•$12Et_2O$		4.9
3c	$[R_4Cu_3Li]$		7.8
	$[R_4Cu_3Li]_2$	5.0±0.5	6.6
	$[R_4Cu_3Li]_2$•$6LiI$•$18\ Et_2O$		4.4
3d	[RCu]		1.2
	$[RCu]_4$		7.8
	$[RCu]_8$	4.6±0.3	4.4*

*) A shape factor for cylindrical geometry was included.[75]

All experimentally determined diffusion coefficients are significantly smaller than calculated for monomers and salt- and solvent-free dimers. For the organocuprate **3a•LiI** the experimental diffusion coefficient indicates aggregates slightly higher than dimers. For the cuprate analogue structures **3b** and **3c** the experimental diffusion coefficients cross over from a structure close to the salt-containing model dimer of **3b** to the salt-free dimer of **3c**. Despite the fact that a higher aggregation trend for higher salt contents is expected because of previously investigated aggregation trends of salt-containing in comparison to salt-free organocuprates,[51] this effect presumably is overcompensated by the strong dilution of the sample (c = 0.07-0.13 mol/L). Probably, this dilution prevents the coordination of all salt units to the dimeric structure of **3b** and **3c** and therefore leads to a disaggregation, which is in accordance with previous investigations.[51,52] The experimental diffusion coefficient of the organocopper compound **3d** excludes a monomer and also the tetrameric structure, which had been reported in X-ray studies,[8] and favors a higher aggregate. The theoretical diffusion coefficient for an octameric linear aggregate fits the experimental data, but in principle, also a cyclic system is conceivable. In summary, based on the structure of the highly soluble **3a•LiI**, with our NMR spectroscopic approach, we derived structures for the complexes **3b-d**. The structures **3b** and **3c** consist of extended cuprate monomers, form equal core structures and show similar aggregation trends as organocuprates. Interestingly, for the organocopper compound **3d** a higher aggregate than in the solid state structure was observed. For visualization, schematic structures for **3a•LiI-3c** are shown in Figure 6. They match the

common bonding features of organocuprates and organocopper compounds with almost linearly coordinated Cu atoms bridged by alkyl moieties.

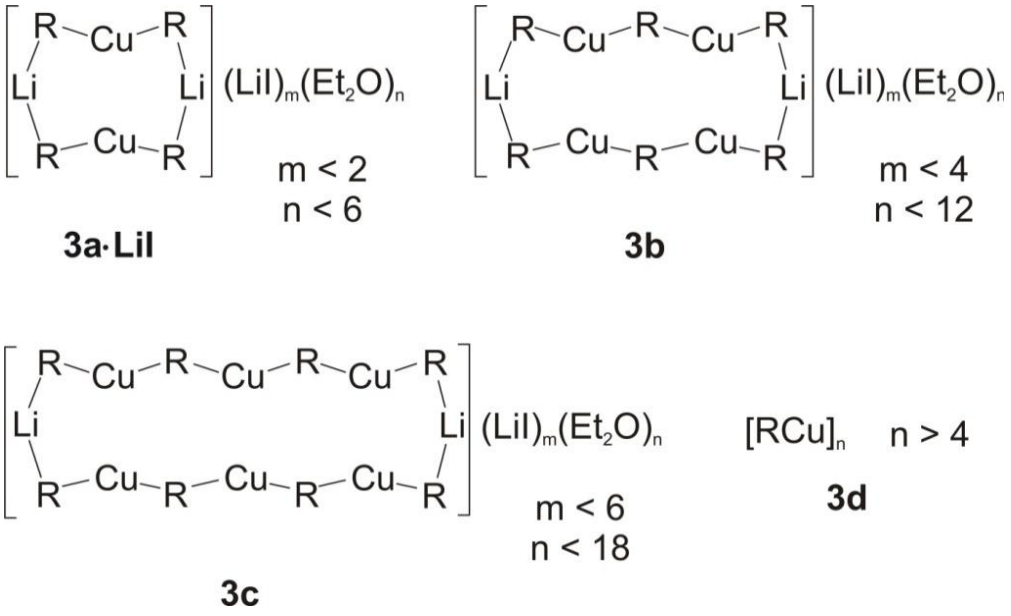

Figure 6: Schematic structures **3a•LiI-3d** (R = Me_3SiCH_2) based on common structural features of organocuprates and copper(I) compounds.

3.3.4. Formation and Structures of Cyanocopper(I) Complexes in Diethyl Ether

Since a higher reactivity for cyanocuprates was discussed during the controversy about higher-order cuprates,[22] next, the complex formation with $Cu^{13}CN$ **2b** was studied. In this case soluble heteroleptic cyanocuprates RCuCNLi are known,[22] which give rise to the question, whether there are still additional copper rich complexes, which remained undetected until now. Therefore, six samples were prepared with **1a** to **2b** ratios of 3.0:1 to 0.3:1 and investigated by 1D as well as DOSY measurements (for details see SI).

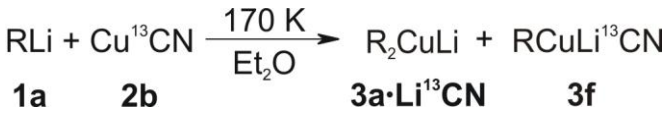

Scheme 1: Formation of the copper(I) complexes $R_{1\text{-}2}CuLi^{13}CN_{0,1}$ (R = Me_3SiCH_2) **3a•Li^{13}CN** and **3f** in reactions of Me_3SiCH_2Li **1a** with $Cu^{13}CN$ **2b** at 170 K in Et_2O.

Depending on the stoichiometric ratio, exclusively Me_3SiCH_2Li **1a**, homoleptic cyanocuprate **3a•Li^{13}CN** (orange in SI Figure 3) and heteroleptic cyanocuprate **3f** (magenta in SI Figure 3) were detected, but not any trace of additional copper rich complexes or higher-order cuprates. The DOSY investigations indicate the formation of moderately higher aggregates than dimers for **3a•Li^{13}CN** and **3f** and only slightly higher aggregation trends for the homo- and heteroleptic cyanocuprate than for the iodide containing **3a•LiI**. Despite the

fact that for cyanocuprates a higher aggregation trend than for iodocuprates is expected from previous aggregation studies,[51] probably the strong dilution overcompensates this trend, which also was discussed above for the iodocomplexes **3a•LiI**-**3c**.

3.3.5. Reactivity of Iodo- and Cyanocopper(I) Complexes in Cross Coupling Reactions with Methyl Iodide

The decreased polarization of the organic moieties of copper rich complexes **3b-e** with respect to **3a•LiI** suggests a decreased reactivity in C-C bond formation reactions and additionally the reactive organocuprate species is over-stoichiometrically consumed at the moment copper rich complexes are formed. Both effects are expected to reduce the reactivity of iodocuprates compared to cyanocuprates. Because such reactivity differences were reported mainly for substitution reactions (vide supra), the reactivity of **3a•LiI** and **3a•Li^{13}CN** in the cross coupling reactions with methyl iodide **4a** was tested.

To elucidate the influence of the copper rich Cu(I) complexes on the reactivity, an exact one to one stoichiometric ratio of Gilman cuprate and alkyl halide (**3a•LiI/3a•Li^{13}CN**:**1a**:**4a** = 1.0:0.0:1.0) was selected for both iodo and cyanocuprate. To enable the regeneration of the reactive Gilman cuprates during the reaction, the reaction was performed additionally in the presence of one equivalent excess of the alkyl lithium reagent **1a** (**3a•LiI/3a•Li^{13}CN**:**1a**:**4a** = 1.0:1.0:1.0). For both conditions two concentrations (0.05-0.06 mol/L and 0.13 mol/L) were chosen to test the influence of the aggregate size. Each mixture was reacted 20 minutes at 170 K, then ^{1}H-NMR spectroscopy was used to detect the existent copper species and to determine the reaction yields by integration. Without rapid-injection NMR technique[76,77] this is the minimum time necessary for temperature equilibration, tuning and shimming. ^{1}H NMR investigations at a later point of time showed that the reactions were already completed after that minimal 20 minutes (see SI Figure 6). A further reduction of the reaction rate by lower temperatures is not possible due to the close melting point of Et_2O (157K) and relatively small line widths necessary for reliable spectra integration. In addition, extensive reactivity investigations of Bertz and Oagle showed that it is extremely difficult to obtain reliable and highly reproducible kinetic data for substitution reactions of organocuprates.[49,65,78] Therefore, in this study only yields are discussed.

Table 2: Test reactions of 0.05-0.06 mol/L (0.13 mol/L) **3a•LiX** (X = I, ^{13}CN) with one equivalent MeI **4a** without and with excess of $TMSCH_2Li$ **1a**. The yields of the main product **5a** and side product **5b** in % were determined by integral analysis of the proton spectra (see Figure 7).

reaction	ratio	main-product 5a [%]	side-product 5b [%]	
			without 4a	with 4a
3a•LiI+1a+4a	1.0:0.0:1.0	57 (31)	1 (<1)	1 (1)
	1.0:1.0:1.0	95 (91)	3 (1)	5 (2)
3a•Li^{13}CN+1a+4a	1.0:0.0:1.0	95 (81)	1 (--)	2 (--)
	1.0:1.0:1.0	97 (99)	3 (--)	4 (--)

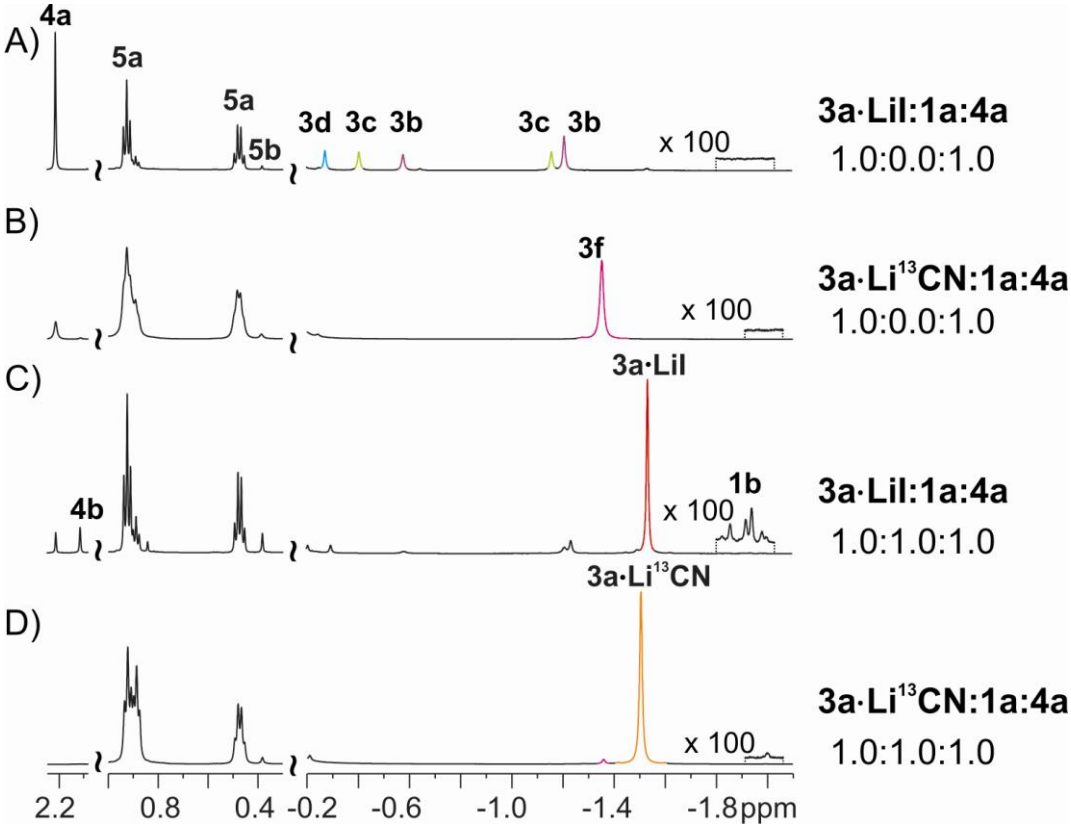

Figure 7: ^{1}H spectra recorded from reactions of 0.05-0.06 mol/L **3a•LiX** (X = I, ^{13}CN) with one equivalent **4a** (A, B) without and (C, D) with excess of **1a** at 170 K in Et_2O illustrate the reaction to **5a** and the side-reaction via **1b** and **4b** to **5b**.

In Figure 7 sections of the representative ^{1}H-spectra of these reactions (0.05-0.06 mol/L) are presented, the respective yields are summarized in Table 2. After the stoichiometric reactions of **3a•LiI** with **4a** indeed substantial amounts of the copper rich complexes **3b-d** are detected (see Figure 7A). After the stoichiometric reactions with **3a•Li^{13}CN** only the heteroleptic cuprate **3f** is observed (see Figure 7B) as expected from the structural investigations. The integrals of the main product 2,2-dimethyl-2-silabutane **5a** (see Scheme 4 course A) show a significantly higher yield for the cyanocuprate **3a•Li^{13}CN** (95 %) than for the reaction with the iodocuprate **3a•LiI** (57.0 %). Besides **5a** only small amounts of the side

product 2,2,5,5-tetramethyl-2,5-disilabutane **5b** were detected (2% for **3a•Li^{13}CN** and 1 % for **3a•LiI**). All other possible side products[65] were below the detection limit. In general **5b** can be generated on two pathways, first during the cuprate preparation and second by metal-halide exchange and subsequent substitution reaction (see Scheme 4 course B and B'). Therefore, the amount of **5b** before and after the reaction with **4a** is given in Table 2. Bertz and Oagle reported in their reactivity study of iodo- and cyanocuprates high amounts of the respective side product for the iodocuprates and low amounts for cyanocuprates formed during the cuprate preparation. Therefore they renormalized the reactivities of both cuprates to their effective concentrations.[65] In our case the concentrations of **5b** before the reaction are negligible for both cuprates (1% for **3a•Li^{13}CN** and 1 % **3a•LiI**), therefore a renormalization is not necessary and the yields can be directly correlated with the reactivity. Next the influence of the concentration, i.e. larger aggregates, was tested using the identical reactions at 0.13 mol/L. Again a significantly higher yield was observed for **3a•Li^{13}CN** (81 %) than for **3a•LiI** (31 %). As expected for substitution reactions, which are faster in THF than in diethyl ether, the absolute yields decreased for both cuprates at higher concentrations i.e. the formation of larger aggregates.

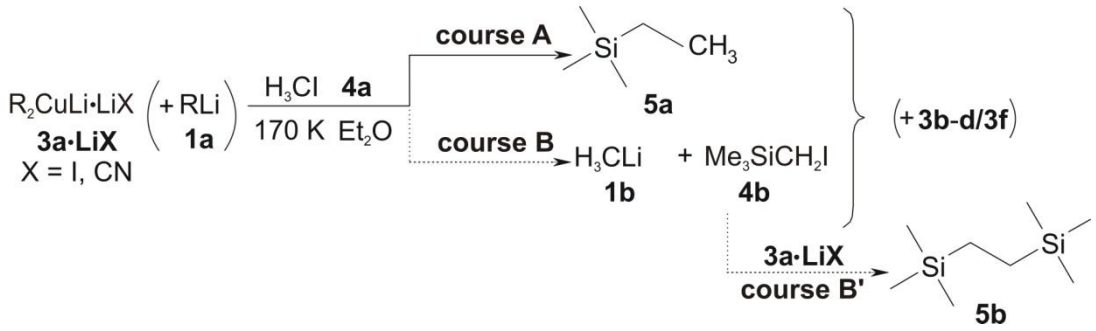

Scheme 4: Reactions of **3a•LiX** (R = Me_3SiCH_2) with **4a** with and without excess of **1a** at 170 K in Et_2O yield the product **5a** via course A and side product **5b** via course B and B'. With excess **1a** as subsequently formed Cu(I) complexes exclusively the homoleptic cuprates **3a•LiX** are detected. Without excess **1a** the changed stoichiometry leads to the formation of copper rich complexes **3b-d** or the heteroleptic cuprate **3f**.

These results raised the question whether the observed higher reactivity of **3a•Li^{13}CN** is an intrinsic effect of the cyano-Gilman cuprate despite its structural equivalence to **3a•LiI** or whether it is an effect of the reduced reactivity of the copper rich complexes **3b-d**, which only occur in the case of iodocuprates. In order to differentiate between these two possibilities additional experiments with one equivalent excess of **1a** were performed, which enable the regeneration of the Gilman cuprates during the reaction. Under these over-stoichiometric conditions the yield with **3a•LiI** increased dramatically up to 95 %, whereas in the case of **3a•Li^{13}CN** only a slightly increased yield of 97 % was observed. Also for the higher

concentrated samples a similarly pronounced trend was found (for spectra see SI Figure 7). There, the yield for **3a•LiI** increased by 60 % up to 91 % and in case of **3a•Li^{13}CN** also a pronounced effect with the highest yield at all (99 %) was detected. In order to exclude that these increased yields are only achieved by the direct reaction between **1a** and **4a**, a blind reaction (**1a**: 0.07 mol/L; **4a**:0.13 mol/L) at 162 K was investigated. This stoichiometric ratio, which yielded 17 % of **5a** was applied in order to assure that the effects of this blind reaction are not underestimated. This blind reaction yielded also the products of metal-halide exchange **1b** and **4b** (see SI Figure 8). In case of the iodocuprate **3a•LiI**, indeed also these products of metal-halide exchange **1b** and **4b** are detected (see Figure 7C), indicating that the blind reaction plays a role. However, with one equivalent of excess alkyl lithium reagent **1a** the increased yields of **5a** (by 38 and 60 %) are far beyond the yield of the blind reaction, which evidences the tremendous influence of the copper rich complexes **3b-d**. In case of the cyanocuprate **3a•Li^{13}CN**, no products of the metal-halide exchange are detected (see Figure 7D), suggesting that the blind reaction plays a minor role in this case. However, the increased yields of **5a** (by 2 % and 18 %) are in the range of the blind reaction (17 % **5a**), but the absolute yields are higher than for the iodocuprate. Nakamura postulated a MeLi-bridged species MeCu(CN)Li•MeLi as possible approach to explain the special reactivity of cyanocuprates.[63,64] The over-stoichiometric use of an alkyl lithium compound is expected to favor the formation of particularly such structures and it is striking that the over-stoichiometric use of **1a** in combination with **3a•Li^{13}CN** leads to the highest yields observed. Therefore, besides the tremendous influence of copper rich iodocomplexes, such alkyl lithium-bridged cyanocuprates definitely also could be an approach to explain the higher reactivity of cyanocuprates compared to iodocuprates.

3.4 Conclusions

In summary, reactions of (trimethylsilyl)methyl lithium **1a** and copper iodide **2a** in various ratios, revealed the formation of the organocuprate **3a•LiI** besides copper rich complexes **3b-e**, with the position of equilibrium being shifted to copper rich complexes with decreasing **1a**:**2a** ratio. With our NMR spectroscopic approach and established solution[51] and X-ray[68] structures of **3a•LiI**, the Cu(I) complexes **3b-d** were structurally characterized and organocuprate analogue structures were suggested for **3b** and **3c**, in which the dimeric core of the organocuprate **3a•LiI** is elongated by one and two RCu units, respectively. Furthermore, passing on from the organocuprate **3a•LiI** to the copper richer complexes **3b-e**, a decreased

polarization of the organic moieties was observed in the proton NMR spectra. In stoichiometric reactions of **3a•LiX** (X = I, ^{13}CN) with methyl iodide **4a**, a tremendous influence of copper rich complexes **3b-d** on the yields of the substitution reaction was evidenced. There, the reduced reactivity of iodocuprates compared to cyanocuprates was found to be mainly the result of such copper rich iodocomplexes, but also an effect of mixed species RCu(CN)Li•RLi, like Nakamura postulated them for cyanocuprates cannot be excluded.[63,64] Hence, from the synthetic point of view, an excess of organolithium compound is essential in conversions of iodocuprates with critical reactivity, i.e. sterically hindered cuprate or substrate. We believe that this is an alternative explanation of the controversy discussed special reactivity observed for cyanocuprates.[22–25] Formerly, this unusual reactivity had been explained by the formation of higher-order cuprates, which had been extensively discussed, but had been excluded as reactive species in organocuprate reactions.[26,32]

3.5 Experimental Section

3.5.1. Sample Preparation

The Me_3SiCH_2Li solution (1.0 M in pentane) was purchased from Aldrich. Et_2O-d_{10} was freshly distilled over K/Na alloy. All manipulations during the synthesis were done under exclusion of moisture and air. All cuprate samples were prepared by a method described by John *et al.*[46] The synthesis was directly done in Et_2O-d_{10} to exclude protonated Et_2O. The pentane from the Me_3SiCH_2Li solution was removed as good as possible before the addition to the Cu salt suspension. The conversions with methyl iodide were performed at 170 K. The NMR titrations were performed at 0.2-0.06 mol/L, DOSY measurement at 0.07-0.18 mol/L and reactions with MeI at 0.05-0.06 and 0.13 mol/L.

3.5.2. NMR Data Collecting and Processing

The NMR spectra were recorded on a Bruker Avance 600 spectrometer equipped with a 5 mm broadband triple resonance Z-gradient probe. ^{1}H,^{13}C HMBC measurements were carried out with a standard Bruker pulse program (hmbcetgpl2nd) using 64 scans, 16 dummy scans, TD(F2) = 4k and TD(F1) = 400 with a relaxation delay of 2 s. All diffusion measurements were performed with a convection-suppressing pulse program[79] in pseudo-2D mode and processed with Bruker software package t1/t2. For each experiment, 2 dummy scans and 8 actual scans were used, with a relaxation delay of 10 s and a diffusion delay of

50 ms. The shape of the gradients was sinusoidal, with a length of 4 ms, and the strength was varied in 24 increments (5-95 %) of the gradient ramp created by Bruker software DOSY. The temperature for all measurements was controlled by a Bruker BVTE 3900 temperature unit.

3.5.3. Determination of Diffusion Coefficients

The diffusion coefficients were determined using the Bruker software package t1/t2 to fit the measured decline of intensity. The diffusion coefficients given in Table and SI Table 3 are the average results of 1-6 experiments of each measurement with sample concentrations between 0.07 and 0.18 mol/L. Due to the concentration range, the experimental diffusion coefficient show higher experimental errors than usual for DOSY measurements: 9 % (**3a·LiI**, 3 experiments, 1x 0.07 mol/L, 2x 0.13 mol/L), 9 % (**3b**, 4 experiments, 2x 0.07 mol/L, 2x 0.13 mol/L), 11 % (**3c**, 4 experiments, 2x 0.07 mol/L, 2x 0.13 mol/L), 7 % (**3d**, 4 experiments, 2x 0.07 mol/L, 2x 0.13 mol/L), 5 % (**3a·Li^{13}CN**, 1 experiment, 0.18 mol/L), and 6 % (**3f**, 3 experiments, 3x 0.07 mol/L).

3.5.4. Internal Viscosity Reference

Since we noticed a strong dependence of the viscosity on the concentration, the temperature, and the kind of Cu(I) complexes, a trace (2-3 drops) of benzene (C_6H_6) was used as an internal reference.[80] By a comparison of the diffusion coefficients of the reference measured in pure DEE-d_{10} and in the cuprate sample, the viscosity correction factors for the Cu(I) complex samples were determined, in order to get comparable experimental diffusion coefficients.

3.5.5. Integral Analysis of the Reactions between 3a·LiX (X = I, ^{13}CN) and 4a

For the determination of yields (%), the sum of integrals of the CH_3 groups, which correspond to unreacted **4a**, the main product **5a** and the product of metal-halide exchange **1b** were correlated to the added amount of **4a** and set to 100 %. Accordingly, the integral of the side product **5b** was correlated to this sum and the yields of **5b** (%) were calculated.

3.6 References

(1) Krause, N. *Modern Organocopper Chemistry*; Wiley-VCH: Weinheim, 2002.

(2) Nakamura, E.; Mori, S. *Angew. Chem. Int. Ed.* **2000**, *39*, 3750-3771.

(3) Whitesides, G. M.; Fischer, W. F.; SanFilippo, J.; Bashe, R. W.; House, H. O. *J. Am. Chem. Soc.* **1969**, *91*, 4871-4882.

(4) House, H. O.; Respess, W. L.; Whitesides, G. M. *J. Org. Chem.* **1966**, *31*, 3128-3141.

(5) Guss, J. M.; Mason, R.; Thomas, K. M.; van Koten, G.; Noltes, J. G. *J. Organomet. Chem* **1972**, *40*, C79-C80.

(6) Gambarotta, S.; Floriani, C.; Chiesi-Villa, A.; Guastini, C. *J. C. S. Chem. Commun.* **1983**, 1156-1158.

(7) Meyer, E. M.; Gambarotta, S.; Floriani, C.; Chiesi-Villa, A.; Guastini, C. *Organometallics* **1989**, *8*, 1067-1079.

(8) Lappert, M. F.; Pearce, R. *J. C. S. Chem. Commun.* **1973**, 24-25.

(9) Olmstead, M. M.; Power, P. P. *J. Am. Chem. Soc.* **1990**, *112*, 8008-8014.

(10) Miyashita, A.; Yamamoto, A. *Bull. Chem. Soc. Jpn.* **1977**, *50*, 1102-1108.

(11) Camus, A.; Marsich, N. *J. Organomet. Chem.* **1970**, *21*, 249-258.

(12) Gilman, H.; Jones, R. G.; Woods, L. A. *J. Org. Chem* **1952**, *17*, 1630-1634.

(13) Lipshutz, B. H.; Sengupta, S. *Organic Reactions*; John Wiley & Sons, Inc, 2004.

(14) Krause, N. In *Metallorganische Chemie*; Spectrum Akademischer Verlag: Heidelberg, Germany, 1996.

(15) Lipshutz, B. H. In *Organometallics in Synthesis*; Schlosser, M., Ed.; Wiley: Chichester, U.K., 1994; pp. 283-382.

(16) Krause, N.; Gerold, A. *Angew. Chem. Int. Ed.* **1997**, *36*, 186-204.

(17) Olmstead, M. M.; Power, P. P. *Organometallics* **1990**, *9*, 1720-1722.

(18) John, M.; Auel, C.; Behrens, C.; Marsch, M.; Harms, K.; Bosold, F.; Gschwind, R. M.; Rajamohanan, P. R.; Boche, G. *Chem. Eur. J.* **2000**, *6*, 3060-3068.

(19) Eaborn, C.; Hitchcock, P. B.; Smith, J. D.; Sullivan, A. C. *J. Organomet. Chem.* **1984**, *263*, C23-C25.

(20) Hope, H.; Olmsted, M. M.; Power, P. P.; Sandell, J.; Xu, X. *J. Am. Chem. Soc.* **1985**, *107*, 4337-4338.

(21) Olmstead, M. M.; Power, P. P. *J. Am. Chem. Soc.* **1989**, *111*, 4135-3136.

(22) Lipshutz, B. H.; Wilhelm, R. S.; Floyd, D. M. *J. Am. Chem. Soc.* **1981**, *103*, 7672-7674.

(23) Lipshutz, B. H.; Kozlowski, J.; Wilhelm, R. S. *J. Am. Chem. Soc.* **1982**, *104*, 2305-2307.

(24) Lipshutz, B. H.; Wilhelm, R. S.; Kozlowski, J. *Tetrahedron Lett.* **1982**, *23*, 3755-3758.

(25) Lipshutz, B. H.; Wilhelm, R. S.; Kozlowski, J. A. *Tetrahedron* **1984**, *40*, 5005-5038.

(26) Krause, N. *Angew. Chem. Int. Ed.* **1999**, *38*, 79-81.

(27) Ashby, E. C.; Watkins, J. J. *J. Am. Chem. Soc.* **1977**, *99*, 5312-5317.

(28) Corey, E. J.; Posner, G. H. *J. Am. Chem. Soc.* **1968**, *90*, 5615-5616.

(29) Lipshutz, B. H.; Wilhelm, R. S. *J. Am. Chem. Soc.* **1982**, *104*, 4696-4698.

(30) Lipshutz, B. H.; Kozlowski, J. A.; Wilhelm, R. S. *J. Org. Chem.* **1983**, *48*, 546-550.

(31) Lipshutz, B. H.; Parker, D.; Kozlowski, J. A.; Miller, R. D. *J. Org. Chem.* **1983**, *48*, 3334-3336.

(32) E. C. Ashby, J. J. W. *Chem. Comm.* **1976**, 784-785.

(33) Bertz, S. H. *J. Am. Chem. Soc.* **1990**, *112*, 4031-4032.

(34) Lipshutz, B. H.; Sharma, S.; Ellsworth, E. L. *J. Am. Chem. Soc.* **1990**, *112*, 4032-4034.

(35) Bertz, S. H. *J. Am. Chem. Soc.* **1991**, *113*, 5470-5471.

(36) Mobley, T. A.; Müller, F.; Berger, S. *J. Am. Chem. Soc.* **1998**, *120*, 1333-1334.

(37) Lipshutz, B. H.; James, B. *J. Org. Chem.* **1994**, *59*, 7585-7587.

(38) Bertz, S. H.; Nilsson, K.; Davidsson, Ö.; Snyder, J. P. *Angew. Chem. Int. Ed.* **1998**, *37*, 314-317.

(39) Stemmler, T. L.; Penner-Hahn, J. E.; Knochel, P. *J. Am. Chem. Soc.* **1993**, *115*, 348-350.

(40) Stemmler, T. L.; Barnhart, T. M.; Penner-Hahn, J. E.; Tucker, C. E.; Knochel, P.; Böhme, M.; Frenking, G. *J. Am. Chem. Soc.* **1995**, *117*, 12489-12497.

(41) Snyder, J. P.; Spangler, D. P.; Behling, J. R.; Rossiter, B. E. *J. Org. Chem.* **1994**, *59*, 2665-2667.

(42) Snyder, J. P.; Bertz, S. H. *J. Org. Chem.* **1995**, *60*, 4312-4313.

(43) Bertz, S. H.; Miao, G.; Eriksson, M. *M. Chem. Commun.* **1996**, 815-816.

(44) Kronenburg, C. M. P.; Jastrzebski, J. T. B. H.; Spek, A. L.; van Koten, G. *J. Am. Chem. Soc.* **1998**, *120*, 9688-9689.

(45) Boche, G.; Bosold, F.; Marsch, M.; Harms, K. *Angew. Chem. Int. Ed.* **1998**, *37*, 1684-1686.

(46) Gschwind, R. M.; Rajamohanan, P. R.; John, M.; Boche, G. *Organometallics* **2000**, *19*, 2868-2873.

(47) Gschwind, R. M.; Xie, X.; Rajamohanan, P. R.; Auel, C.; Boche, G. *J. Am. Chem. Soc.* **2001**, *123*, 7299-7304.

(48) Bertz, S. H.; Miao, G.; Rossiter, B. E.; Snyder, J. P. *J. Am. Chem. Soc.* **1995**, *117*, 11023-11024.

(49) Bertz, S. H.; Chopra, A.; Eriksson, M.; Ogle, C. A.; Seagle, P. *Chem. Eur. J.* **1999**, *5*, 2680-2691.

(50) Ouannes, C.; Dressaire, G.; Langlois, Y. *Tetrahedron Lett.* **1977**, 815-818.

(51) Xie, X.; Auel, C.; Henze, W.; Gschwind, R. M. *J. Am. Chem. Soc.* **2003**, *125*, 1595-1601.

(52) Henze, W.; Vyater, A.; Krause, N.; Gschwind, R. M. *J. Am. Chem. Soc.* **2005**, *127*, 17335-17342.

(53) Nakamura, E.; Mori, S.; Morokuma, K. *J. Am. Chem. Soc.* **1997**, *119*, 4900-4910.

(54) Bertz, S. H.; Carlin, C. M.; Deadwyler, D. A.; Murphy, M. D.; Ogle, C. A.; Seagle, P. *J. Am. Chem. Soc.* **2002**, *124*, 13650-13651.

(55) Bertz, S. H.; Cope, S.; Dorton, D.; Murphy, M.; Ogle, C. A. *Angew. Chem. Int. Ed. Engl.* **2007**, *46*, 7082-7085.

(56) Bertz, S. H.; Cope, S.; Murphy, M.; Ogle, C.; Taylor, B. J. *J. Am. Chem. Soc.* **2007**, *129*, 7208-7209.

(57) Hu, H.; Snyder, J. P. *J. Am. Chem. Soc.* **2007**, *129*, 7210-7211.

(58) Gärtner, T.; Henze, W.; Gschwind, R. M. *J. Am. Chem. Soc.* **2007**, *129*, 11362-11363.

(59) Henze, W.; Gartner, T.; Gschwind, R. M. *J. Am. Chem. Soc.* **2008**, *130*, 13718-13726.

(60) Bartholomew, E. R.; Bertz, S. H.; Cope, S.; Dorton, D. C.; Murphy, M.; Ogle, C. A. *Chem. Commun.* **2008**, 1176-1177.

(61) Bertz, S. H.; Murphy, M. D.; Ogle, C. A.; Thomas, A. A. *Chem. Commun.* **2010**, *46*, 1255-1256.

(62) Gärtner, T.; Yoshikai, N.; Neumeier, M.; Nakamura, E.; Gschwind, R. M. *Chem. Commun.* **2010**, *46*, 4625-4626.

(63) Yoshikai, N.; Nakamura, E. *Chem. Rev.* **2012**, *112*, 2339-2372.

(64) Nakamura, E.; Yoshikai, N. *Bull. Chem. Soc. Jpn.* **2004**, *77*, 1-12.

(65) Bertz, S. H.; Human, J.; Ogle, C. A.; Seagle, P. *Org. Biomol. Chem.* **2005**, *3*, 392-394.

(66) Lipshutz, B. H.; Siegmann, K.; Garcia, E.; Kayser, F. *J. Am. Chem. Soc.* **1993**, *115*, 9276-9282.

(67) Pearson, R. G.; Gergory, C. D. *J. Am. Chem. Soc.* **1976**, *98*, 4098-4104.

(68) van Koten, G.; Noltes, J. G. *J. Organomet. Chem.* **1975**, *102*, 551-563.

(69) Krause, N.; Wagner, R.; Gerold, A. *J. Am. Chem. Soc.* **1994**, *116*, 381-382.

(70) Snyder, J. P. S.; Tipsword, G. E.; Splanger, D. J. *J. Am. Chem. Soc.* **1992**, *114*, 1507-1510.

(71) Yamanaka, M.; Inagaki, A.; Nakamura, E. *J. Comput. Chem.* **2003**, *24*, 1401-1409.

(72) Böhme, M.; Frenking, G.; Reetz, M. T. *Organometallics* **1994**, *13*, 4237-4245.

(73) Ben-Amotz, D.; Willis, K. G. *J. Phys. Chem.* **1993**, *97*, 7736-7742.

(74) Edward, J. T. *J. Chem. Edu.* **1970**, *47*, 261-270.

(75) Bloomfield, V. A. In *On-Line Biophysics Textbook*; Schuster, T. M., Ed.; 2000; Vol. Separation, pp. 1-5.

(76) McGarrity, J. F.; Prodolliet, J. *J. Org. Chem.* **1984**, *49*, 4465-4470.

(77) McGarrity, J. F.; Ogle, C. A.; Brich, Z.; Loosli, H. R. *J. Am. Chem. Soc.* **1985**, *107*, 1810-1815.

(78) Murphy, M. D.; Ogle, C. A.; Bertz, S. H. *Chem. Commun.* **2005**, 854-856.

(79) Jershow, A.; Mueller, N. *J. Magn. Reson.* **1997**, *125*, 372-375.

(80) Cabrita, E. J.; Berger, S. *Magn. Reson. Chem.* **2001**, *39*, 142-148.

3.7 Supporting Information

3.7.1. NMR Data for Starting Materials, Complexes and Products

alkyl lithium compounds	**1a**		**1b**
molecular formula	Me_3SiCH_2Li		MeLi
$\delta(^1H)$ [ppm]	–0.15	–2.2	–1.94
$\delta(^{13}C)$ [ppm]	4.9	4.7	–12.5
assignment	Me_3Si	CH_2	Me
color	**green**		---

Cu(I) complexes	**3a·LiI**		**3b**			**3c**		
molecular formula (R = Me_3SiCH_2)	$R_2CuLi{\cdot}LiI$		R_3Cu_2Li			R_4Cu_3Li		
$\delta(^1H)$ [ppm]	–0.07	–1.53	–0.08	–0.54	–1.19	–0.08	–0.36	–1.14
$\delta(^{13}C)$ [ppm]	4.2	–2.6	4.5	–7.0	–3.8	4.5	–6.8	–3.2
assignment	Me_3Si	CH_2	Me_3Si	CH_2	CH_2	Me_3Si	CH_2	CH_2
color	**red**		**purple**			**light green**		

Cu(I) complexes	**3d**		**3e**	**3a·Li^{13}CN**		**3f**		
molecular formula (R = Me_3SiCH_2)	RCu		R_2ICu_3	$R_2CuLi{\cdot}Li^{13}CN$		$RCuLi^{13}CN$		
$\delta(^1H)$ [ppm]	0.06	–0.24	0.09	–0.11	–1.50	–0.15	–1.37	
$\delta(^{13}C)$ [ppm]	4.2	–3.3	4.5	4.8	–2.8	4.4	–5.2	152.1
assignment	Me_3Si	CH_2	Me_3Si /CH_2	Me_3Si	CH_2	Me_3Si	CH_2	^{13}CN
color	**blue**		**black**	**orange**		**magenta**		

alkyl halides	**4a**	**4b**	
molecular formula	MeI	Me_3SiCH_2I	
$\delta(^1H)$ [ppm]	2.18	2.10	0.14
$\delta(^{13}C)$ [ppm]	–23.2	–13.1	–2.3
assignment	CH_3	CH_2	Me_3Si

products	**5a**			**5b**	
molecular formula	$Me_3SiCH_2CH_3$			$Me_3SiCH_2CH_2SiMe_3$	
$\delta(^1H)$ [ppm]	0.93	0.48	–0.02	0.39	–0.02
$\delta(^{13}C)$ [ppm]	7.2	8.4	–2.7	8.8	–2.5
assignment	CH_3	CH_2	Me_3Si	CH_2	Me_3Si

3.7.2. Appropriate Temperature for NMR Investigations on Complexes 3a-f

In order to find the appropriate temperature for the NMR investigations on the copper rich complexes, a temperature screening was performed. Therefore, exemplarily a 1.7:1 mixture of **1a** and **2a** in Et_2O was investigated by proton NMR spectroscopy at variable temperatures. Starting from 170 K, the sample was heated stepwise to 300 K, measuring a spectrum every 10 K. In order to check for reversibility of the process, the sample was cooled down again.

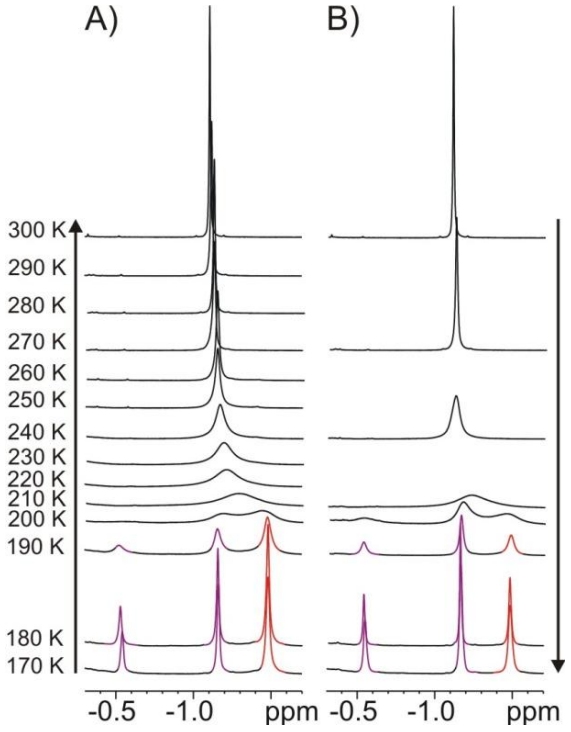

SI Figure 1: Cu(I) sections of the temperature dependent ^1H spectra showing the CH_2 signals of **3a•Li** (red) and **3b** (purple). The measurements were performed on a 1.7:1 mixture of **1a** and **2a** in Et_2O from (A) 170 K to 300 K and (B) in reversed order to test for reversibility of the chemical exchange. The arrows aside indicate the order in which the spectra were recorded.

The signals of **3a•LiI** and **3b** are clearly resolved at 170 K, visibly start to broaden at 190 K and finally collapse into one signal by further heating the sample. Upon cooling down, the signals split up again. This reversibility indicates a chemical exchange that can be slowed down at low temperatures. Therefore, throughout our studies all NMR investigations were performed at 170 or 185 K.

3.7.3. Signal Assignment for the Complexes 3a•LiI-3e

By adding different amounts of **1a** to an ethereal suspension of **2a** at 170 K, the formation of the respective soluble Cu(I) complexes started immediately. This could be followed in the corresponding ^1H spectra (see Figure 4) and was visible due to a specific color change. Upon

addition of 3.0 equivalents of **1a**, the white powder **2a** dissolved completely to give a clear colorless solution. Simultaneously, in the ^{1}H spectrum two signals appeared at –1.53 ppm (red in Figure 4) and –2.23 ppm (green in Figure 4), showing an integral ratio of 2.0:1.0. Moreover, both signals shared a cross peak in the ^{1}H,^{13}C HMBC spectrum to proton signals at –0.07 and –0.15 ppm, respectively (see SI Figure 5) The complete dissolution of **2a** indicated its full conversion to the well characterized colorless homoleptic organocuprate $(Me_3SiCH_2)_2CuLi$ **3a•LiI** with a known chemical shift of –1.57 ppm for the CH_2 groups in diethyl ether.[1] The formula of **3a•LiI** (R_2CuLi) displays the incorporation of two molecules of **1a** (R) per **2a** (Cu). In other words, the conversion of **2a** with **1a**, left 1.0 equivalent of the latter unconsumed, which gave the signal at –2.23 ppm with its corresponding Me_3Si signal at –0.15 ppm. Besides that, the ^{1}H NMR spectrum reflected the expected 1:1 ratio of **3a•LiI** to **1a**. Accordingly, the addition of 2.0 equivalents of **1a** to **2a** gave exclusively **3a•LiI**. By reducing the amount of **1a** further with respect to **2a** to 1.8:1, the clear solution adopted a pale brown somewhat metallic looking color. The proton NMR spectrum of this mixture revealed a new set of signals downfield from the CH_2 chemical shifts of **3a•LiI**. The former were observed at –0.54 and –1.19 ppm (purple in Figure 4) with a 1:2 ratio and a mutual cross signal in the ^{1}H,^{13}C HMBC spectrum (see Figure 4). From the integrals of the proton signals we calculated that 75 % of **1a** was consumed by the reaction to **3a**, leaving 31 % of **2a** unconsumed. With this, the ratio of **1a**:**2a** in the new compound **3b** is 3:2, which leads to the molecular formula R_3Cu_2Li ($R = Me_3SiCH_2$) (for details see SI Table 1). Furthermore, the 1:2 ratio of the proton NMR signals indicated structural equivalence of two out of three CH_2 groups. These interpretations agree with the observations of Ashby *et al.*, who reported a similar Cu(I) compound in the reaction of MeLi and CuI in ratios < 2:1 with comparable chemical shifts (–0.22 and –1.17 ppm).[2] For this analogue, likewise, two different CH_3 proton NMR signals downfield from Me_2CuLi (–1.38 ppm) with an integral ratio of 1:2 were observed. The continued decrease of **1a** with respect to **2a** to a 1.6:1 mixture resulted in a clear, yellow solution. This time, the main component was **3b** and the minor one was **3a•LiI**. This was in agreement with the expectation that a decreased amount of **1a** shifts the equilibrium towards Cu(I) complexes with less than 2 units of **1a** per **2a**. Besides, two further sets of signals appeared downfield from the CH_2 groups of **3b**. One set of signals were observed with a 1:1 ratio at $\delta = -0.34$ as well as –1.14 ppm (light green in Figure 4) and the other signal was detected at $\delta = -0.24$ ppm (blue in Figure 4). For the pair of signals at –0.34 and –1.14 ppm, the ^{1}H,^{13}C HMBC spectrum revealed a cross signal (see SI Figure 2) and

from the integral analysis, we calculated a ratio of 1.33:1, which led to the molecular formula R_4Cu_3Li ($R = Me_3SiCH_2$) **3c**. The intensity analysis of the signal at –0.24 ppm indicated a complex with the molecular formula RCu ($R = Me_3SiCH_2$) **3d**, for which the solid state structure consists of tetramers leading to a quite good solubility of the otherwise insoluble alkyl copper compounds (see Figure 1).[3] Upon mixing 1.4 equivalents of **1a** with **2a** the proton signals of **3a•LiI** vanished completely. The reduction of **1a** to 1.4 equivalents with respect to **2a** shifted the equilibrium further towards the copper richer complexes. The signals of **3c** and **3d** grew as the signals of **3b** diminished. Accordingly, by the addition of one equivalent of **1a** to **2a**, exclusively complex **3d** was formed. Below a 1:1 ratio of **1a**:**2a**, the solution was still clear and yellow, but **2a** partly remained at the bottom of the NMR tube. Aside from **3d**, another complex was detected at $\delta = 0.09$ ppm (black in Figure 4). In this complex, the CH_2 signal was shifted as far downfield as the Me_3Si moiety, resulting in one big signal for all protons. This was considered in the intensity analysis by assigning 22 protons to the integral, instead of two. The signal at $\delta = 0.00$ ppm was assigned to tetramethylsilane (TMS), which can be formed from **1a** with traces of moisture, stemming from imperfections in the sample preparation. As **2a** was not dissolved completely, the Cu content of the last complex could not be calculated from the integral analysis. Despite, with the equilibrium being shifted towards this complex at **1a**:**2a** stoichiometry lower than 1:1, it is probable that the R:Cu ratio ($R = Me_3SiCH_2$) is less than one. Therefore, according to the literature, we assigned the signal to a Cu(I) complex with the molecular formula R_2Cu_3I ($R = Me_3SiCH_2$) **3e**. Such a complex composition, earlier, had been reported by van Koten *et al.* in the X-ray analysis of $[R_2Cu_3I]_2$ (R = 2-(dimethyl-amino)phenyl).[4] In summary, the chemical equations for the formation of complexes **3a**-**e** were derived (see SI Scheme 1).

$$CuI + 2\,RLi \longrightarrow R_2CuLi + LiI$$

$$2\,CuI + 3\,RLi \longrightarrow R_3Cu_2Li + 2\,LiI$$

$$3\,CuI + 4\,RLi \longrightarrow R_4Cu_3Li + 3\,LiI$$

$$CuI + RLi \longrightarrow RCu + LiI$$

$$3\,CuI + 2\,RLi \longrightarrow R_2Cu_3I + 2LiI$$

SI Scheme 1: Formation of Cu(I) complexes in Et_2O solution depending on the stoichiometry of copper iodide **1a** and alkyl lithium compound **2a**.

3.7.4. Integral Analysis of the ^{1}H NMR Data of Complexes 3a•LiI-3e

Samples of Me_3SiCH_2Li **1a** and CuI **2a** were prepared in seven different stoichiometries. ^{1}H NMR spectra were recorded at 170 K in diethyl ether. The resulting CH_2 signals were then divided into different groups, each referring to one Cu(I) complex **3a•LiI-3e**. The sum of integrals of the latter was set to 100 % and related to the employed concentration **1a**. The amount of **1a** consumed by the reaction to the respective complexes was then calculated. The employed amount of **2a** was then distributed over the individual complexes. With this, a **1a**:**2a** ratio was calculated for each complex in order to derive molecular formulas for the complexes **3a•LiI-3e**. In addition, the percentage of each complex in the individual samples was calculated.

SI Table 1: Intensity analysis of the ^{1}H NMR spectra (see Figure 5). The contents of **1a** and **2a** in the different Cu(I) complexes **3a•LiI-3e** as well as the complex compositions were calculated from the integrals with respect to the used Me_3SiCH_2Li:CuI **1a**:**2a** ratio.

1a:**2a**	**complex**	**1a**	**3a•LiI**	**3b**	**3c**	**3d**	**3e**	check Σ
	δ(^{1}H) [ppm]	–2.23	–1.53	–0.54	–0.36	–0.24	0.09	
	$(CH_3)_3SiCH_2$:Cu	0.00	2.00	1.50	1.33	1.00	0.67	
3.0:1	integral	1.9647	4.0000					
	1a in complex [%]	32.9	67.1					100.0
	2a in complex [%]	0.0	100.6					100.6
	complex [%]	49.6	50.4					100.0
2.0:1	integral		4.0000					
	1a in complex [%]		100.0					100.0
	2a in complex [%]		100.0					100.0
	complex [%]		100.0					100.0
1.8:1	integral		4.0000	1.3219				
	1a in complex [%]		75.2	24.8				100.0
	2a in complex [%]		69.4	30.6				100.0
	complex [%]		81.9	18.1				100.0
1.6:1	integral		1.5797	5.9963	1.1159	0.3287		
	1a in complex [%]		17.5	66.5	12.4	3.6		100.0
	2a in complex [%]		13.6	68.9	14.4	5.7		102.7
	complex [%]		21.5	54.4	15.2	8.9		100.0
1.4:1	integral		0.4573	6.0906	4.2066	2.0992		
	1a in complex [%]		3.6	47.7	32.7	16.3		100.0
	2a in complex [%]		2.4	42.8	33.2	22.1		100.5
	complex [%]		3.5	31.4	32.6	32.5		100.0
1.0:1	integral					2.0000		
	1a in complex [%]					100.0		100.0
	2a in complex [%]					101.5		101.5
	complex [%]					100.0		100.0
0.6:1	integral					0.4912	22.0000	
	1a in complex [%]					2.2	97.8	100
	2a in complex [%]					1.2	81.5	82.7
	complex [%]					19.7	80.3	100.0

3.7.5. Elucidation of the Monomeric Structure 3c

Accordingly to the structure elucidation of the monomer **3b** structure **3c** was investigated. Therefore, for **3c**, based on the common binding feature of linear copper coordination for all Cu(I) complexes (see Figures 1-3) and our proton NMR investigations, which showed two chemically non-equivalent CH_2 groups in a 1:1 ratio, two possible monomeric structures are conceivable (see SI Figure 2A). Structure **3c i** can be considered as the simple adduct of an organocuprate with two alkyl copper units bridged by a lithium ion and one equivalent of lithium iodide, hence no cross signal between the chemically non-equivalent CH_2 groups is expected. In contrast, in **3c ii** all organic moieties are bridged by Cu atoms, which, enables magnetization transfers between the chemically non-equivalent CH_2 groups. Such a cross signal was observed in the $^{1}H,^{13}C$ HMBC spectrum (see SI Figure 2C), which excludes **3c i** and favors **3c ii**.

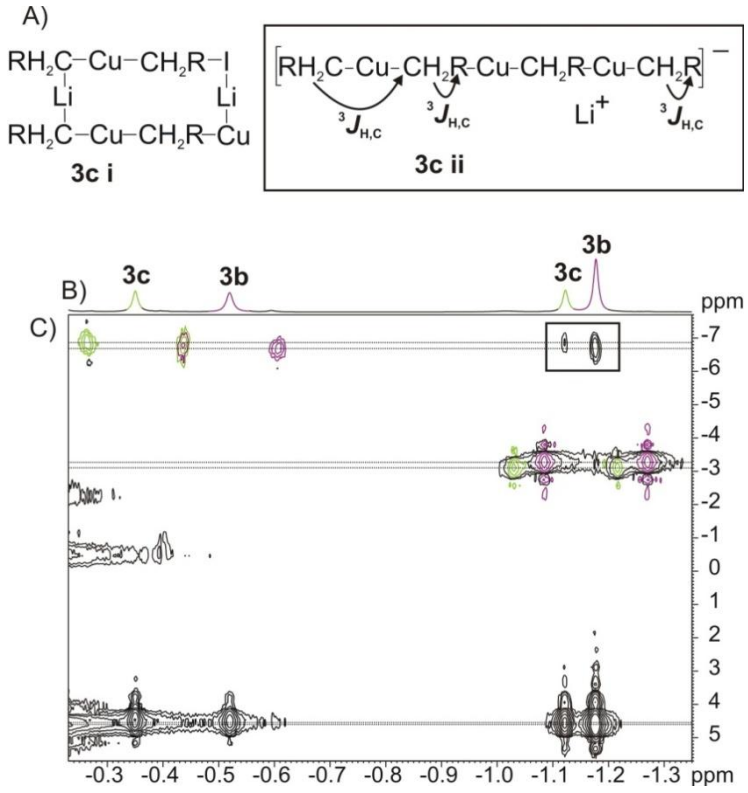

SI Figure 2: Identification of the monomeric structure of **3c** as **3c ii**: (A) Possible structures **3c i** and **3c ii** (R = Me_3Si) on the basis of (B) ^{1}H NMR spectrum. (C) High-field section of the $^{1}H,^{13}C$ HMBC spectrum at 185 K in Et_2O. The signals of the Cu(I) complexes **3b** and **3c** are depicted in purple and light green, respectively. The decisive cross signal, which allows for the unambiguous identification of **3c** as **3c ii** is indicated by a black square. The observed couplings are indicated by arrows in structure **3c ii**.

3.7.6. Calculation of Theoretical Diffusion Coefficients

The theoretical diffusion coefficients were calculated from hard-sphere increments[5] and the Stokes-Einstein theory[6] modified by a shape factor,[7] when indicated by an asterisk in Table 1 and SI Table 3. The original Stokes-Einstein theory[6] is valid only for molecules of spherical form. Therefore, for non-spherical molecules such as oligomeric and polymeric chains presented in this study the Stokes-Einstein theory[6] has to be modified by a shape factor.[7] The applied methodology had been already used in previous investigations of the solid state structures of organocuprates in Et_2O and will be explained briefly in the following.[1] Generally, the diffusion coefficient is given by the Stokes-Einstein equation: [6]

$$D = \frac{kT}{F \cdot 6\pi\eta r_H} \tag{1}$$

D is the diffusion coefficient, k is the Boltzmann constant, T is the absolute temperature, η the viscosity of the sample solution and F is the shape factor. For a cylindrical shape F can be described as:[7]

$$F = \frac{[2p^2/3]^{1/3}}{\ln p + 0.312 + 0.565/p + 0.1/p^2} \tag{2}$$

p is defined as $p = L/(2r)$, with L and r as the length and radius of the cylinder, respectively. In our structure elucidation of oligomeric chains (see Table 1 and SI Table 3), we can assume: $r = r_c$ and $L = n \cdot (2r_c)$, where r_c is the radius of the core unit (which is assumed to be spherical) and n equals the number of the core units in the oligomeric chain. Thus, $p = n$ and eq. (2) can be re-written as:

$$F = \frac{[2n^2/3]^{1/3}}{\ln n + 0.312 + 0.565/n + 0.1/n^2} \tag{3}$$

The length index n is simultaneously defined as $n = (r_H/r_c)^3$.[8] With a combination of Eqs. (1) and (3) the unknown parameter n can be iteratively determined. The final length indices n, which were calculated for the different Cu(I) complexes in Et_2O, including such a shape factor, are marked by an asterisk in Table 1 and SI Table 3.

3.7.7. Signal Assignment for the Complexes 3a·Li^{13}CN and 3f

The proton spectra of the seven samples (**1a**:**2b** = 3.0:1to **1a**:**2b** = 0.3:1) were recorded at 170 K in diethyl ether. The spectra (see SI Figure 3) show two signals in the CH_2 section at

δ = –1.50 and –1.37 ppm and accompanying signals at δ = –0.11 and –0.15 ppm, pair wise sharing cross peaks in the $^{1}H,^{13}C$ HMBC (see SI Figure 3). Furthermore, the signal at δ = –1.37 ppm shows a cross signal to $\delta(^{13}C)$ = 152.1 ppm in the $^{1}H,^{13}C$ HMBC.

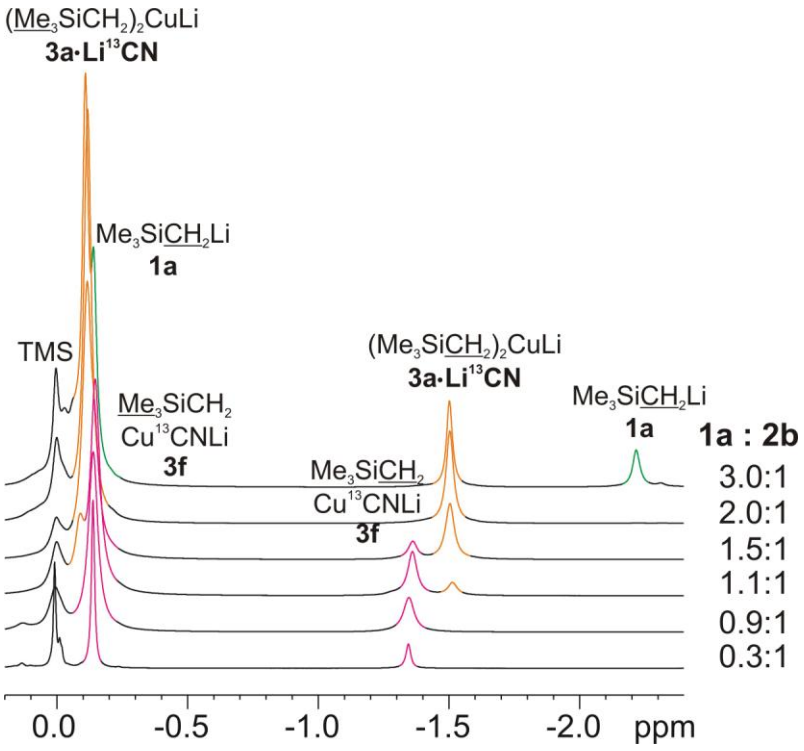

SI Figure 3: Cu(I)-sections of the ^{1}H spectra of Me_3SiCH_2Li **1a** (green), the homoleptic (**3a•Li^{13}CN**, orange) and heteroleptic (**3f**, magenta) cyanocuprate in diethyl ether at 170 K with accompanying ratios of **1a** to $Cu^{13}CN$ **2b**.

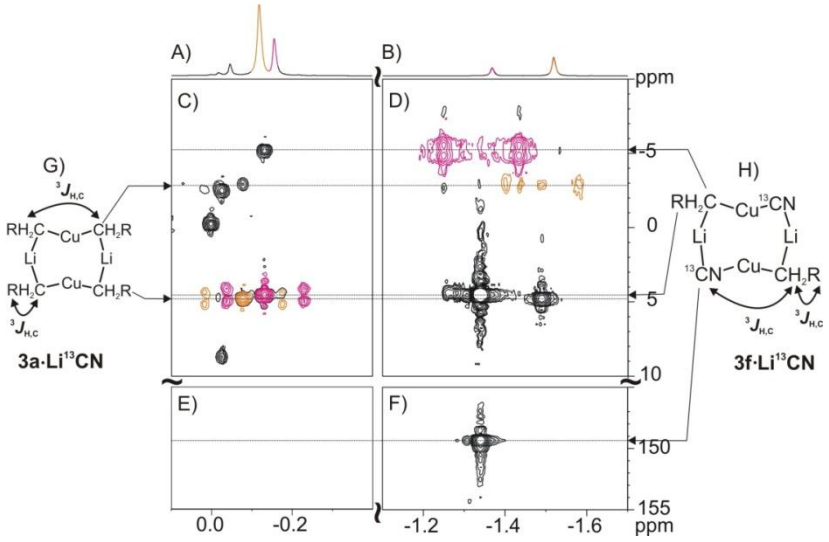

SI Figure 4: (A, B) High-field sections of a 1D ^{1}H spectrum and sections of the $^{1}H,^{13}C$ HMBC spectrum of (C) the Me_3Si region (scaled down for better resolution), (D) the corresponding CH_2 region and accordingly, (E,F) the ^{13}CN regions at 185 K in diethyl ether. Besides, (G) the dimeric core structures of **3a•Li^{13}CN** and (H) **3f•Li^{13}CN** with the observed $^{3}J_{H,C}$ couplings (indicated by double arrows) are given for better visualization of the coupling pattern. The signals of **3a•Li^{13}CN** and **3f•Li^{13}CN** are depicted in orange and magenta, respectively.

According to previous investigations, the signals at $\delta = -1.50$ and -0.11 ppm were assigned to the homoleptic cyanocuprate $R_2CuLi{\cdot}Li^{13}CN$ (R = Me_3SiCH_2) **3a•Li^{13}CN** and the signals at $\delta = -1.37$ and -0.15 ppm to the heteroleptic cyanocuprate $RCu^{13}CNLi$ (R = Me_3SiCH_2) **3f**.[1] The integral analysis is given in SI Table 2 and fits this assignment very well.

SI Table 2: Intensity analysis of the ^{1}H NMR spectra (see SI Figure 3). The contents of **1a** and **2b** in the different Cu(I) complexes **3a•Li^{13}CN** and **3f** as well as the complex compositions were calculated from the integrals with respect to the used Me_3SiCH_2Li:CuI **1a**:**2a** ratio.

1a:**2b**	**complex**	**1a**	**3a•Li^{13}CN**	**3f**	check Σ
	$\delta(^1H)$ [ppm]	–2.23	–1.50	–1.37	
	Me_3SiCH_2:Cu	0.00	2.00	1.00	
3.0:1	integral	1.9758	4.0000		
	1a in complex [%]	33.1	66.9		100.0
	2a in complex [%]	0.0	105.2		105.2
	complex [%]	49.7	50.3		100.0
2.0:1	integral		4.0000		
	1a in complex [%]		100.0		100.0
	2a in complex [%]		100.0		100.0
	complex [%]		100.0		100.0
1.5:1	integral		4.0000	1.4053	
	1a in complex [%]		74.0	26.0	100.0
	2a in complex [%]		57.0	40.0	97.0
	complex [%]		58.7	41.3	100.0
1.1:1	integral		0.6136	2.0000	
	1a in complex [%]		23.5	76.5	100.0
	2a in complex [%]		13.4	87.5	100.9
	complex [%]		13.3	86.7	100.0
0.9:1	integral			2.0000	
	1a in complex [%]			100.0	100.0
	2a in complex [%]			85.7	85.7
	complex [%]			100.0	100.0
0.3:1	integral			2.0000	
	1a in complex [%]			100.0	100.0
	2a in complex [%]			28.6	28.0
	complex [%]			100.0	100.0

3.7.8. Structure Elucidation of 3a•Li^{13}CN and 3f

For the DOSY analysis, for **3a•Li^{13}CN** a model dimer analogue to **3a•LiI** with two $Li^{13}CN$ and six Et_2O units was used. In contrast, for **3f** the known crystal structure $\{[t\text{BuCu(CN)Li}]_2(Et_2O)_4]\}_\infty$, in which dimeric building blocks are elongated to chains,[9] was used as model structure. For the monomers and dimers of **3a•Li^{13}CN** and **3f**, the model free approach was used. Additionally, for higher aggregates of **3a•Li^{13}CN** and **3f** shape factors for

cylindrical geometry were included (vide supra).[7] In SI Table 3 the experimental and calculated diffusion coefficients for **3a•Li^{13}CN** and **3f** are listed.

SI Table 1: Experimental diffusion coefficients (D_{exp}) compared to calculated diffusion coefficients (D_{calc}) for monomers, dimers and higher aggregates of 0.07 mol/L-0.18 mol/L **3a•Li^{13}CN** and **3f** (R = Me_3SiCH_2) obtained by a model free approach including hard-sphere increments[5] and the Stokes-Einstein theory.[6]

compound		D_{exp} [10^{-8} m^2s^{-1}]	D_{calc} [10^{-8} m^2s^{-1}]
3a	$[R_2CuLi]$		9.7
	$[R_2CuLi]_2$		7.7
	$[R_2CuLi]_2$•$2Li^{13}CN$•$6Et_2O$		5.9
	$\{[R_2CuLi]_2$•$2Li^{13}CN$•$6Et_2O\}_{1.5}$	5.1±0.3	5.1*
3f	[RCuCNLi]		11.6
	$[RCuCNLi]_2$		9.2
	$[RCuCNLi]_2$•$4Et_2O$		7.2
	$\{[RCuCNLi]_2$•$4Et_2O\}_{1.2}$	6.8±0.4	6.8*

*) A shape factor for cylindrical geometry was included.[7]

Like already observed in the case of the iododcopper(I) complexes, for **3a•Li^{13}CN** and **3f** the comparison of the experimental and the calculated diffusion coefficients exclude simple monomers and dimers as well. For **3a•Li^{13}CN** and **3f** the experimental diffusion coefficients indicate higher aggregates than dimers.

3.7.9. Additional NMR Spectra

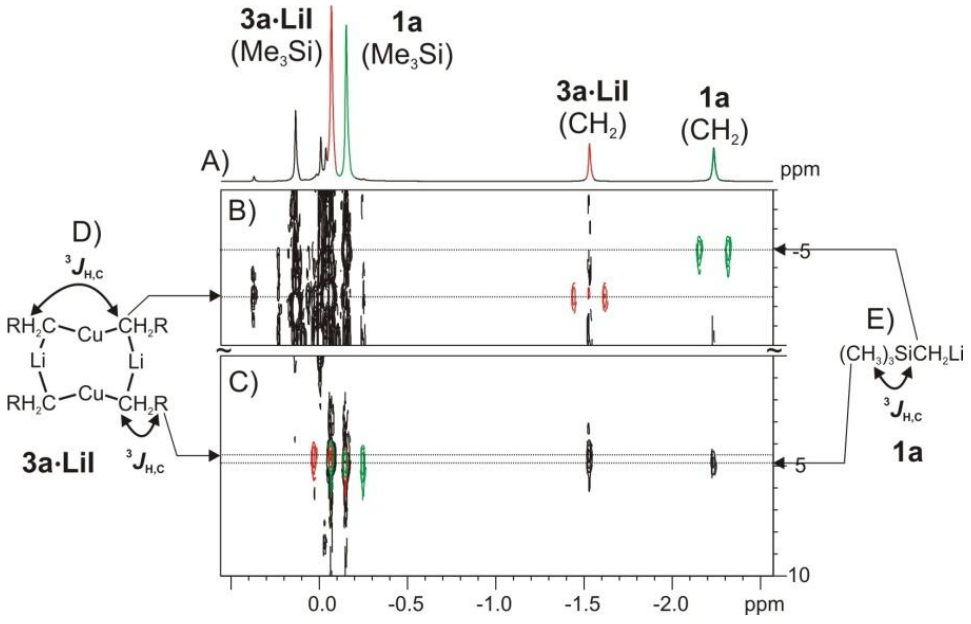

SI Figure 5: High-field sections of (A) a 1D ^1H spectrum, (B) sections of the $^1H,^{13}C$ HMBC spectrum of the CH_2 region and (C) the corresponding Me_3Si region (scaled down for better resolution) at 185 K in diethyl ether. Besides, (D) the dimeric core structure of **3a•LiI** with the observed $^3J_{H,C}$ couplings (indicated by double arrows) and (E) the formula of **1a** is given for better visualization of the coupling pattern. The signals of **1a** and **3a•LiI** are depicted in green and red, respectively (R = Me_3Si).

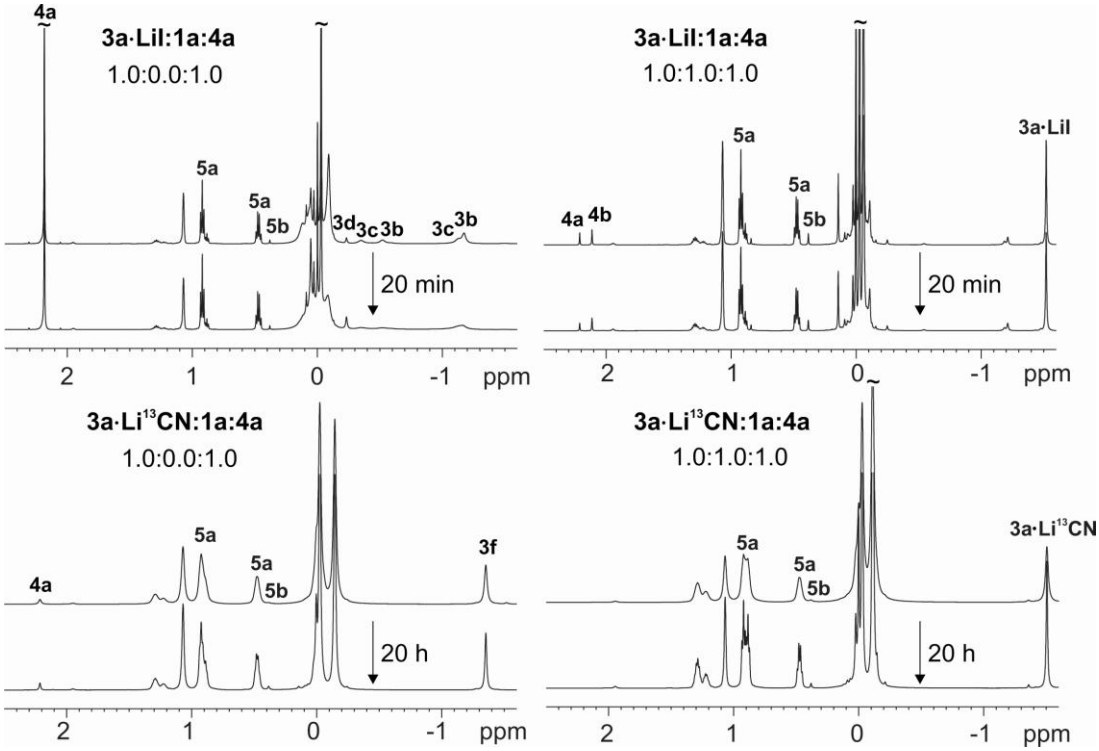

SI Figure 6: ^{1}H spectra recorded of reactions of **3a•LiX** (X = I, ^{13}CN) with one equivalent **4a** without and with excess of **1a** at 170 K in Et_2O show the reaction to **5a** and the side-reaction via **4b** to **5b**. The spectra after 20 minutes and after a certain time delay (indicated by arrow) illustrate the completeness of the reactions already after 20 minutes.

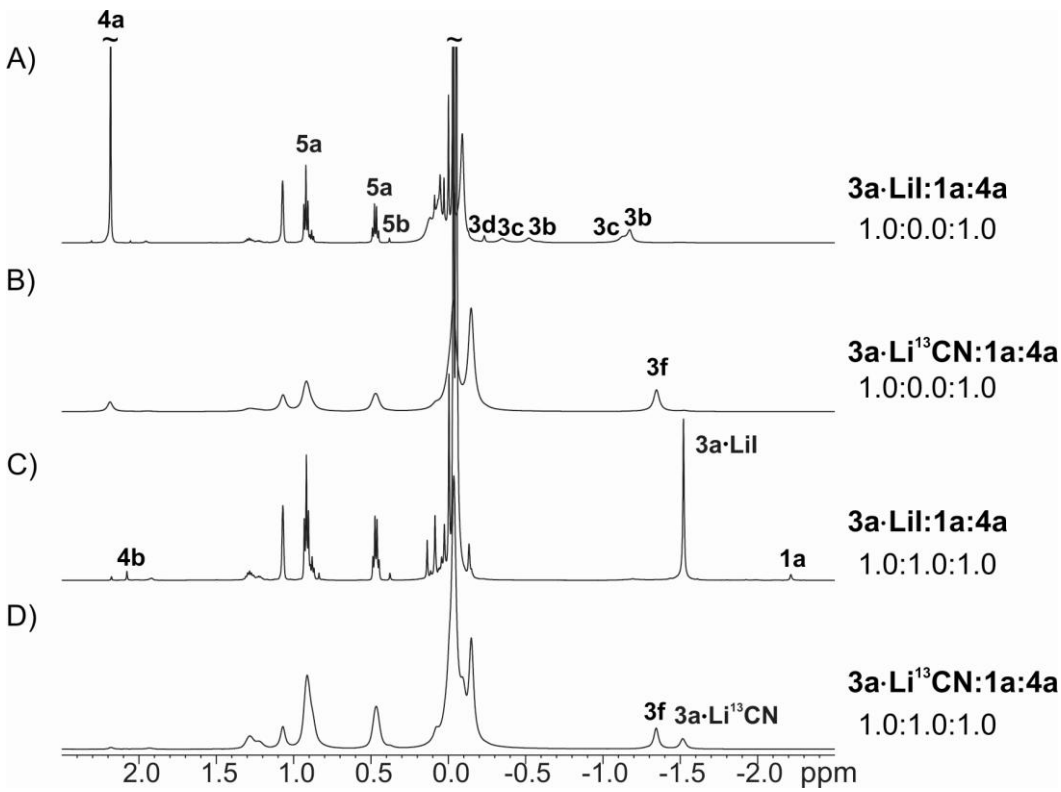

SI Figure 7: ^{1}H spectra recorded from reactions of 0.13 mol/L **3a•LiX** (X = I, ^{13}CN) with one equivalent **4a** (A, B) without and (C, D) with excess of **1a** at 170 K in Et_2O illustrate the reaction to **5a** and the side-reaction via **1b** and **4b** to **5b**.

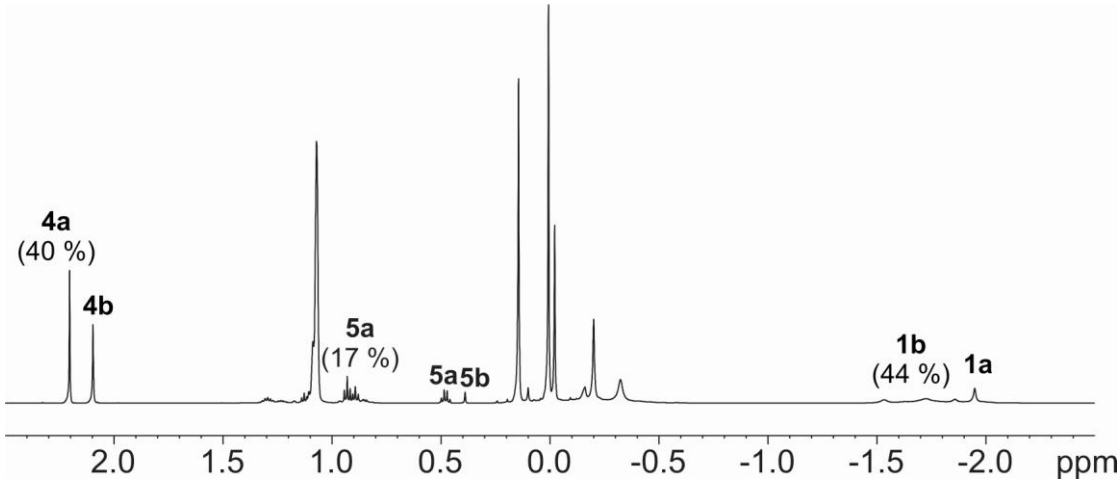

SI Figure 8: ^{1}H spectrum of the blind reaction of the alkyl lithium reagent **1a** (0.13 mmol/L) with methyl iodide **4a** (0.7 mmol/L) at 162 K in Et_2O yields 17 % of the product **5a**, 44 % MeLi **1b** as a result of the metal-halide exchange and 40 % of **4a** remain unreacted in solution.

3.7.10. References

(1) Xie, X.; Auel, C.; Henze, W.; Gschwind, R. M. *J. Am. Chem. Soc.* **2003**, *125*, 1595-1601.

(2) E. C. Ashby, J. J. W. *Chem. Comm.* **1976**, 784-785.

(3) Lappert, M. F.; Pearce, R. *J. C. S. Chem. Commun.* **1973**, 24-25.

(4) van Koten, G.; Noltes, J. G. *J. Organomet. Chem.* **1975**, *102*, 551-563.

(5) Ben-Amotz, D.; Willis, K. G. *J. Phys. Chem.* **1993**, *97*, 7736-7742.

(6) Edward, J. T. *J. Chem. Edu.* **1970**, *47*, 261-270.

(7) Bloomfield, V. A. In *On-Line Biophysics Textbook*; Schuster, T. M., Ed.; 2000; Vol. Separation, pp. 1-5.

(8) Jiang, Q.; Rüegger, H.; Venanzi, L. M. *Inorg. Chim. Acta* **1999**, *290*, 64-79.

(9) Boche, G.; Bosold, F.; Marsch, M.; Harms, K. *Angew. Chem. Int. Ed.* **1998**, *37*, 1684-1686.

4. The Elusive Highly Charged Zintl Anions: NMR Detection of Si_4^{4-} and Sn_4^{4-} in Liquid Ammonia

For these studies, I performed the ^{119}Sn NMR spectroscopic investigations in solution and Carina Koch joined the ^{29}Si measurements in solution. The ^{29}Si MAS-NMR measurements were performed by Tobias Gärtner. The synthesis and the characterization of the solids as well as the sample preparation were carried out by Franziska Fendt and Stefanie Gärtner.

Maria Neumeier, Franziska Fendt, Stefanie Gärtner, Carina Koch, Tobias Gärtner, Nikolaus Korber, Ruth M. Gschwind

to be published

4.1 Abstract

The negatively charged Zintl ions of group 14 and 15 are element-element-bound clusters with a versatile and fascinating chemistry. Some representatives and their reaction products show very promising properties with regard to the application as cluster-assembled nanomaterials. However, an experimental approach for the targeted synthesis of such new materials has severely been hampered by the limited knowledge about dissolution processes of Zintl ions and stabilizing influences on these compounds in solution. Previously, the binary phases A_4E_4 (A = alkali metal, E = Si, Ge, Sn) had been assumed to be completely insoluble, but now the dissolution of Rb_4Sn_4 is described. Thus, due to the stabilizing influence of chelating [2.2.2]-cryptand, the first ^{119}Sn signal of Sn_4^{4-} in liquid ammonia was detected. In addition, this stabilizing effect was used in the solvation of $K_6Rb_6Si_{17}$, where it allowed for the first observation of a silicide (Si_4^{4-}) in solution at all. Furthermore, with the NMR spectroscopic detection of amide during the oxidation of the highly charged clusters E_4^{4-} (E = Sn, Si) to Sn_9^{4-} and SiH_3^-, respectively, we provide an experimental evidence for the long-standing assumption of solvent deprotonation during these oxidation processes.

4.2 Introduction

Anionic homoatomic discrete molecular building blocks of main group elements, namely Zintl anions, are very interesting and promising starting materials in terms of developing new hybrid materials of transition metals and main group elements.[1] The naked clusters themselves in solution also offer the possibility to find new elemental modifications by oxidative coupling or create potential semiconducting amorphous or crystalline films by anodic deposition like it was shown for germanium.[2,3] The underlying analytical characterization method for most of the reported materials is single crystal x-ray structure analysis which is most suitable to describe the nature of polyanions in solid state. In contrast, transformations of such anions taking place in solution suffer from a lack of knowledge. If one wants to understand these complicated solution and transition processes involving several reagents, the behavior of the naked polyanions in pure solutions need to be investigated at first. The target is a better understanding for this class of substances in solution to enable straightforward synthesis of transformation reactions. Solutions of group 15 polyanions were studied intensely by Baudler *et al.*,[4] in contrast, a systematic investigation of ligand-free group 14 polyanions in solution is still missing. Therefore, our studies were focused on the determination of such group 14 polyanions in solution by using NMR spectroscopy. In former

^{119}Sn NMR studies Rudolph *et al.* reported the detection of Sn_9^{4-}. They documented a further upfield shifted signal, which was tentatively assigned to Sn_4^{2-}. Moreover, Eichhorn *et al.* recently demonstrated the influence of [2.2.2]-cryptand on the Sn_9^{4-} species in solution. Their ^{119}Sn NMR studies showed that a stoichiometric excess of [2.2.2]-cryptand led to HSn_9^{3-} besides several different K^+ coordinated species $K_xSn_9^{(4-x)-}$ (x = 0−3).[5] More highly reduced clusters, like Sn_4^{4-} and Pb_4^{4-}, have, until now, only been proven to exist in solution by the circumstantial evidence of solvate crystal structures, which were obtained from direct reduction experiments in liquid ammonia.[6] For the lighter homologues, Si and Ge, the only known analogues solvate crystal structure is a functionalized tetrahedral silicide.[7] An alternative route to access these E_4^{4-} (E = element of group 14) clusters, would be the solvation of the precursor phases A_4E_4 (A = alkali metal), but they were supposed to be completely insoluble for the lighter congeners E = Si, Ge and Sn.[1] Further, there is no signal of a naked homoatomic polyanion of silicon in solution reported so far. The only ^{29}Si signal for a negatively charged silicon cluster in solution stems from the $R_3Si_4^-$ anion (R = $SiMeDis_2$; Dis = $CH(SiMe_3)_2$), studied in toluene by Sekiguchi *et al.*[8] However, starting from binary phases $A_{12}Si_{17}$ with one Si_9^{4-} and two Si_4^{4-} anions per formula unit, Sevov *et al.* were able to show that silicides may be dissolved in liquid ammonia to yield the oxidized polyanions Si_9^{3-}, Si_9^{2-} and Si_5^{2-} in cryptand-containing solvate compounds.[9,10] In previous recrystallization experiments of a solid starting material with the nominal composition $K_6Rb_6Si_{17}$ in liquid ammonia, we additionally were able to indirectly evidence the existence of unoxidized Si_9^{4-} in solution[11,12] and we also used this ternary material to form the complex ion $[\{Ni(CO)_2\}_2(\mu\text{-}Si_9)_2]^{8-}$.[13] Also, Fässler *et al.* succeeded in the synthesis of a functionalized silicide, $[(MesCu)_2(\eta^3\text{-}Si_4)]^{4-}$, which contains Si_4 tetrahedral bonded to copper, in liquid ammonia from a similar starting material.[7] Given these results, the question if and which silicide species may be detected in solution became urgent.

So, here we present the first NMR signal of a naked silicide in solution at all. To our knowledge, this is the most highfield shifted ^{29}Si signal of a Si atom in a molecular environment without the involvement of any transition metal complex. Therefore, the highfield border of the NMR scale of all measured ^{29}Si signals is extended from −274.2 ppm[14] to −323 ppm. Additionally, we provide the first experimental evidence that Rb_4Sn_4 is soluble in liquid ammonia and that Sn_4^{4-} can be stabilized in solution in the presence of [2.2.2]-cryptand. Aside from that, we could observe the oxidation of Sn_4^{4-} to Sn_9^{4-} in these solutions and, based on the detection of NH_2^-, unambiguously identify protons as the

oxidizing agent. This knowledge about solution processes of group 14 polyanions might provide the possibility of targeted synthesis of functionalized Zintl clusters and give an approach for rational material design.

4.3 Results and Discussion

To study highly charged Sn_4^{4-} and Si_4^{4-} cluster in solution we selected stannides as start system. For the detection of stannides a NMR approach is established, in which ^{119}Sn is observed and the ^{117}Sn satellite pattern is used for the assignment of the cluster sizes Sn_x (for details see SI).[5,15–17] Furthermore, stannides provide higher stability towards moisture and oxidation processes as well as better solubility than silicides. For the synthesis, we chose the direct reduction of elemental tin with elemental rubidium (1:1) in liquid ammonia, because this additive-free preparation method minimizes external influences on the properties and the preferred cluster sizes and allowed for the crystallization of the solvates $A_4Sn_4 \cdot 2NH_3$ (A = Rb, Cs) in previous studies.[6] With this setup a small ^{119}Sn signal at −1727 ppm with a coupling constant of 1466 Hz and a ^{117}Sn satellite pattern of 0.13:1.00:0.12 was observed (see Figure 1a), despite the fact that the solubility of pure Sn_4^{4-} in solution is expected to be very limited. In additive-free crystal structures exclusively Sn_9^{4-} and Sn_4^{4-} have been reported so far[1] and for A_4Sn_9 cluster (A = alkali metals) the chemical shift range as well as the scalar coupling constants in ethylenediamine (en) is well known (−1115−−1241 ppm; 256−293 Hz).[17] The upfield shift of the detected ^{119}Sn signal at −1727 ppm indicates a higher negative charge per Sn atom than Sn_9^{4-} and the large coupling constant of 1466 Hz hints at a smaller cluster size. Both parameters as well as the ^{117}Sn satellite pattern are in accordance with the assignment to Sn_4^{4-}, but due to the limited signal to noise ratio (S/N) in the direct reduction slightly larger or smaller stannide clusters with five or three Sn atoms cannot be unambiguously excluded. Therefore, the solubility improving and stabilizing effect of [2.2.2]-cryptand[18,19] was used for dissolution experiments on Rb_4Sn_4 in liquid ammonia. Prior to dissolution, the solid Rb_4Sn_4 was characterized by Raman spectroscopy and X-ray diffraction (see SI), which confirmed the presence of Sn_4^{4-} as the exclusive anionic moiety (see Figure 1b). Despite the fact that Rb_4Sn_4 has been assumed to be insoluble so far,[1] already after 7.5 hours of dissolution plus 7.5 hours of acquisition a broad signal covering 21000 Hz appeared in the ^{119}Sn spectrum and sharpened within 4 days to a signal at −1825 ppm which shows a surprisingly high S/N of 196 (see Figure 1c). This allowed for the unambiguous assignment to Sn_4^{4-} by simulation of the

experimental ^{117}Sn satellite pattern (0.133:1.000:0.132, 1423 Hz, see Figure 1d). The signal of Sn_4^{4-} in the presence of [2.2.2]-cryptand is significantly shifted upfield compared to the additive-free direct reduction ($\Delta\delta = -98$ ppm). This is in agreement with previous reports about the effect of different counter ions or [2.2.2]-cryptand on the chemical shift of Sn_9^{4-}, where the degree of ion dissociation or sequestration correlates with upfield shifts.[5,17] The larger absolute upfield shift for Sn_4^{4-} compared to Sn_9^{4-} is in accordance with the higher negative charge per Sn atom. In contrast, in dissolution experiments on Rb_4Sn_4 without [2.2.2]-cryptand exclusively Sn_9^{4-} was detected (–1248 ppm, $J = 263$ Hz). Interestingly, the intensity of this signal grew over time and simultaneously the signal of NH_2^- appeared in the proton spectrum (see SI). This is to our knowledge the first experimental evidence for the long standing suggestion that protons of ammonia act as oxidizing agent in the oxidation of Sn_4^{4-} to Sn_9^{4-}. Thus, direct reduction experiments of elemental tin with elemental rubidium (1:1) in combination with dissolution experiments of Rb_4Sn_4 with and without [2.2.2]-cryptand allowed not only for the first detection and the assignment of the highly charged cluster Sn_4^{4-} but also for the identification of ammonia as potential oxidizing agent.

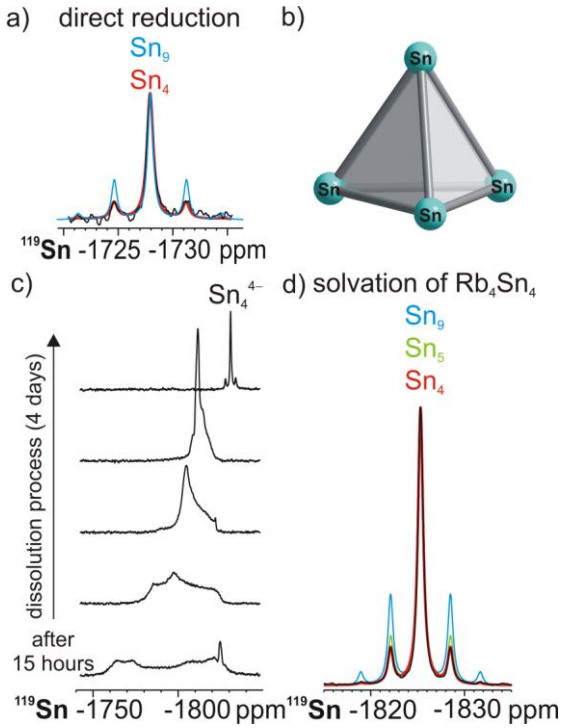

Figure 1: Sn_4^{4-} in liquid ammonia: a) Experimental (black) and simulated (colored) ^{119}Sn spectra of Sn_4^{4-} at 195 K resulting from direct reduction; b) Sn_4^{4-} cluster present in Rb_4Sn_4; c) ^{119}Sn spectra showing the dissolution process of Rb_4Sn_4 in the presence of [2.2.2]-cryptand at 233 K; d) assignment to Sn_4^{4-} based on simulations of the ^{117}Sn satellite pattern.

Next, we concentrated on the detection of naked silicides in solution, as to date, there is only circumstantial evidence for their existence (vide supra), but a ^{29}Si NMR signal in solution has not been reported so far. The only known NMR signals of silicides are reported in solid state MAS-NMR studies of the binary phases ASi (A = alkali metal). There, from Cs to Na an upfield trend of the signals is observed in accordance with a reduced electron transfer between cluster anion and counter ion.[20] For Rb and K it was even possible to resolve the two crystallographic sites, which resulted in separated NMR signals for each phase (Rb: –290 ppm, –305 ppm; K: –320 ppm, –340 ppm). Given the tremendous intensity enhancement of Sn_4^{4-} in the dissolution experiments with [2.2.2]-cryptand compared to the direct reduction (vide supra), the applied dissolution method was also chosen for the detection of silicides. Based on our experience with recrystallization experiments[11,12] and conversion[13] of silicides, as starting material a solid with the nominal composition $K_6Rb_6Si_{17}$ was used. In order to facilitate the NMR detection in solution ^{29}Si isotope labeling was applied. For $K_6Rb_6Si_{17}$ an enrichment of 20 % ^{29}Si was chosen, providing a compromise between absolute signal enhancement and intensity reduction due to ^{29}Si-^{29}Si scalar couplings e.g. expected for Si_9^{4-}. Prior to the solvation experiments, the characterization of the mixed cationic solid $K_6Rb_6Si_{17}$ by Raman spectroscopy showed the presence of both, Si_4^{4-} and Si_9^{4-} cluster precast in the solid state (see Figure 2a and SI). Deviating, the X-ray powder diffraction pattern showed only the presence of the binary Si_4^{4-} containing phase Rb_4Si_4 (see SI), which was attributed to the poor crystallinity and the plural phase character of the solid starting material. In the solid state MAS-NMR of $K_6Rb_6Si_{17}$, only elemental Si and a broad signal at –311 ppm was observed (see Figure 2b), which is exactly in between the known chemical shifts of Rb_4Si_4 and K_4Si_4.[20] Again no signal for Si_9^{4-} was detected, probably due to line broadening effects caused by scalar coupling and the poor crystallinity of the material, prohibiting also its detection in the X-ray powder diffraction pattern. Next, $K_6Rb_6Si_{17}$ was dissolved in the presence of cryptand in liquid ammonia and the first ^{29}Si spectrum of the sample was started after 19 hours. Unexpectedly, already after 4.5 hours of acquisition time and without further optimization of the NMR parameters, an extremely broad signal covering 180 Hz appeared in the ^{29}Si NMR spectrum, which sharpened within 11 days to a signal at –323 ppm with a tremendous signal to noise ratio of 80 (see Figure 2c and SI).

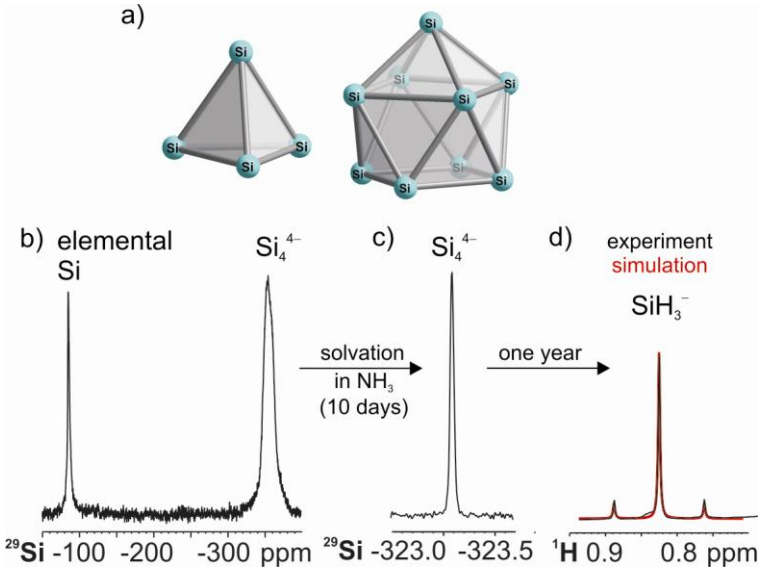

Figure 2: NMR-detection of Si_4^{4-} in the solid state and in solution plus identification of the degradation product SiH_3^-: a) Si_4^{4-} and Si_9^{4-} cluster present in $K_6Rb_6Si_{17}$; b) ^{29}Si MAS-NMR spectrum of $K_6Rb_6Si_{17}$ with 20 % ^{29}Si labeling at room temperature c) ^{29}Si NMR spectrum after dissolution of the 20 % ^{29}Si labeled $K_6Rb_6Si_{17}$ in the presence of [2.2.2]-cryptand in liquid ammonia at 195 K; d) ^{1}H NMR spectrum at 195 K after dissolution of the 20 % ^{29}Si labeled $K_6Rb_6Si_{17}$ without [2.2.2]-cryptand in liquid ammonia and one year storage at 195 K including the simulation (red) of SiH_3^-.

Following, this signal was assigned to a specific silicide cluster. ^{29}Si is the only NMR active isotope, hence exclusively the chemical shift can be used to differentiate between Si_4^{4-} and Si_9^{4-}, which are both present in the starting material. The ^{29}Si signal detected in solution shows with −323 ppm only a slight upfield shift compared to the solid state MAS-NMR signal of Si_4^{4-} in $K_6Rb_6Si_{17}$ at −311 ppm. For Si_9^{4-} no MAS-NMR signal has been reported so far, thus the exact chemical shift range is unknown. However, from the trends observed for the stannides, a lower charge per atom shifts the signal considerably downfield (Sn_4^{4-}: −1727 ppm; Sn_9^{4-}: −1248 ppm). Thus, the signal of Si_9^{4-} is expected to be in between the solid state signal of Si_4^{4-} and elemental Si. The chemical shift reported for $R_3Si_4^-$ in solution (δ = −153.6 ppm; R = $SiMeDis_2$; Dis = $CH(SiMe_3)_2$) corroborates this trend.[8] Furthermore, theoretical calculations suggest a higher rigidity for Si_9^{4-} than for Sn_9^{4-},[11] which would result in three separated signals for Si_9^{4-} (see Figure 2a). This fact and all chemical shift trends for silicides and stannides known so far corroborate the assignment to Si_4^{4-}. Next, the slight upfield shift between Si_4^{4-} in solution and in the MAS-NMR spectrum is addressed. As discussed above for stannides, the dissociation of cations from Zintl anions induces upfield shifts. For the highly charged Sn_4^{4-} signal without and with cryptand an upfield shift of $\Delta\delta$ = −98 ppm is observed (vide supra). For ^{29}Si the absolute chemical shift range is significantly smaller. Thus, the upfield shift of Si_4^{4-} in solution by only 12 ppm with respect

to the MAS-NMR signal fits to the ion sequestration during the dissolution process. Beyond that, Si_4^{4-} was observed to be surprisingly stable in the presence of [2.2.2]-cryptand. Even in a sample of $K_6Rb_6Si_{17}$, which was stored at 195 K for one further month and measured at an elevated temperature of 233 K, the Si_4^{4-} signal was detected in 87 % of the maximal intensity observed after 11 days at 195 K (see SI). After an extended storage (one year) of $K_6Rb_6Si_{17}$ in liquid ammonia without [2.2.2]-cryptand, a variety of degradation products was observed in the proton spectrum (see SI). Among these, the signal at 0.83 ppm with a $^1J_{H,Si} = 75$ Hz could be identified as SiH_3^- . The simulation considering the 20 % ^{29}Si labeling (see Figure 2d) and the coupling constant of the previously reported signal of $KSiH_3$ in benzene[21] corroborate this assignment. Recently, Eichhorn *et al.* reported the protonated stannide HSn_9^{3-} in a reversible equilibrium with Sn_9^{4-} in the presence of [2.2.2]-cryptand in en.[5] For the less stable silicides without the stabilizing influence of [2.2.2]-cryptand, the protonation is expected to be irreversible, resulting in the formation of SiH_3^- as final degradation product.

4.4 Conclusions

In summary, the long time elusive detection of silicides in solution is presented on the example of Si_4^{4-}. In addition, the likewise elusive first NMR-observation of the highly charged stannide Sn_4^{4-} is reported. Amazingly high signal intensities and stabilities were observed for both highly charged Zintl anions, Si_4^{4-} and Sn_4^{4-}, by utilizing the stabilizing effect of [2.2.2]-cryptand and in the case of Si_4^{4-} the enhanced solubility of the plural phase $K_6Rb_6Si_{17}$. Furthermore, by observing the generation of NH_2^- the first experimental evidence for the long-standing assumption of solvent protons as oxidizing agent for Zintl anions is given and in case of silicides, SiH_3^- was detected as degradation product.

4.5 References

(1) Scharfe, S.; Kraus, F.; Stegmaier, S.; Schier, A.; Fässler, T. F. *Angew. Chem. Int. Ed.* **2011**, *50*, 3630-3670.

(2) Guloy, A. M.; Ramlau, R.; Tang, Z.; Schnelle, W.; Baitinger, M.; Grin, Y. *Nature* **2006**, *443*, 320-323.

(3) Chandrasekharan, N.; Sevov, S. C. *J. Elchem. Soc.* **2010**, *157*, C140-C145.

(4) Baudler, M.; Glinka, K. *Chem. Rev.* **1993**, *93*, 1623-1667.

(5) Kocak, F. S.; Downing, D. O.; Zavalij, P.; Lam, Y.-F.; Vedernikov, A. N.; Eichhorn, B. *J. Am. Chem. Soc.* **2012**, *134*, 9733-9740.

(6) Wiesler, K.; Brandl, K.; Fleischmann, A.; Korber, N. *Z. Anorg. Allg. Chem.* **2009**, *635*, 508-512.

(7) Waibel, M.; Kraus, F.; Scharfe, S.; Wahl, B.; Fässler, T. F. *Angew. Chem. Int. Ed.* **2010**, *49*, 6611-6615.

(8) Ichinohe, M.; Toyoshima, M.; Kinjo, R.; Sekiguchi, A. *J. Am. Chem. Soc.* **2003**, *125*, 13328-13329.

(9) Goicoechea, J. M.; Sevov, S. C. *Journal of the American Chemical Society* **2004**, *126*, 6860-6861.

(10) Goicoechea, J. M.; Sevov, S. C. *Inorganic Chemistry* **2005**, *44*, 2654-2658.

(11) Joseph, S.; Suchentrunk, C.; Kraus, F.; Korber, N. *Eur. J. Inorg. Chem.* **2009**, 4641-4647.

(12) Joseph, S.; Hamberger, M.; Mutzbauer, F.; Härtl, O.; Meier, M.; Korber, N. *Z. Naturforsch.* **2010**, *65b*, 1059-1065.

(13) Joseph, S.; Hamberger, M.; Mutzbauer, F.; Härtl, O.; Meier, M.; Korber, N. *Angew. Chem. Int. Ed.* **2009**, *48*, 8770-8772.

(14) Abersfelder, K.; White, A. J. P.; Berger, R. J. F.; Rzepa, H. S.; Scheschkewitz, D. *Angewandte Chemie International Edition* **2011**, *50*, 7936-7939.

(15) Rudolph, R. W.; Wilson, W. L.; Parker, F.; Taylor, R. C.; Young, D. C. *J. Am. Chem. Soc.* **1978**, *100*, 4629-4630.

(16) Rudolph, R. W.; Wilson, W. L.; Taylor, R. C. *J. Am. Chem. Soc.* **1981**, *103*, 2480-2481.

(17) Wilson, W. L.; Rudolph, R. W.; Lohr, L. L.; Taylor, R. C.; Pyykko, P. *Inorg. Chem.* **1986**, *25*, 1535-1541.

(18) Corbett, J. D.; Edwards, P. A. *J. C. S. Chem. Commun.* **1975**, 984-985.

(19) Teixidor, F.; Luetkens, M. L.; Rudolph, R. W. *J. Am. Chem. Soc.* **1983**, *105*, 149-150.

(20) Stearns, L. A.; Gryko, J.; Diefenbacher, J.; Ramachandran, G. K.; McMillan, P. F. *J. Solid State Chem.* **2003**, *173*, 251-258.

(21) Fehér, F.; Krancher, M.; Fehér, M. *Z. Anorg. Allg. Chem.* **1991**, *606*, 7-16.

4.6 Supporting Information

4.6.1. Synthesis

4.6.1.1 General Considerations

All manipulations described below were performed in a purified argon atmosphere (Glove box) by using glass vessels dried at least four times in vacuum. [2.2.2]-cryptand was purchased from Sigma-Aldrich and used without further drying. Elemental rubidium was synthesized by the reduction of RbCl and purified through distillation. Elemental potassium was obtained from a commercial source and distilled on our own. By condensing the commercially acquired gaseous ammonia onto elemental sodium and storing this cooled Na/ammonia-solution for about three days, residual moisture traces were removed.

4.6.1.2 Solid Phase Synthesis of the Zintl Anions (High Temperature Synthesis)

Rb_4Sn_4: Rb_4Sn_4 was obtained by gradually heating (60 °C/h) stoichiometric amounts of elemental rubidium (0.64 g, 7.5 mmol) and elemental tin (0.78 g, 6.6 mmol) in a Duran glass ampoule to 450 °C and holding it at this temperature for 20 h. Subsequently, the reaction mixture slowly cooled to room temperature (25 °C/h). Due to its sensitivity towards moisture and air the solid state phase was handled and stored under argon atmosphere.

$K_6Rb_6Si_{17}$ (20 % ^{29}Si): $K_6Rb_6Si_{17}$ was synthesized by a high temperature fusion of stoichiometric amounts of the elements, where 0.294 g (7.5 mmol) potassium, 0.644 g (7.5 mmol) rubidium and 0.5 g (17.8 mmol, 20 % 29Si) were placed in a Duran glass ampoule and heated to 460 °C at a rate of 25 °C/h and held at this temperature for 72 h. Afterwards the mixture was gradually cooled down to room temperature (20 °C/h). Due to its sensitivity towards moisture and air the solid state phase was handled and stored under argon atmosphere.

4.6.1.3 Direct Reduction in Liquid Ammonia (Low Temperature Synthesis)

All direct reduction experiments were carried out directly in an NMR tube. Therefore, at first 39 mg (0.46 mmol) elemental Rb and 60 mg (0.51 mmol) Sn were placed in a tube and subsequently anhydrous liquid ammonia was directly condensed onto the mixture at −78 °C. In order to guarantee the permanent absence of moisture and air, the tube was sealed under ammonia atmosphere. Before NMR measurements on these solutions were performed, the fresh samples were stored at low temperature until the blue color turned to deeply red.

4.6.1.4 Solvation of Zintl Phases in Liquid Ammonia

Under completely inert conditions (Glove box), the respective solid material (Rb_4Sn_4: 25 mg, 0.031 mmol; $K_6Rb_6Si_{17}$: 20 mg, 0.016 mmol) was transferred into an NMR tube. The dissolution of Rb_4Sn_4 in liquid ammonia was carried out in the presence of [2.2.2]-cryptand (18 mg, 0.048 mmol) and the dissolution of $K_6Rb_6Si_{17}$ in the presence of [2.2.2]-cryptand (6 mg, 0.016 mmol) and a small amount of $RbNH_2$. Therefore, anhydrous liquid ammonia was directly condensed onto the respective sample at −78 °C. In order to guarantee permanently the absence of moisture and air, the tube was sealed under ammonia atmosphere.

4.6.2. Phase Determination

4.6.2.1 General Considerations

The FT-Raman spectra were recorded at room temperature under inert conditions from powdered samples sealed in pyrex tubes (∅ = 0.7−1.0 mm) using a Raman module coupled to a Varian FTS 7000e spectrometer (Nd:YAG-laser, λ = 1064 nm). Data were processed with OriginPro 7.5 and Microsoft Excel 2007. Structure determinations were investigated by X-ray powder diffraction. Data were collected on a transmission powder diffraction system (STADI P, Fa. Stoe Cie, Darmstadt, Cu-K_α radiation with λ = 1.540598 Å). Therefore, capillaries were charged with powdered samples, respectively, and air-proof sealed. Data were processed with WinXPow.[1] Solid state ^{29}Si MAS-NMR spectra were recorded with a 400 MHz spectrometer using a standard Bruker pulse program (hpdec.av), 128 number of scans, TD = 16k, a MAS-frequency of 12k and a relaxation delay of 180 s. Data were processed with the Bruker software TOPSPIN 2.1 using SI = 16k. The chemical shifts are reported in ppm relative to $SiMe_4$.

1. Sheldrick, G., SHELX97 - Programs for the solution and refinement of crystal structures, Universität Göttigen, **1997**.

4.6.2.2 Rb_4Sn_4

The Raman spectrum of Rb_4Sn_4 showed the characteristic vibrational resonances of Sn_4^{4-} at 133.1 cm^{-1} and 184.2 cm^{-1} (see SI Figure 1).[1] Furthermore, the solution and refinement of the experimental powder diffraction data yielded a tetragonal body centered cell of the space group $I4_1/acd$ which relates to Rb_4Sn_4 (see SI Figure 2).[2-4] So, we assume that Rb_4Sn_4 is a phase pure solid and contains Sn_4^{4-} as the exclusive anionic moiety due to missing peaks of Sn_9^{4-} in terms of Raman spectroscopy[5] and X-ray diffraction.

1. Somer, M.; Aydemir, U.; Baitinger, M.; von Schnering, H. G. *Z. Anorg. Allg. Chem*. **2006**, *632*, 1281-1286.
2. von Schnering, H. G.; Grin, Y.; Baitinger, M.; Kniep, R. *Zeitschrift für Kristallographie – New Crystal Strucutres* **1999**, *214*, 453.
3. von Schnering, H. G.; Baitinger, M.; Grin, Y.; Kniep, R. *Zeitschrift für Kristallographie – New Crystal Strucutres* **1999**, *214*, 457-458.
4. Klemm, W.; Hewaidy, I. F.; Busmannn, E. *Z. Anorg. Allg. Chem*. **1964**, *328*, 283.
5. von Schnering, H. G.; Baitinger, M.; Bolle, U.; Carrillo-Cabrera, W.; Curda, J.; Grin, Y.; Heinemann, F.; Llanos, J.; Peters, K.; Schmeding, A., Somer, M., *Z. Anorg. Allg. Chem*. **1997**, *623*, 1037-1039.

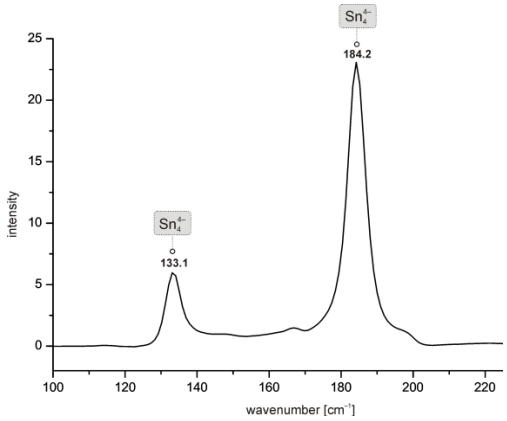

SI Figure 1: The Raman spectrum shows the characteristic vibrations of Rb_4Sn_4.

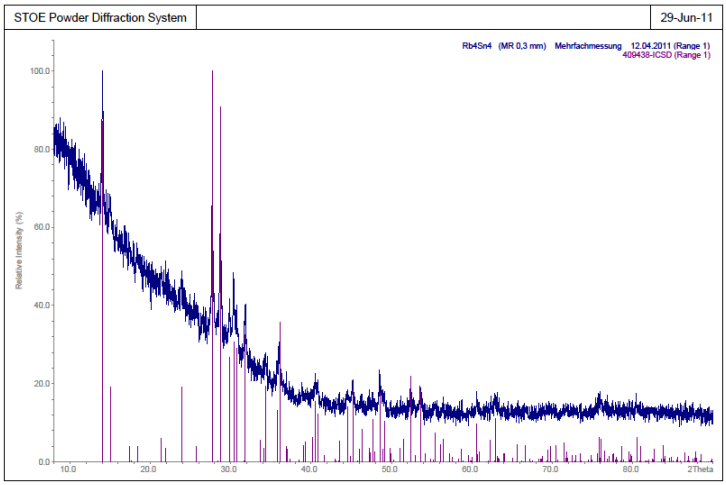

SI Figure 2: Comparison of experimental (blue) and theoretical (violet) reflection pattern of Rb_4Sn_4. The latter was calculated from single crystal data as there is no powder data available.

4.6.2.3 $K_6Rb_6Si_{17}$

$K_6Rb_6Si_{17}$ can be considered as a mixed phase of $(K,Rb)_4Si_4$ and $(K,Rb)_{12}Si_{17}$ as the Raman spectrum showed the vibrational resonances of Si_4^{4-} (286.2 cm^{-1}, 355.9 cm^{-1} and 479.3 cm^{-1}) and Si_9^{4-} (391.6 cm^{-1}) (see SI Figure 3).[1] The experimental reflection pattern presented in Figure 4a relates to $(K_2Rb_2)Si_4$. The missing reflections of $A_{12}Si_{17}$ (with A = K, Rb) (see Figure 4b), presumably, are superimposed by the broad reflection of the amorphous solid material. So, both, Powder diffraction and MAS-NMR experiments (see main article Figure 2b) confirmed the

presence of Si_4^{4-} in solid state, but as the crystallinity of the sample is poor, Si_9^{4-} could not be detected.

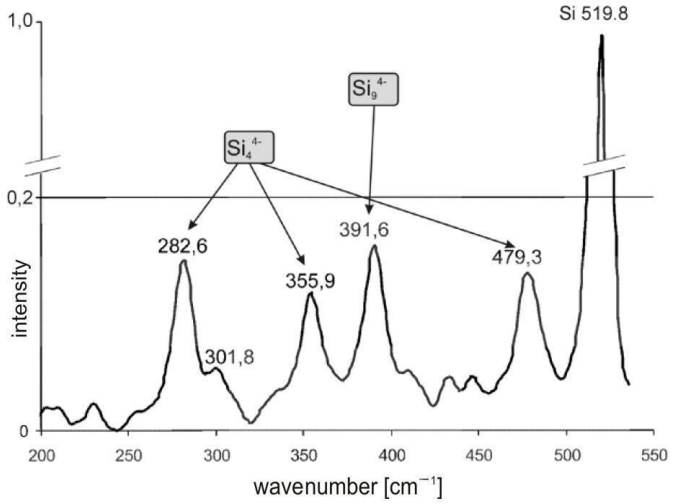

SI Figure 3: The Raman spectrum shows the characteristic vibrational resonances of, both, Si_4^{4-} and Si_9^{4-} clusters.

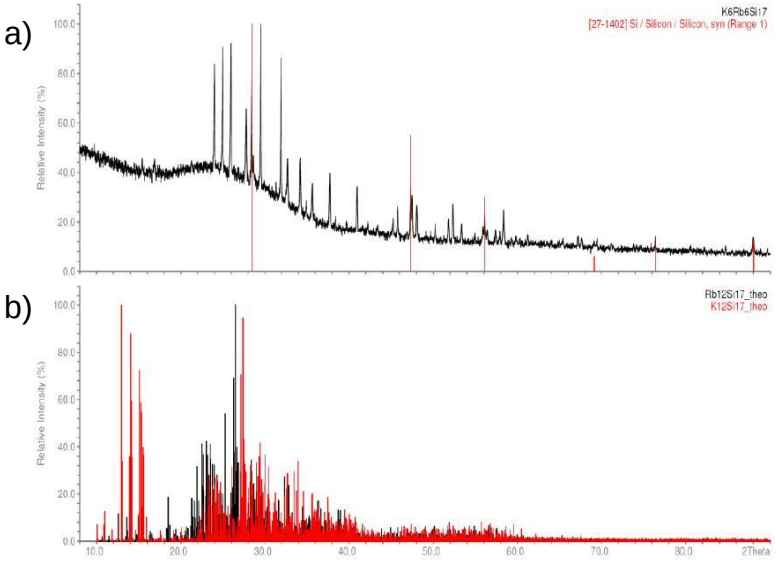

SI Figure 4: (a) Comparison of the experimental reflection pattern of $K_6Rb_6Si_{17}$ (black) and unreacted silicon (red). (b) Theoretical reflection patterns of $K_{12}Si_{17}$ (black) and $Rb_{12}Si_{17}$ (red).

1. Hoch, C.; Wendorff, M.; Röhr, C.; *Journal of Alloys and Compounds* **2003**, *361*, 206.

4.6.3. NMR Investigations in Solution

4.6.3.1 Data Collecting and Processing

The NMR spectra were recorded on a Bruker Avance 600 spectrometer equipped with a 5 mm broadband triple resonance Z-gradient probe. The temperatures for all measurements were controlled by a Bruker BVTE 3900 temperature unit. ^{119}Sn measurements were carried

out with a standard Bruker pulse program (zg) using 70k number of scans, 2 dummy scans, TD = 8k with a relaxation delay of 0.3 s. Data were processed with the Bruker software TOPSPIN 3.1 using the processing parameters SI = 16 k, WDW = EM and LB = 50 Hz. The chemical shifts are reported in ppm relative to $SnMe_4$. ^{29}Si measurements were carried out with a standard Bruker pulse program (zg30) using 3k number of scans, 8 dummy scans, TD = 8k with a relaxation delay of 5 s. Data were processed with the Bruker software TOPSPIN 3.1 using the processing parameters SI = 16k, WDW = EM and LB = 1 Hz. The chemical shifts are reported in ppm relative to $SiMe_4$. All signal to noise ratios were determined by using the Bruker analysis tool for S/N calculations.

4.6.3.2 Signal Assignment

The more abundant ^{119}Sn was used as observe nucleus and the ^{117}Sn-^{119}Sn scalar coupling for signal assignment. Therefore, the coupling patterns for all possible cluster sizes (4, 5 and 9) were calculated from the statistical distribution of both NMR active nuclei over the respective polyanion (see SI table 1). Based on these calculations and for a better visualization, theoretical NMR spectra were simulated for these patterns and compared to the experimental ones.

SI Table 1: Calculation of the theoretical coupling pattern

Possible clusters	Theoretical coupling pattern
E_4^{4-}	0.047:0.324:1.000:0.324:0.047
E_5^{2-}	0.011:0.170:1.000:0.170:0.011
E_9^{4-}	0.006:0.128:1.000:0.128:0.006

4.6.3.3 Additional NMR Spectra

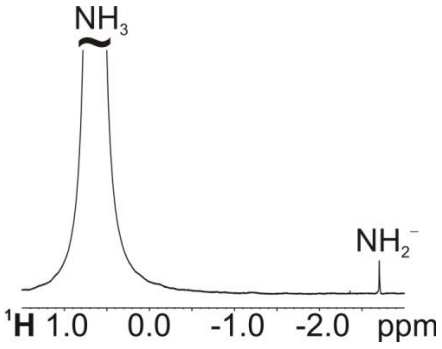

SI Figure 5: ^1H spectrum of pure $RbNH_2$ at 195 K in liquid ammonia serves as reference for further signal assignment.

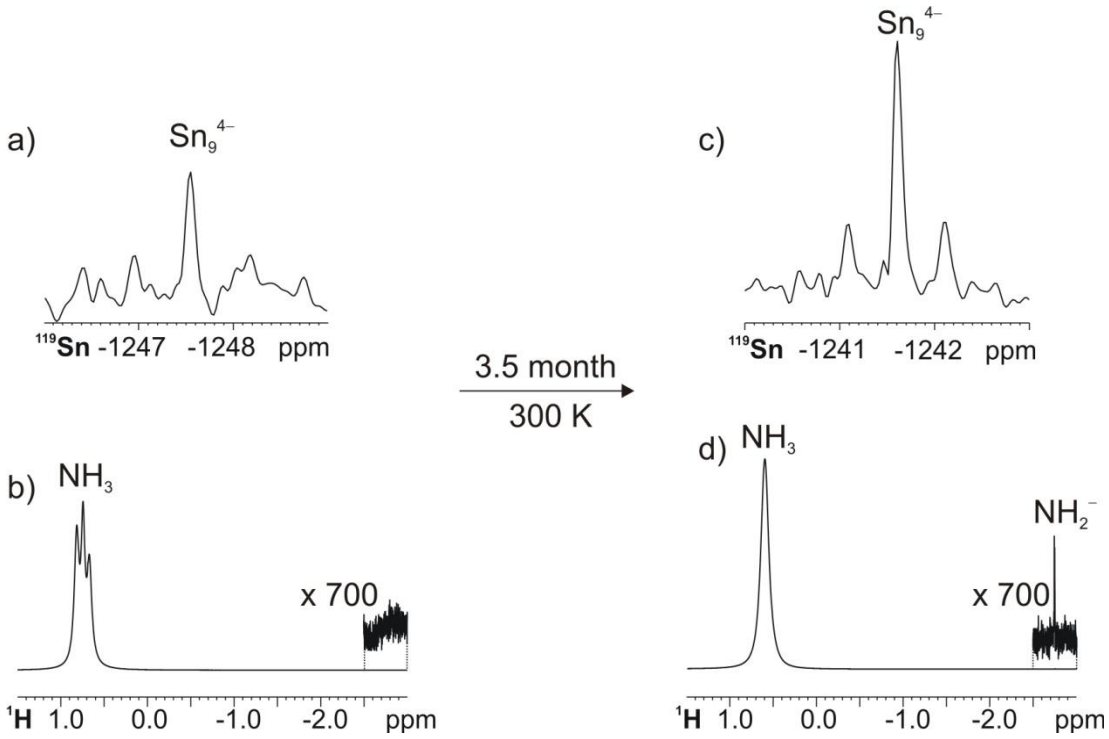

SI Figure 6: Solvation of Rb_4Sn_4 in liquid ammonia. The ^{119}Sn spectrum recorded from the freshly prepared sample at 195 K (a) shows a small Sn_9^{4-} signal at −1247.5 ppm. The corresponding proton spectrum (b) shows a triplet for liquid ammonia and no detectable amount of NH_2^- (assigned by comparison with the reference spectrum of NH_2^- in liquid ammonia shown in SI Figure 5). Upon storing the sample at room temperature for 3.5 month, the signal grows significantly, which is visible in the ^{119}Sn spectrum (c) recorded at 300 K. Probably, the chemical shift offset of 6 ppm is due to a temperature effect. The signal growth of Sn_9^{4-} is accompanied by (d) the evolution of NH_2^-, which is detectable alongside of NH_3. Simultaneously, the coupling pattern of ammonia breaks down. Presumably, this effect is due to chemical exchange with the amide.

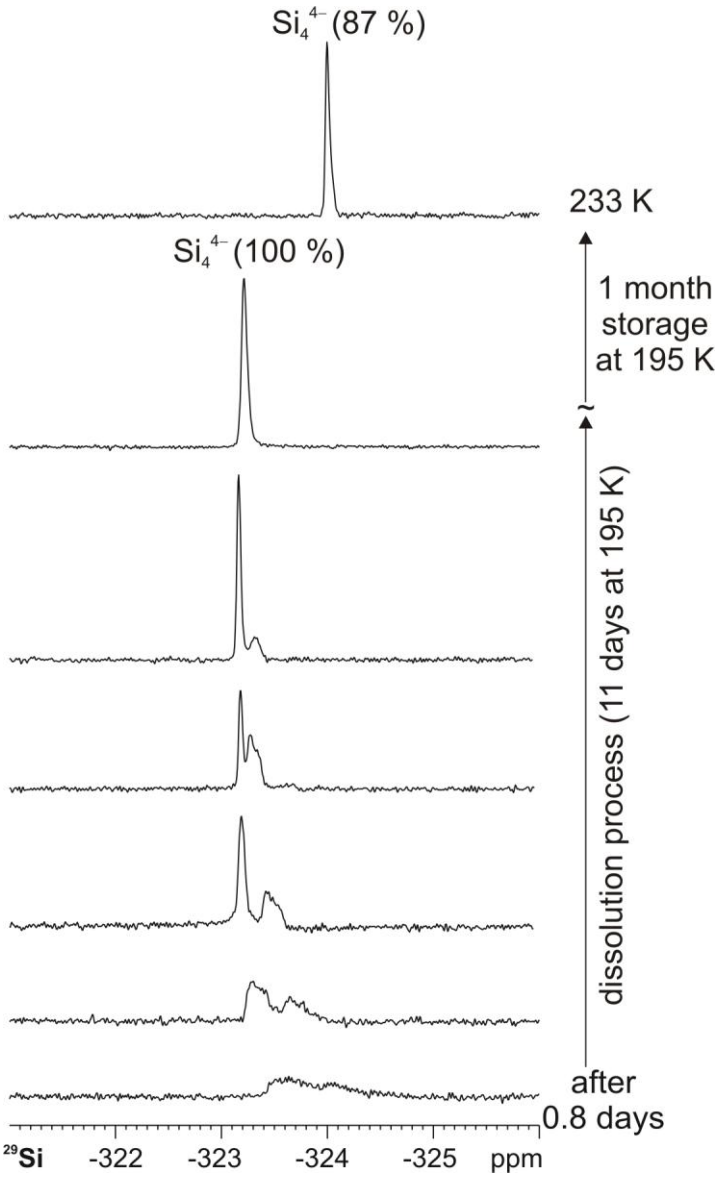

SI Figure 7: ^{29}Si spectra recorded at 195 K from the solvation of $K_6Rb_6Si_{17}$ (20 % enriched in ^{29}Si) and [2.2.2]-cryptand in liquid ammonia. The spectra clearly show the solvation process of the solid state material. In the beginning, this process is characterized by a 1.6 ppm extended signal, which results in one narrow line after 10 days. Due to the unexpected stability, this signal is also detectable at 233 K with an upfield shift of 0.9 ppm, which agrees with the greater cation mobility at elevated temperatures.

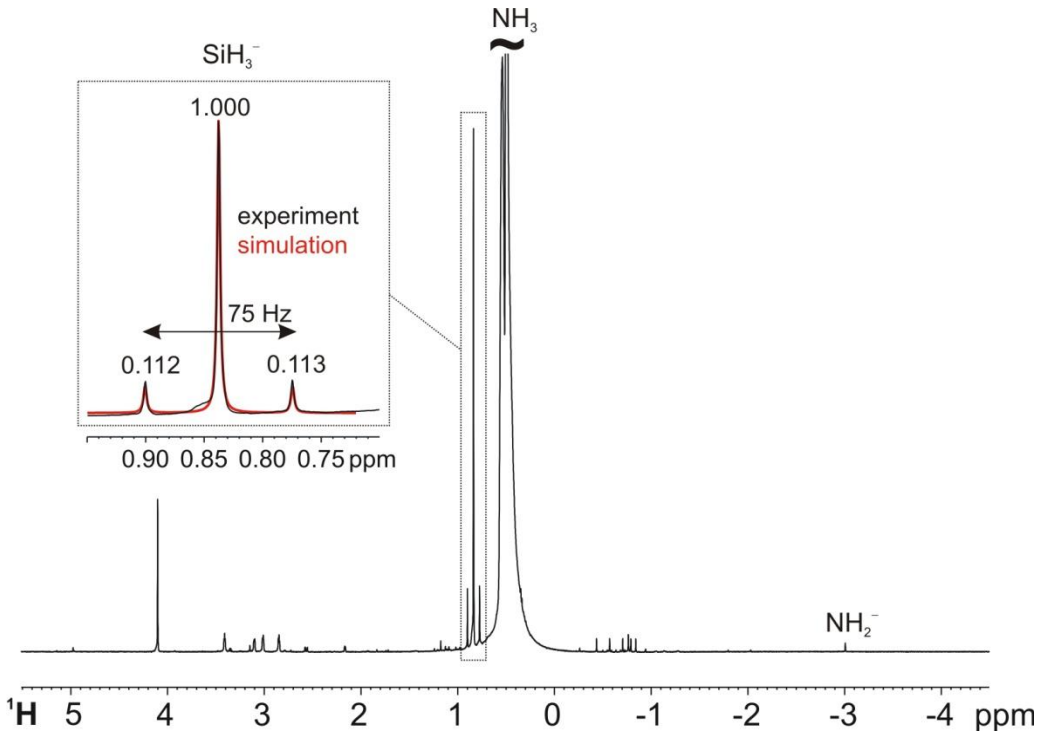

SI Figure 8: After one year storage of the solvation sample of $K_6Rb_6Si_{17}$ in liquid ammonia at 195 K in the absence of stabilizing [2.2.2]-cryptand, the ^1H spectrum shows a variety of degradation products. The signals for SiH_3^- and NH_2^-could be unambiguously assigned in comparison to the simulated signal of SiH_3^- including the 20 % ^{29}Si labeling and a reference spectrum of NH_2^- in liquid ammonia (see SI Figure 5).

5. ^{119}Sn NMR Investigations on the Solution Chemistry of Polystannides in Liquid Ammonia: On the Way to a Targeted Material Research

For these studies, I performed the NMR spectroscopic investigations, while the synthesis and the characterization of the binary phases as well as the sample preparation were performed by Franziska Fendt. The synthesis and the characterization of the ternary phases as well as the sample preparation were performed by Ute Friedrich.

Maria Neumeier, Franziska Fendt, Ute Friedrich, Nikolaus Korber, Ruth M. Gschwind

to be published as soon as possible

5.1 Abstract

The fascinating and versatile chemistry of group 14 Zintl anions is contrary to the fragmentary knowledge about their properties and stabilities in solution. Reactions of Zintl anions with transition metal complexes yielded manifold new materials with polyanions as ligands, interstitial intermetallic phases and even a new modification of the element germanium. Since the knowledge about the solvation process and the properties of polyanions in solution is rather limited to date, the discovery of such new materials is quite coincidental. Here, we present the first systematic ^{119}Sn NMR study of the transformations of stannides in liquid ammonia, which occur during the solvation process. Moreover, we gained insight into the stabilizing effect of [2.2.2]-cryptand on the highly reduced tetrastannide, which over time gets oxidized to Sn_9^{4-} and Sn_5^{2-}. Finally, we used this knowledge to address different polyanions in chemical reactions with mesitylcopper. Two reactions of Rb_4Sn_4 with mesitylcopper with and without [2.2.2]-cryptand show that the cluster structures present in solution are really decisive for the product formation. This knowledge will be helpful on the way to a more targeted material research.

5.2 Introduction

The various group 14 elements show an extreme versatile chemistry. Carbon is a non-metal and forms covalent bonds, lead (in its predominantly occurring modification) is a metal of cubic closest packing and forms preferentially salts with more electronegative reaction partners. In contrast, silicon takes up an intermediate position and, predominantly, forms polar bonds. Furthermore, the elements Si-Pb can form intermetallic phases with alkali or alkaline earth metals.[1] These so-called Zintl phases have come a long way, since, more than 120 years ago, Joannis had observed the dissolution of Pb in blue solutions of alkali metals in liquid ammonia.[2] Later on, the German chemist Eduard Zintl, attributed this observation to the formation of Pb_9^{4-}.[3] Henceforth, intermetallic phases, which are characterized by a complete electron transfer from the more electropositive to the more electronegative reactant, were named Zintl phases.[4] More than 70 years after their discovery, Kummer and Diehl published the first X-ray structure analysis of a homoatomic polyanion, Sn_9^{4-}.[5] Over time, further achievements have been made, including improved dissolution and crystallization properties by the addition of [2.2.2]-cryptand.[6,7] Based on this, first conversions of homoatomic polyanions[8] and X-ray crystallographic investigations on their reaction products became

possible.[9] In the first observed transition metal complex, a Sn_9^{4-} anion was presented to be coordinated as ligand to chromium.[9] In 1996, the first interstitial transition metal complex was reported, which represents another reaction route for Zintl anions.[10,11] Also, the oxidative coupling of two Ge_9^{4-} anions, was shown[12] and even a new Ge modification was discovered in 2006.[13,14] This brief historical overview illustrates the manifold and fascinating chemistry of Zintl phases. Today, a multitude of homoatomic polyanions with different geometries are known from X-ray crystallography. E_4^{4-} (E = Si-Pb) are electron precise tetrahedrons, which are iso-structural to the uncharged group 15 tetrahedrons (Figure 1a). For E_9^{x-} (x = 2: E = Si, Ge; x = 3, 4: E = Si-Pb) the so far known geometries are in between a single capped quadratic antiprism with C_{4v} symmetry and a threefold capped trigonal prism with D_{3h} symmetry (see Figure 1b).[15] Both geometric limits can be converted from one form into the other via the "diamond-square" process,[16] for which SCF-CNDO-MO calculations[17] suggested a negligible barrier along the path. E_5^{2-} (E = Si-Pb) is a trigonal bipyramidal cluster (see Figure 1c).

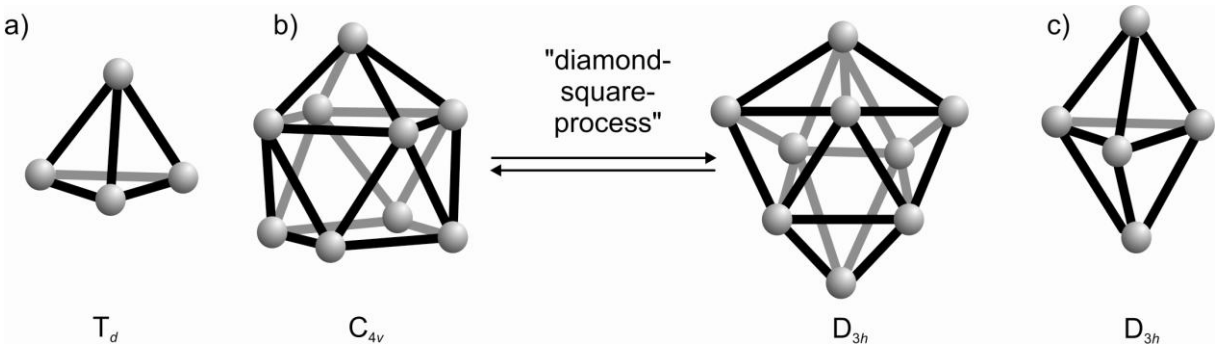

Figure 1: Geometries of the in liquid NH_3 detected polyanions a) E_4^{4-}, b) E_9^{x-} and c) E_5^{2-} (E = Si-Pb).

It is striking that four- and nine-atomic clusters can be obtained by solid state synthesis, in which the respective group 14 element (E) is reacted with an alkali or alkaline earth metal (A). Depending on the stoichiometric ratio, the reaction products are intermetallic phases with the composition A_4E_4 (E = Si-Pb),[18–22] A_4E_9 (E = Ge, Sn, Pb)[23–25] and $A_{12}E_{17}$ (E = Si-Pb).[23,26] They contain either E_4^{4-} (A_4E_4) or E_9^{4-} (A_4E_9) or both clusters ($A_{12}E_{17}$). They are partly soluble in polar aprotic solvents, like ethylenediamine or liquid ammonia. Depending on the conditions, different solvate crystals can be obtained from these solutions. Whereas additive-free solutions of A_4E_9 and $A_{12}E_{17}$ yield structures with E_9 clusters, E_5 clusters can be obtained among others from [2.2.2]-cryptand-containing solutions. A_4E_4 was assumed to be insoluble,[15] except Rb_4Pb_4, which yields crystals with Pb_4 clusters.[27] Interestingly, crystals with Sn_4^{4-} moieties are accessible by the direct reduction of tin with alkali metals in liquid ammonia.[27] Furthermore, Si_4^{4-} had been successfully extracted from $K_6Rb_6Si_{17}$ and stabilized

in solution by two MesCu moieties (Mes = 2,4,6-$Me_3C_6H_2$).[28] Further sizes and geometries can be observed in reactions of E_9 cluster with transition metal complexes. $[Ir@Sn_{12}]^{3-}$,[29] $[Pt_2@Sn_{17}]^{4-}$ or $[Pd_2@Sn_{18}]^{4-}$, are examples for larger clusters.[30,31] Another geometry, E_6^{2-}, is known from $[\{E\text{-}Cr(CO)_5\}_6]^{2-}$ with (E = Ge, Sn), in which the polyanion is exo-bonded to the transition metal and acts as a ligand.[32,33] These experimental results indicate transformations of polyanions in solution. Whereas many examples for reactions with the most stable clusters E_9^{4-} are known, reactions with other polyanions are rare. One example is the conversion of Si_4^{4-} with MesCu, which yielded $[(MesCu)_2(Si_4)]^{4-}$.[28] Such highly charged clusters are much more sensitive to changes in solution conditions and, presumably, often suffer from redox instability.[34] Up to now, the stability of different cages in solution never has been investigated systematically. Moreover, often uncharacterized alloys are used as starting materials and therefore, new materials are often produced rather coincidentally. In order to develop a more targeted material research, a detailed understanding of the processes during the solvation of Zintl phases is desirable. There, the main goal is to understand the conditions under which a distinct polyanion is stable in solution and, potentially, can be addressed in a chemical reaction.

In order to gain more insight into these transformations in solution, we developed a dual strategy. The first step includes the synthesis of different solids, whose characterization enables a detailed knowledge about the polyanions, which are precast in the Zintl phase. Appropriate investigations are X-ray diffraction or Raman spectroscopy. The second step includes the dissolution of these solids in liquid ammonia and a detailed NMR study of the respective polyanions in solution. For comparison, another method of sample preparation was used, namely the direct reduction of group 14 elements with alkali metals in liquid ammonia. These investigations might clarify the transformations in solution and enable targeted reactions with transition metals. Based on the results of Rudolph *et al.*, we chose the stannides as a model system. They had detected the first stannide signals of Sn_9^{4-} and Sn_4^{2-} in ethylenediamine.[35–37] As tin possesses two excellent NMR active nuclei, ^{119}Sn (8.58 %) and ^{117}Sn (7.61 %), both with spin = ½, and provide reasonable magnetogyric ratios (–9.578, –10.021 10^7 rad $T^{-1}s^{-1}$), they used ^{119}Sn as observe nucleus and the ^{117}Sn satellite pattern for unambiguous assignment of the cluster size. According to this procedure, we calculated the statistically expected coupling patterns for all from solid state known naked clusters (Sn_4^{4-}, Sn_5^{2-}, Sn_9^{4-}) (see SI).[15] Based on these calculations, we simulated the theoretical NMR spectra for these patterns and compared them to the experimental ones. Besides the possibility

of unambiguous signal assignment, a further advantage of the solutions of stannides is the greater stability towards moisture and oxidation processes and a better solubility compared to silicides.

In chapter 4 the first ^{119}Sn signal of the highly charged Sn_4^{4-} in the direct reduction of elemental tin with elemental rubidium (1:1) without further additives was shown (δ = –1727 ppm). Despite the expectation that the solubility of Sn_4^{4-} is rather limited, we were able to directly evidence the existence of such a highly charged cluster anion in solution. In addition, even though Rb_4Sn_4 has been assumed to be completely insoluble,[38] the co-solvation of Rb_4Sn_4 with [2.2.2]-cryptand yielded enormous amounts of Sn_4^{4-} with a chemical shift of –1825 ppm, which shows an upfield shift of 98 ppm with respect to the Sn_4^{4-} signal in additive-free solution, indicating the sequestration of the counterion by [2.2.2]-cryptand.[39] Even the up to 21000 Hz broad Sn_4^{4-}signal, in the beginning of the dissolution process were visible. In contrast, in solvation experiments of Rb_4Sn_4 without [2.2.2]-cryptand a fast oxidation of Sn_4^{4-} to Sn_9^{4-} (δ = –1248 ppm) was observed. Beyond that, the simultaneous detection of NH_2^- provided the experimental evidence for the long-standing assumption of solvent deprotonation during this oxidation process. Thus, the salient increase of solubility and stability of Sn_4^{4-} by the addition of [2.2.2]-cryptand impressively demonstrates once more the potential of this additive.

5.3 The Chemistry of Pure Polystannide Solutions

5.3.1. Additive-Free Solutions: Direct Reduction

Having revealed the direct reduction of tin with alkali metals in liquid ammonia as an efficient access for studying four-atomic clusters of tin in solution, we widened the scope of reducing agents from rubidium to sodium in order to study the counterion effect. In chapter 4 we discussed a greater effect of [2.2.2]-cryptand on the chemical shift offset of Sn_4^{4-} than Sn_9^{4-}. For Sn_9^{4-}, Rudolph *et al.* reported an upfield shift of 31 ppm, from –1205 to –1236 ppm, by the addition of [2.2.2]-cryptand. In contrast, in our own studies, we observed a 98 ppm upfield shift for Sn_4^{4-} and explained it by the higher charge density of tetrastannide, which therefore possesses a stronger cation affinity. In order to corroborate our explanation, we investigated the counterion effect of Sn_4^{4-}, which should be also more pronounced for Sn_4^{4-} than for Sn_9^{4-}. For comparison, we used the direct reduction procedure with the alkali

metal sodium as reducing agent (see SI). The progress of the reaction could be monitored visually and the blue to orange-red color change was used for timing the measurements. In this sample we found the signal of Sn_9^{4-} at −1298 ppm and that of Sn_4^{4-} at −1969 ppm (see Figure 2). Hence, both anions are shifted upfield when replacing the rubidium by sodium cations. This is in agreement with the HSAB concept, which predicts a stronger interaction of the soft Rb^+ and the Zintl anions compared to the much harder Na^+. This effect reduces the coordination of harder cations and leads to a greater electron density located on the cage anions, which explains the shift.

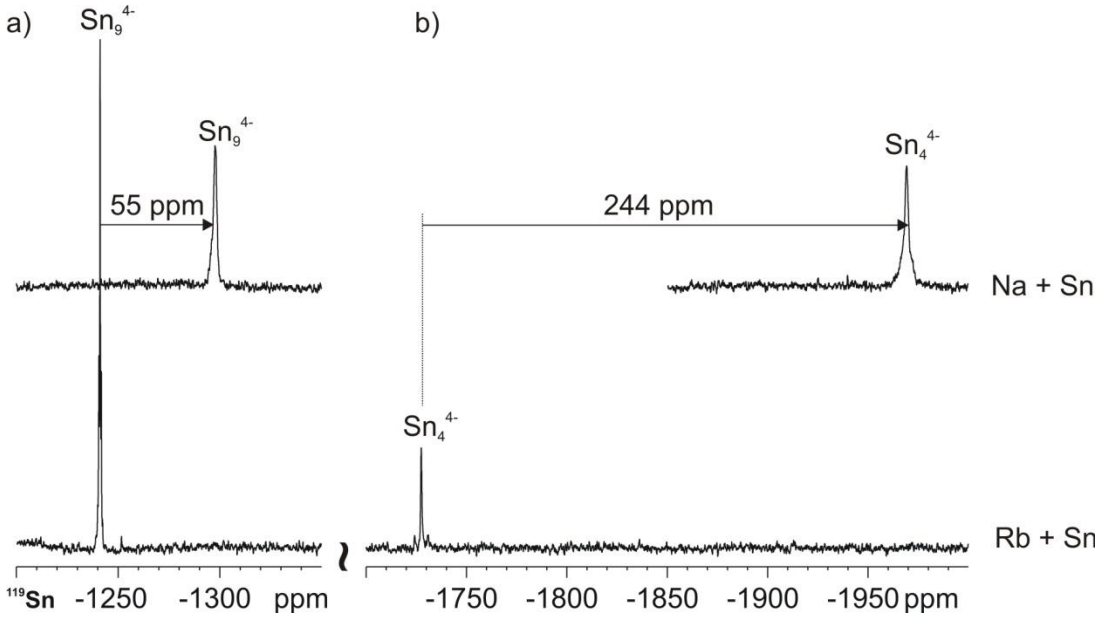

Figure 2: Sections of the ^{119}Sn spectra recorded at 195 K in liquid ammonia from the direct reduction of tin with rubidium and sodium, respectively. The spectra illustrate the counterion effect, which can be observed by exchanging the reducing agent rubidium by sodium. Both, the Sn_9^{4-} signal (a) and the Sn_4^{4-} signal (b) are shifted upfield, with the effect being more pronounced for Sn_4^{4-}, which is probably due to the higher charge density in this anionic cluster.

Here, the counterion effect is significantly more pronounced for the highly charged Sn_4^{4-}. While the signal of Sn_9^{4-} is shifted 55 ppm upfield by replacing Rb^+ by Na^+, Sn_4^{4-} even shifts by 244 ppm. The counterion effect of Sn_9^{4-} is in agreement with the one observed by Rudolph *et al.*, who reported a shift of 40 ppm by replacing Rb^+ by Na^+ at room temperature in ethylenediamine.[35] The significantly increased effect on the chemical shift of Sn_4^{4-} is due to its greater electron density compared to Sn_9^{4-}, which corroborates our previous hypothesis, which also attributed the more distinct upfield shift of Sn_4^{4-} by the ion sequestration reagent [2.2.2]-cryptand, to the higher charge density compared to Sn_9^{4-}.

Up to here, we observed that parameters like preparation method, time of storage and temperature are decisive for the observation of different polyanions in solution. In solvation samples exclusively Sn_9^{4-} was detected, whereas the direct reduction procedure additionally yielded Sn_4^{4-} at 195 K. Over time or by heating the sample up to 300 K, the latter gets oxidized to Sn_9^{4-} (see SI Figure 4).

5.3.2. Additive-Containing Solutions

5.3.2.1 Solvation of Rb_4Sn_4 in Liquid Ammonia in the Presence of [2.2.2]-Cryptand

As discussed above and in chapter 4, both, the conditions in solution and the method of sample preparation are decisive for the type of Zintl anions observable in solution. In order to prove this concept, we used a further alternative preparation method. This brought us back to the solvation technique. For the latter, in 1977, by adding [2.2.2]-cryptand to ammonia solutions of binary tin-alkali metal phases, Edwards and Corbett reported a crystal structure, containing the until then unknown polystannide Sn_5^{2-}.[17] This technique was later on taken up by von Schnering *et al.*, who intended to prepare Sn_4^{4-}-containing solutions for Raman measurements by reacting a solution of $K_{1.33}Sn$ in liquid ammonia and instead yielded amorphous K_4Sn_4 besides crystals of $[K\text{-}[2.2.2]\text{-crypt})]_2Sn_5$.[40] The origin of the Sn_5^{2-} anion remained unclear, but was attributed to the presence of cryptand, as equally prepared solutions, in the absence of cryptand, yielded only K_4Sn_4. Also, the latest report of Eichhorn *et al*. describes the crucial influence of cryptand on the Sn_9^{4-} species in ethylenediamine.[39] They observed a competition of K^+ binding between the complexing agent and the Sn polyanions, which they attributed to a strong affinity of Sn_9^{4-} to K^+. In a titration of Sn_9^{4-} in ethylenediamine with [2.2.2]-cryptand solutions, they found a stepwise removal of K^+ from the polyanion. There, the ^{119}Sn signal was shifted upfield from −1205 ppm (without [2.2.2]-cryptand) to −1236 ppm (with 4.5-7.5 equiv of [2.2.2]-cryptand) and in addition, the signal broadened severely ($b_{1/2}$ = 10-25 ppm), which was rationalized by a chemical exchange between at least two different coordinated Sn_9 species (KSn_9^{3-}, Sn_9^{4-}). Finally, by adding a stoichiometric excess of [2.2.2]-cryptand, an additional signal appeared, which they assigned to HSn_9^{3-} by ^{1}H and ^{119}Sn spectroscopy.

According to these results, we used an analogous preparation technique in order to clarify the origin of Sn_5^{2-}. Therefore, we further studied the influence of [2.2.2]-cryptand on the solvation of Rb_4Sn_4. Hence, we used the phase pure solid and dissolved it in liquid ammonia

in the presence of 1.5 equivalents [2.2.2]-cryptand. This sample was then investigated by ^{119}Sn NMR measurements at 233 K, as previous studies showed the crystallization of Sn_5^{2-} solvates at this temperature. In the fresh sample we detected mainly two ^{119}Sn signals at $\delta = -1302$ and -1815 ppm in a 1:6.7 ratio (see Figure 3a). The line shapes of both signals did not allow a coupling pattern analysis of ^{117}Sn satellites, but are known from earlier studies and could be assigned to Sn_9^{4-} and Sn_4^{4-}. In comparison to the additive-free solutions (solvation, direct reduction) both signals are shifted upfield, which is in good agreement with the ion sequestration by [2.2.2]-cryptand, discussed above and previously observed by Eichhorn *et al.*[39]

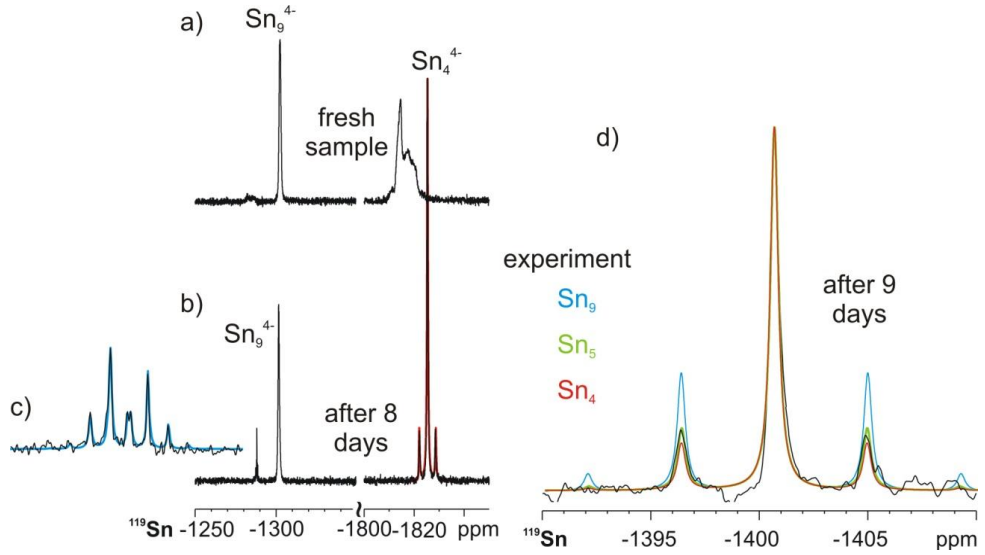

Figure 3: Sections of the ^{119}Sn spectra recorded at 233 K from the solvation of Rb_4Sn_4 in liquid ammonia in the presence of [2.2.2]-cryptand show (a) the solvation of Rb_4Sn_4 and illustrate (b-d) the conversion of the in the solid precast Sn_4^{4-} to further polyanions. Obviously, there are distinct time-frames, in which a specific species can be detected. In addition, simulated spectra, which were used for signal assignment, are shown in (b-d) (colored lines).

In addition, after eight days, besides the Sn_9 cluster (−1302 ppm) a new signal was detected at −1288 ppm (see Fb). The expansion of the latter shows well resolved ^{117}Sn satellites, for which the simulation of the spectrum indicate two nine-atomic clusters (see Figure 3c). These two separately detectable signals outline two slightly different chemical surroundings. Altogether, after eight days, three different Sn_9 signals were detected, two very similar ones ($\Delta\delta$ = 1ppm) and one, which shows a greater separation from the others ($\Delta\delta$ = 11 and 12 ppm). This matches the report of Eichhorn *et al.*, who also detected different cation coordinated Sn_9 clusters in the presence of [2.2.2]-cryptand at room temperature in ethylenediamine.[39] Because of chemical exchange, they observed one broad signal ($b_{1/2}$ = 10-25 ppm) for all Sn_9 clusters. Probably, in our case, at 233 K in liquid ammonia, the

intermolecular chemical exchange is slow enough to give separated signals. Here, probably the two groups of signals, which are separated by 11.5 ppm (average) stem from different Rb^+-coordinations. Furthermore, we speculate that the additional splitting of the more downfield shifted set of signals by 1 ppm might stem from different solvent-coordinations. Upon aging the sample nine days, a further signal appeared at –1401 ppm with two ^{117}Sn satellites (see Figure 3d). The spectrum best fits a simulation of a five-atomic cluster, but because of marginal intensity difference, a four-atomic cluster cannot be excluded completely. But, as Sn_4^{4-} shows a significantly different chemical shift, in our view, it is likely that here we have detected the first Sn_5^{2-} NMR signal in solution. This interpretation is corroborated by the fact that Sn_5^{2-} had been crystallized from analogously prepared solutions at the same temperature and, therefore in principle, should be detectable. Interestingly, the chemical shift does not fit the charge per atom, which would suggest the Sn_5^{2-} downfield from Sn_9^{4-}. Further aging of the sample does not lead to additional species, but results in the loss of signals. Probably, from here onwards, the solvation of Rb_4Sn_4 and its transformations get superimposed by crystallization or degradation processes, which might reduce the detectable amount of dissolved tin clusters. In summary, in the presence of [2.2.2]-cryptand we were able to stabilize and detect Sn_4^{4-} in the solvation of Rb_4Sn_4 in liquid ammonia. Despite the long-lasting stability of Sn_4^{4-}, the conversion to different Sn_9^{4-} species was observed to be fast. Large quantities of one nine-atomic cluster could be detected directly after the preparation and two others appeared within eight days. In accordance to the interpretations of Eichhorn *et al.*, our observations could be attributed to differently Rb^+ coordinated Sn_9^{4-} clusters, which are formed because of a competition between the polyanion and the cryptand for the cation.[39] Additionally, different solvent-coordinations might lead to further signal splitting at 233 K, which remains speculative. Upon further aging of the sample, we observed the formation of Sn_5^{2-}, which never had been detected in solution before. From here onwards, the solvation and transformations in solution probably got superimposed by crystallization or degradation processes, which are accompanied by a loss of signal. It seems that there are distinct time-frames, in which the amount of a specific species is high enough for detection by NMR spectroscopy. In fresh solvations of Rb_4Sn_4 and [2.2.2]-cryptand, mainly Sn_4^{4-}, which is precast in the solid, can be detected and stabilized over a long period of time. This cluster gradually becomes oxidized to Sn_9^{4-} (three differently coordinated species) and finally to Sn_5^{2-}, which is the highest oxidation level known for polyanions of tin. Obviously, the presence of [2.2.2]-cryptand is crucial for the stabilization of the four- and five-atomic tin

clusters in liquid ammonia and leads to an equilibrium of differently cation- and solvent-coordinated nine-atomic clusters.

Up to now, our discussions included the solvation and detection of Sn_4^{4-} and the first observation of Sn_5^{2-} in liquid ammonia. Furthermore, we reported three different nine-atomic clusters, with two of them showing narrow line widths and presumably possessing only slightly different chemical surroundings, which speculatively outline different solvent-coordinations ($\Delta\delta$ = 1 ppm). Interestingly, the third signal, which is shifted upfield from the others by 11 and 12 ppm and, most likely, represents a different cation-coordinated Sn_9 cluster, is comparatively broad ($b_{1/2}$ = 214 Hz). This observation is unusual for a nine-atomic cluster, for which ^{117}Sn-^{119}Sn couplings could be observed in the additive-free solvation (263 Hz) as well as in the direct reduction (267 Hz). As protonation was excluded for all species by comparing proton coupled and decoupled spectra, potentially, this line broadening might indicate intra- or intermolecular dynamics, which were studied in further investigations by temperature depending NMR spectroscopy. In principal, one intermolecular and two intramolecular processes are conceivable. The intermolecular process can take place between differently cation-coordinated clusters and must be considered as real chemical exchange. The intramolecular processes concern the fluxion of the nine-atomic cage and, most likely, occur without breaking chemical bonds via the "diamond-square" model.[17] Here, again, a distinction can be drawn between two different situations. The first possibility is the interconversion between the two possible conformations of the nine-atomic clusters (D_{3h}, C_{4v}), the second is the freeze of one conformation, which cancels the chemical equivalence of the tin atoms. In order to study these dynamics, the solvation of Rb_4Sn_4 together with [2.2.2]-cryptand in liquid ammonia was investigated at 197 and 233 K (see Figure 4).

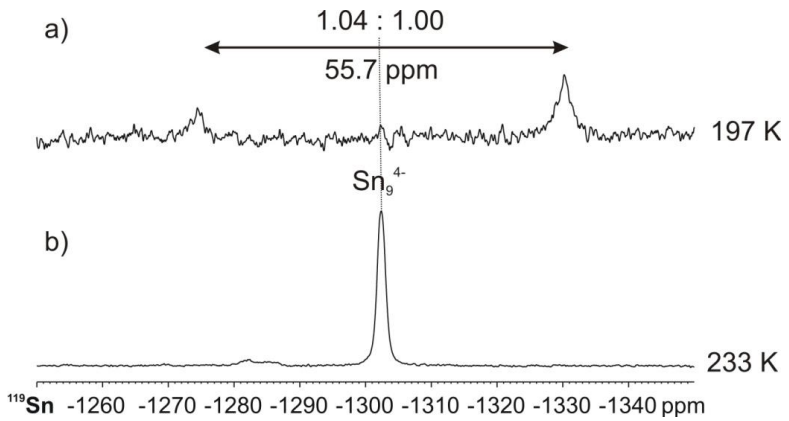

Figure 4: Sections of the ^{119}Sn spectra recorded at 197 K (a) and 233 K (b) from the solvation of Rb_4Sn_4 together with [2.2.2]-cryptand in liquid ammonia. The spectra illustrate the splitting of the broad Sn_9^{4-} signal in the transition from 233 to 197 K. This behavior indicates dynamics between two different configurations.

Compared to the spectrum at 233 K, the spectrum at 197 K[2] clearly shows a nearly symmetrical splitting of the Sn_9^{4-} signal. Furthermore, integral analysis of the low temperature spectrum reveals a 1:2 population of two distinct states. Theoretically, according to this population, an asymmetric splitting would be expected. Therefore, we believe that the splitting is superimposed by an upfield shift of the Sn_9 cluster at lowered temperatures. This seems to be a general trend, which already had been discussed in connection with the additive-free solvation of Rb_4Sn_4 and the direct reduction. As these phenomena are difficult to separate, we did not attempt any line shape fitting. Hence, the low temperature spectrum indicates dynamics, but does not provide the opportunity to distinguish between the possible processes. About the most probable, we can only speculate. We believe that the intermolecular exchange may be excluded, because, as we have seen from the two sharp Sn_9 signals, in principle, only slightly different surroundings result in separated Sn_9 signals. The intramolecular case seems to be much more likely. There, one can imagine a 1:2 population of both possible conformers or the exclusive presence of the D_{3h} symmetry. The latter is represented by a threefold capped trigonal prism, for which two different signals are expected in a 1:2 ratio. For us, this is the most conceiving possibility, but remains speculative. Further investigations with different amounts of [2.2.2]-cryptand might clarify the assignment. A higher amount of ion sequestering reagent should shift the position of equilibrium towards separated ion pairs, which should result in more upfield shifted signals, as observed in ethylenediamine by Eichhorn *et al.*[39] Further low temperature measurements at 195 K for a different position of equilibrium also should clarify the point of intra- or intermolecular exchange of the signal observed at −1302 ppm, for which we suppose the freezed "diamond-square" process. If our hypothesis is right, the signal should split into the same 1:2 population of two distinct states. In contrast, if our assumption is not correct and the signal splitting is due to an intermolecular process, the shifted position of the equilibrium should result in a different population of the two distinct states. In addition, the variation of the amount of [2.2.2]-cryptand might also clarify the assignment of Sn_5^{2-}, for which the concentration should rise with the amount of cryptand in solution.

[2] The signal to noise ratio severely dropped, because of much worse solubility at 197 K.

5.3.2.2 Summary

In the previous sections and in chapter 4, we have addressed the solution properties and transformations of polystannides and got insight into the conditions under which different species are stable enough to yield quantities, which are detectable by NMR spectroscopy. In the solvation of phase pure Rb_4Sn_4, only Sn_9^{4-} was present in solution, which outlines poor solubility and stability of Sn_4^{4-} in additive-free solvation. In the direct reduction we were able to detect the first Sn_4^{4-} signal in liquid ammonia, which was observed to be converted to Sn_9^{4-} over time. Finally, the transition from additive-free to [2.2.2]-cryptand-containing solutions, enabled the detection of the first Sn_5^{2-} cluster. The latter was observed to be formed in an oxidation reaction from Sn_4^{4-} to Sn_5^{2-}. Obviously, the presence of [2.2.2]-cryptand is decisive for the stability of Sn_4^{4-} and Sn_5^{2-} and also the preparation method (direct reduction or solvation) seems to affect the equilibriums in solution. This observation is not fully understood to date, but the knowledge about the stabilities of a respective species opens up new possibilities for more targeted conversions of the polystannides. Possibly, the versatile chemistry, which has been developed so far for Sn_9^{4-}, can be transferred to Sn_4^{4-} and Sn_5^{2-}. Unclear points, such as the reliable assignment of Sn_5^{2-} and the three respectively four differently coordinated Sn_9^{4-} clusters, might be clarified by the variation of the amount of [2.2.2]-cryptand used in the solvation of Rb_4Sn_4 combined with low temperature NMR measurements. This should shift the position of the equilibrium and hence, give further insight into the transformation processes in solution.

5.4 Conversions of Polystannides with Mesitylcopper

With the previous studies, we have explored the stability of different polystannides in liquid ammonia, which depends on the preparation method (direct reduction or solvation) as well as additives in solution ([2.2.2]-cryptand). With this vital knowledge, we are now able to investigate the chemistry of these clusters systematically, which might enable targeted reactions of distinct tin clusters. Various complexes $[M(\eta^4\text{-}Sn_9)(CO)_3]^{4-}$ (M = Cr, Mo, W) had been reported, in which intact Sn_9^{4-} act as ligands for transition metals.[9] There, the tin cluster is side-on coordinated and forms covalent exo-bonds to the transition metal, which results in a twofold capped quadratic antiprismatic closo-cluster. Furthermore, ligand-free intermetallic clusters, like $[Ir@Sn_{12}]^{3-}$ [29] or $[Cu@Sn_9]^{3-}$ [41] can be formed, in which the transition metal is encapsulated. Despite the diversity of reactions of Sn_9^{4-}, to date, the

conversion of Sn_4^{4-} or Sn_5^{2-} has not been possible. However, for the lighter homologue, silicon, the crystal structure of $[(MesCu)_2(Si_4)]^{4-}$ had been reported.[28] According to these results, we chose MesCu as transition metal compound, as it seemed to be most promising for, potentially, studying reactions of all polyanions of tin, which we had observed in liquid ammonia. Therefore, in two different samples, Rb_4Sn_4 and MesCu were dissolved in liquid ammonia. Afterwards, the reaction mixtures were investigated by ^{119}Sn spectroscopy at 233 K. Planning to get mainly Sn_4^{4-}-containing products, one reaction was performed in the presence of [2.2.2]-cryptand. For comparison, the same reaction was performed without additives. In both samples, the expected polyanions were detected. For the additive-free solvation the signal of Sn_9^{4-} was detected at –1245 ppm, showing the typical ^{117}Sn satellite pattern. In the [2.2.2]-cryptand-containing sample three different coordinated Sn_9^{4-} clusters at –1191, –1292 and -1303 ppm as well as Sn_4^{4-} at –1816 ppm and Sn_5^{2-} at –1409 ppm were detected. These species, which before had been studied in detail, now can act as starting materials for reactions with MesCu. Indeed, besides Sn_4^{4-}, Sn_9^{4-} and Sn_5^{2-}, in the [2.2.2]-cryptand-containing sample one and in the additive-free reaction mixture two new signals were observed. In the presence of [2.2.2]-cryptand we detected a new species at δ = –1609 ppm (see Figure 5a). The signal shows ^{117}Sn satellites with $J_{117Sn,119Sn}$ = 1190 Hz. The integration gave an intensity pattern of 0.13:1.00:0.16, which best fits a four-atomic tin cluster, for which, statistically, a 0.128:1.000:0.128 ratio is expected. This can be visualized by comparing the experimental spectrum to the simulated ones of four-, five- and nine-atomic clusters (colored lines in Figure 5a).

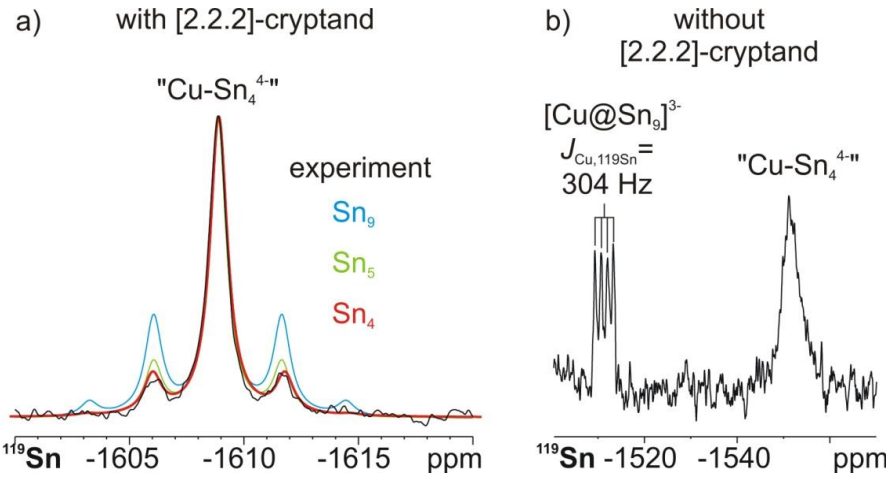

Figure 5: Sections of the ^{119}Sn spectra recorded at 233 K in liquid ammonia from the co-solvation of Rb_4Sn_4 with MesCu (a) in the presence and (b) without [2.2.2]-cryptand illustrate an increased concentration of the copper-Sn_4 complex in the presence of [2.2.2]-cryptand (a), which can be deduced to the greater stability of Sn_4^{4-} in these solutions. The faster reaction to Sn_9^{4-} without [2.2.2]-cryptand enables the detection of $[Cu@Sn_9]^{3-}$ (b). In (a) additionally the simulated spectra of four-, five- and nine-atomic tin clusters are shown (colored lines).

This signal at δ = –1609 ppm appears 207 ppm downfield from Sn_4^{4-} and outlines a lower electron density on the tin atoms of this species. This indicates a transformation of Sn_4^{4-} to another four-atomic tin-compound. Since no differently charged four-atomic cluster than Sn_4^{4-}, has ever been unambiguously demonstrated, it is likely that we detected the first transition metal complex with Sn_4^{4-} cages. Up to now, we were not able to get a crystal structure of this complex, therefore, we can only speculate about its composition. The smallest sized transition metal filled complexes reported so far include at least an E_9 cluster, e.g. $[Cu@Sn_9]^{3-}$.[41] The latter shows an averaged ^{119}Sn-$^{63/65}$Cu coupling of 286 Hz because of a nearly spherical surrounding of the Cu(I) ion, which ensures a small electric field gradient across the Cu atom. Therefore, we suggest that in our complex the Sn_4^{4-} moiety is exo-bonded to the copper ion. In this case the electric field gradient across copper is much higher, which might explain the missing ^{119}Sn-$^{63/65}$Cu coupling. In analogy to the known complex $[(MesCu)_2(Si_4)]^{4-}$, in which the copper atoms cap two sides of the tetrahedral Si_4 cluster,[28] we suggest $[(MesCu)_2(Sn_4)]^{4-}$ for our signal at –1609 ppm.

In the additive-free co-solvation of Rb_4Sn_4 with MesCu, besides Sn_9^{4-} at –1245 ppm, two further complexes were observed at δ = –1511 and –1552 ppm (see Figure 5b). The more downfield shifted signal shows a 1:1:1:1 quartet with J = 304 Hz. This signal is in accordance with $[Cu@Sn_9]^{3-}$, for which Fässler *et al.* had reported a chemical shift of –1440 ppm in acetonitrile and a ^{119}Sn-$^{63/65}$Cu coupling with J = 286 Hz.[41] The other signal at –1552 ppm is broad with a halfwidth of 865 Hz. Therefore, the ^{117}Sn satellite pattern is not resolved, which obscures an independent assignment. However, the signal is 57 ppm shifted upfield compared to the above discussed signal, for which we suggest $[(MesCu)_2(Sn_4)]^{4-}$. This chemical shift offset presumably displays the stronger coordination of Rb^+ in the absence of [2.2.2]-cryptand, which also was discussed for Sn_4^{4-} (direct reduction and co-solvation of Rb_4Sn_4 with [2.2.2]-cryptand) and also had been previously reported by Eichhorn *et al.* for K_4Sn_9 in ethylenediamine.[39] Thus, for the signal at –1552 ppm we suggest $[(MesCu)_2(Sn_4)]^{4-}$, which was already observed in the [2.2.2]-cryptand-containing sample. The reduced concentration of this Cu-Sn-complex also fits the fact that in the additive-free solvation the concentration of naked Sn_4^{4-} is below the detection limit of NMR spectroscopy. We believe that we have detected the first exo-complex between a four-atomic tin cluster and a transition metal. Furthermore, we could show that the concentration of this new complex is dependent on the concentration of Sn_4^{4-} in solution, which was observed to be stabilized by adding

[2.2.2]-cryptand to the solvation of Rb_4Sn_4. In summary, certain conditions must be kept to target a distinct tin-complex for a conversion and to yield the desired transition metal complex. In order to achieve transition metal complexes with better NMR properties, in future experiments, metals like Pd or Pt can be used, for which quadrupolar relaxation plays a minor role. In addition, for Pt complexes, ^{195}Pt spectroscopy can be used to gain further insight into the structures of stannide complexes.

5.5 Conclusions

In our investigations we studied the stability and the transformations of polystannides in solutions. We presented a significantly increased counterion effect for Sn_4^{4-} than for Sn_9^{4-}, which corroborates the higher charge density of Sn_4^{4-}. In addition, the co-solvation of Rb_4Sn_4 with [2.2.2]-cryptand enabled not only the mere detection of Sn_4^{4-}, but also allowed for the detection of the first Sn_5^{2-} signal and at least three differently salt and solvent coordinated nine-atomic tin clusters. For one of these Sn_9-clusters, low temperature NMR investigations suggest the freeze of the diamond-square process in the conformation of a threefold capped trigonal prism. The equilibriums occurring in solution are not fully understood until today, but the knowledge about the stabilities of different tin species was used for reactions of distinct tin clusters. In principle, the performance of two different reactions of Rb_4Sn_4 and MesCu with and without [2.2.2]-cryptand show promising results regarding targeted reactions. There, most likely, we have found the first exo-complex between a four-atomic tin cluster and a transition metal, $[(MesCu)_2(Sn_4)]^{4-}$. The best yields were achieved in the co-solvation of Rb_4Sn_4 with MesCu and [2.2.2]-cryptand, which ensures highest Sn_4^{4-} concentrations over a long period of time. We believe that our investigations prepared the ground for further optimizations on the way to targeted reactions. These might enable the systematic extension of the versatile Zintl chemistry and the rational design of new materials.

5.6 References

(1) Holleman, A. F.; Wiberg, E.; Holleman, N. *Lehrbuch der Anorganischen Chemie*; 101. ed.; Walter de Gruyter: Berlin, New York, 1995; p. 797.

(2) Joannis, A. C. *C. R. Acad. Sci.* **1891**, *29*, 795.

(3) Zintl, E.; Harder, A. *Physik. Chem.* **1931**, *A 154*, 47.

(4) Laves, F. *Naturwissenschaften* **1941**, *29*, 244-255.

(5) Kummer, D.; Diehl, L. *Angew. Chem. Int. Ed.* **1970**, *9*, 895.

(6) Corbett, J. D.; Edwards, P. A. *J. C. S. Chem. Commun.* **1975**, 984-985.

(7) Belin, C. H. E.; Corbett, J. D.; Cisar, A. *J. Am. Chem. Soc.* **1977**, *99*, 7163-7169.

(8) Teixidor, F.; Luetkens, M. L.; Rudolph, R. W. *J. Am. Chem. Soc.* **1983**, *105*, 149-150.

(9) Eichhorn, B. W.; Haushalter, R. C.; Pennington, W. T. *J. Am. Chem. Soc.* **1988**, *110*, 8704-8706.

(10) Gardner, D. R.; Fettinger, J. C.; Eichhorn, B. W. *Angew. Chem. Int. Ed.* **1996**, *35*, 2852-2854.

(11) Esenturk, E. N.; Fettinger, J.; Eichhorn, B. *Polyhedron* **2006**, *25*, 521-529.

(12) Xu, L.; Sevov, S. C. *J. Am. Chem. Soc.* **1999**, *121*, 9245-9246.

(13) Guloy, A. M.; Ramlau, R.; Tang, Z.; Schnelle, W.; Baitinger, M.; Grin, Y. *Nature* **2006**, *443*, 320-323.

(14) Fässler, T. F. *Angew. Chem. Int. Ed.* **2007**, *46*, 2572-2575.

(15) Scharfe, S.; Kraus, F.; Stegmaier, S.; Schier, A.; Fässler, T. F. *Angewandte Chemie* **2011**, *123*, 3712-3754.

(16) Guggenberger, L. J.; Muetterties, E. L. *J. Am. Chem. Soc.* **1976**, *98*, 7221-7225.

(17) Edwards, P. A.; Corbett, J. D. *Inorg. Chem.* **1977**, *16*, 903-907.

(18) Hewaidy, I. F.; Busmann, E.; Klemm, W. *Z. Anorg. Allg. Chem.* **1964**, *328*, 283-293.

(19) Goebel Y., Haarmann, F., T. P. *Z. Kristallogr. - New Crystall Structures* **2008**, *223*, 187.

(20) Witte, J.; Schnering, H. G.; Klemm, W. *Z. Anorg. Allg. Chem.* **1964**, *327*, 260-273.

(21) Busmann, E. *Z. Anorg. Allg. Chem.* **1961**, *313*, 90-106.

(22) Schäfer, R.; Klemm, W. *Z. Anorg. Allg. Chem.* **1961**, *312*, 214-220.

(23) Hoch, C.; Wendorff, M.; Röhr, C. *Journal of Alloys and Compounds* **2003**, *361*, 206-221.

(24) Ponou, S.; Fässler, T. F. *Z. Anorg. Allg. Chem.* **2007**, *633*, 393-397.

(25) Queneau, V.; Sevov, S. C. *Angew. Chem. Int. Ed.* **1997**, *36*, 1754-1756.

(26) Queneau, V.; Todorov, E.; Sevov, S. C. *J. Am. Chem. Soc.* **1998**, *120*, 3263-3264.

(27) Wiesler, K.; Brandl, K.; Fleischmann, A.; Korber, N. *Z. Anorg. Allg. Chem.* **2009**, *635*, 508-512.

(28) Waibel, M.; Kraus, F.; Scharfe, S.; Wahl, B.; Fässler, T. F. *Angew. Chem. Int. Ed.* **2010**, *49*, 6611-6615.

(29) Wang, J.-Q.; Stegmaier, S.; Wahl, B.; Fässler, T. F. *Chem. Eur. J.* **2010**, *16*, 1793-1798.

(30) Kesanli, B.; Halsig, J. E.; Zavalij, P.; Fettinger, J. C.; Lam, Y.-F.; Eichhorn, B. W. *J. Am. Chem. Soc.* **2007**, *129*, 4567-4574.

(31) Kocak, F. S.; Zavalij, P.; Lam, Y.-F.; Eichhorn, B. W. *Inorg. Chem.* **2008**, *47*, 3515-3520.

(32) Kircher, P.; Huttner, G.; Heinze, K.; Renner, G. *Angew. Chem. Int. Ed.* **1998**, *37*, 1664-1666.

(33) Schiemenz, B.; Huttner, G. *Angew. Chem. Int. Ed.* **1993**, *32*, 297-298.

(34) Joseph, S.; Hamberger, M.; Mutzbauer, F.; Härtl, O.; Meier, M.; Korber, N. *Z. Naturforsch.* **2010**, *65b*, 1059-1065.

(35) Wilson, W. L.; Rudolph, R. W.; Lohr, L. L.; Taylor, R. C.; Pyykko, P. *Inorg. Chem.* **1986**, *25*, 1535-1541.

(36) Rudolph, R. W.; Wilson, W. L.; Parker, F.; Taylor, R. C.; Young, D. C. *J. Am. Chem. Soc.* **1978**, *100*, 4629-4630.

(37) Rudolph, R. W.; Wilson, W. L.; Taylor, R. C. *J. Am. Chem. Soc.* **1981**, *103*, 2480-2481.

(38) Scharfe, S.; Kraus, F.; Stegmaier, S.; Schier, A.; Fässler, T. F. *Angew. Chem. Int. Ed.* **2011**, *50*, 3630-3670.

(39) Kocak, F. S.; Downing, D. O.; Zavalij, P.; Lam, Y.-F.; Vedernikov, A. N.; Eichhorn, B. *J. Am. Chem. Soc.* **2012**, *134*, 9733-9740.

(40) Somer, M.; Carrillo-Cabrera, W.; Peters, E.-M.; Peters, K.; Kaupp, M.; von Schnering, H. G. *Z. Anorg. Allg. Chem.* **1999**, *625*, 37-42.

(41) Scharfe, S.; Fässler, T. F.; Stegmaier, S.; Hoffmann, S. D.; Ruhland, K. *Chem. Eur. J.* **2008**, *14*, 4479-4483.

5.7 Supporting Information

5.7.1. Synthesis

5.7.1.1 General Considerations

All manipulations described below were performed in a purified argon atmosphere (glove box) by using glass vessels dried at least four times in vacuum. [2.2.2]-cryptand was purchased from Sigma-Aldrich and used without further drying. Elemental rubidium was synthesized by the reduction of RbCl and purified through distillation. Elemental potassium was obtained from a commercial source and distilled on our own. By condensing the commercially acquired gaseous ammonia onto elemental sodium and storing this cooled Na/ammonia-solution for about three days, residual moisture traces were removed.

5.7.1.2 Solid Phase Synthesis of the Zintl Anions (High Temperature Synthesis)

Rb_4Sn_4: Rb_4Sn_4 was obtained by gradually heating (60 °C/h) stoichiometric amounts of elemental rubidium (0.64 g, 7.5 mmol) and elemental tin (0.78 g, 6.6 mmol) in a Duran glass ampoule to 450 °C and holding it at this temperature for 20 h. Subsequently, the reaction mixture slowly cooled to room temperature (25 °C/h). Due to its sensitivity towards moisture and air the solid state phase was handled and stored under argon atmosphere.

$Rb_{12}Sn_{17}$: $Rb_{12}Sn_{17}$ was obtained by gradually heating (60 °C/h) appropriate amounts of elemental rubidium (0.40 g, 4.7 mmol) and elemental tin (1.09 g, 9.2 mmol) in a Duran glass ampoule up to 450 °C and holding it at this temperature for 20 h. Subsequently, the reaction mixture slowly cooled to room temperature (25 °C/h). Due to its sensitivity towards moisture and air the solid state phase was handled and stored under argon atmosphere.

5.7.1.3 Solvation of Zintl Phases in Liquid Ammonia

Under completely inert conditions (glove box), the respective solid material (Rb_4Sn_4: 25 mg, 0.031 mmol; $Rb_{12}Sn_{17}$: 20 mg, 0.007 mmol) was transferred into an NMR tube. Depending on the sample, the dissolution in liquid ammonia was carried out without further additives or in the presence of $RbNH_2$ (4.5 mg, 0.44 mmol) or [2.2.2]-cryptand (18 mg, 0.048 mmol). Therefore, anhydrous liquid ammonia was directly condensed onto the respective sample at −78 °C. In order to guarantee the permanent absence of moisture and air, the tube was sealed under ammonia atmosphere.

5.7.1.4 Direct Reduction of Tin with Alkali Metals in Liquid Ammonia (Low Temperature Synthesis)

All direct reduction experiments were carried out directly in an NMR tube.

Rb/Sn: Under exclusion of oxygen and moisture, Sn (60 mg, 0.51 mmol) and Rb (39 mg, 0.46 mmol) were transferred into a NMR tube. Liquid ammonia was condensed onto the mixture at -78 °C. In order to guarantee the permanent absence of moisture and air, the tube was sealed under ammonia atmosphere. Before NMR measurements on these solutions were performed, the fresh samples were stored at low temperature until the blue color turned to deeply red.

Na/Sn: Under exclusion of oxygen and moisture, Sn (60 mg, 0.51 mmol) and Na (11 mg, 0.48 mmol) were transferred into a NMR tube. Liquid ammonia was condensed onto the sample at -78 °C. In order to guarantee the permanent absence of moisture and air, the tube was sealed under ammonia atmosphere. Before NMR measurements on these solutions were performed, the fresh samples were stored at low temperature until the blue color turned to deeply red.

5.7.2. Phase Determination

5.7.2.1 General Considerations

The FT-Raman spectra were recorded at room temperature under inert conditions from powdered samples sealed in Pyrex tubes (∅ = 0.7−1.0 mm) using a Raman module coupled to a Varian FTS 7000e spectrometer (Nd:YAG-laser, λ = 1064 nm). Data were processed with OriginPro 7.5. Structure determinations were investigated by X-ray powder diffraction. Data were collected on a transmission powder diffraction system (STADI P, Fa. Stoe Cie, Darmstadt, Cu-K_α radiation with λ = 1.540598 Å). Therefore, capillaries were charged with powdered samples, respectively, and air-proof sealed. Data were processed with WinXPow.[1]

5.7.2.2 Rb_4Sn_4

The Raman spectrum of Rb_4Sn_4 showed the characteristic vibrational resonances of Sn_4^{4-} at 133.1 and 184.2 cm^{-1}.[1] Furthermore, the solution and refinement of the experimental powder diffraction data yielded a tetragonal body centered cell of the space group $I4_1/acd$ which relates to Rb_4Sn_4.[2,3] So, we assume that Rb_4Sn_4 is a phase pure solid and contains Sn_4^{4-} as the exclusive anionic moiety due to missing resonances of Sn_9^{4-} in the term of Raman spectroscopy.[4]

1. von Schnering *et. al.*; *Z. Anorg. Allg. Chem.* **2006**, *632*, 1281-1286.

2. von Schnering, H. G. *et al.*; *Zeitschrift für Kristallographie – New Crystal Strucutres* **1999**, *214*, 457.
3. W. Klemm *et al.*; *Z. Anorg. Allg. Chem.* **1964**, *328*, 283.
4. H. G. von Schnering *et al.*; *Z. Anorg. Allg. Chem.***1997**, *623*, 1037-1039.

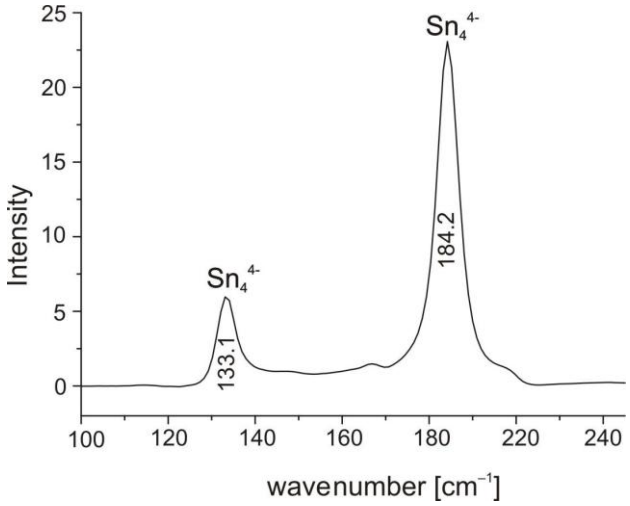

SI Figure 1: The Raman spectrum shows the characteristic vibrations of Rb_4Sn_4.

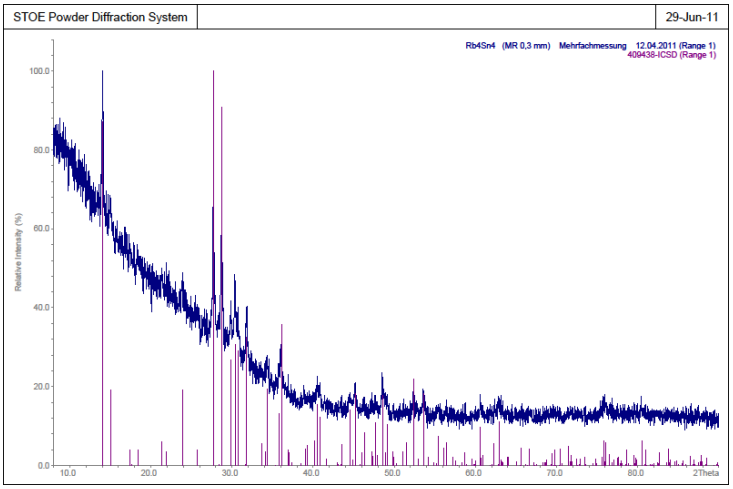

SI Figure 2: Comparison of experimental (blue) and theoretical (red) reflection pattern of Rb_4Sn_4. The latter was calculated from single crystal data as there is no powder data available.

5.7.2.3 $Rb_{12}Sn_{17}$

The Raman spectrum of $Rb_{12}Sn_{17}$ showed the characteristic vibrational resonances of Sn_4^{4-} at 150.1 cm^{-1} and Sn_9^{4-} at 191.0 cm^{-1}.[1] The characterization by X-ray diffraction was prevented by the poor crystallinity of the solid.

1. von Schnering, H. G.; Somer, M.; Aydemira, U.; Baitingerb, M.; *Z. Anorg. Allg. Chem.* **2006**, *632*, 1281-1286.

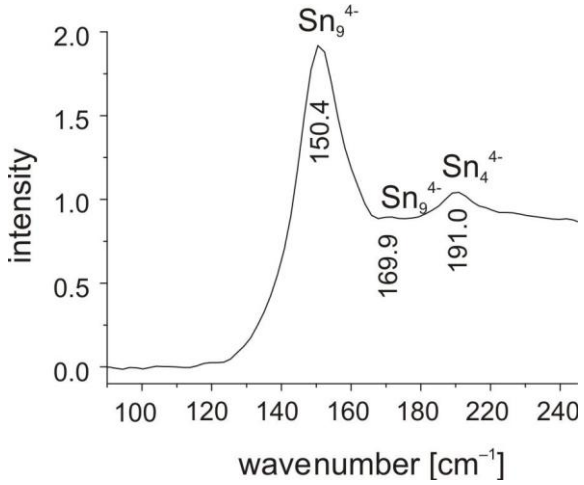

SI Figure 3: The Raman spectrum shows the characteristic vibrations of $Rb_{12}Sn_{17}$.

5.7.3. NMR Investigations in Solution

5.7.3.1 Data Collecting and Processing

The NMR spectra were recorded on a Bruker Avance 600 spectrometer equipped with a 5 mm broadband triple resonance Z-gradient probe. The temperatures for all measurements were controlled by a Bruker BVTE 3900 temperature unit. ^{119}Sn measurements were carried out with a standard Bruker pulse program (zg) using 70k number of scans, 4 dummy scans, TD = 8k with a relaxation delay of 0.3 s. Data were processed with the Bruker software TOPSPIN 3.1 using the processing parameters SI = 16k, WDW = EM and LB = 50 Hz. The chemical shifts are reported in ppm relative to $SnMe_4$. The theoretical NMR spectra were obtained with the TOPSPIN 3.1 simulation tool Daisy.

5.7.3.2 Signal Assignment

The more abundant ^{119}Sn was used as observe nucleus and the ^{117}Sn-^{119}Sn scalar coupling for signal assignment. Therefore, the coupling patterns for all possible cluster sizes (2, 5 and 9) were calculated from the statistical distribution of both NMR active nuclei over the respective polyanion.

Possible clusters	Theoretical coupling pattern
Sn_4^{4-}	0.047:0.324:1.000:0.324:0.047
Sn_5^{2-}	0.011:0.170:1.000:0.170:0.011
Sn_9^{4-}	0.006:0.128:1.000:0.128:0.006

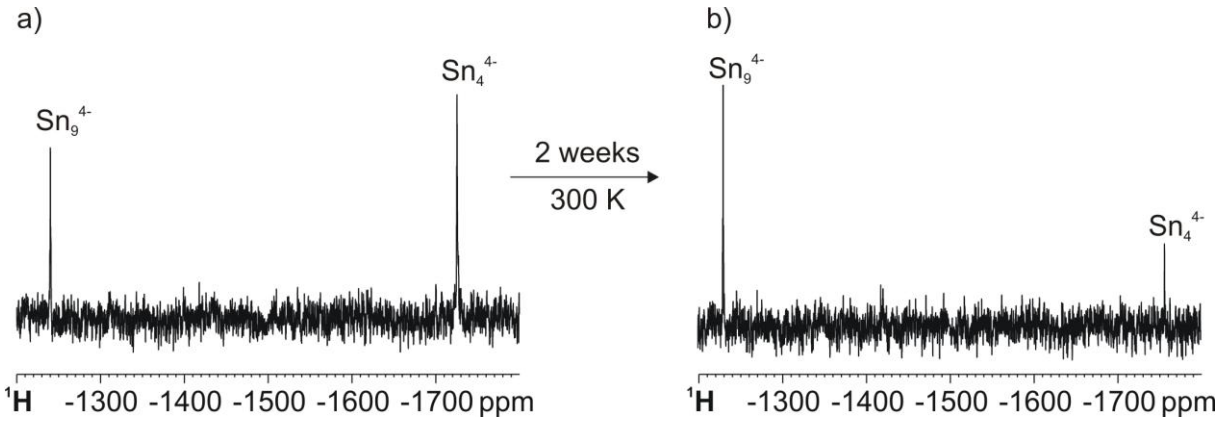

SI Figure 4: ^{119}Sn spectra recorded from the direct reduction of tin with rubidium in liquid ammonia at 195 K (a) and 300 K (b). The spectra illustrate the oxidation of Sn_4^{4-} to Sn_9^{4-}, which results in the accumulation of Sn_9^{4-} in solution.

5.8 Additional Findings

Throughout the studies on the solution chemistry of homoatomic Zintl ions in liquid ammonia, also solutions of the ternary phases KSnBi and CsSnBi were investigated. In the solution of KSnBi and [18]-crown-6, the ^{119}Sn spectrum showed three sets of signals (see AF Figure 1) Each of these can be assigned to a special cluster size $[Sn_{4-x}Bi_x]^{(x-4)-}$, $[Sn_{9-x}Bi_x]^{(x-4)-}$ and $[Sn_{10-x}Bi_x]^{(x-2)-}$.

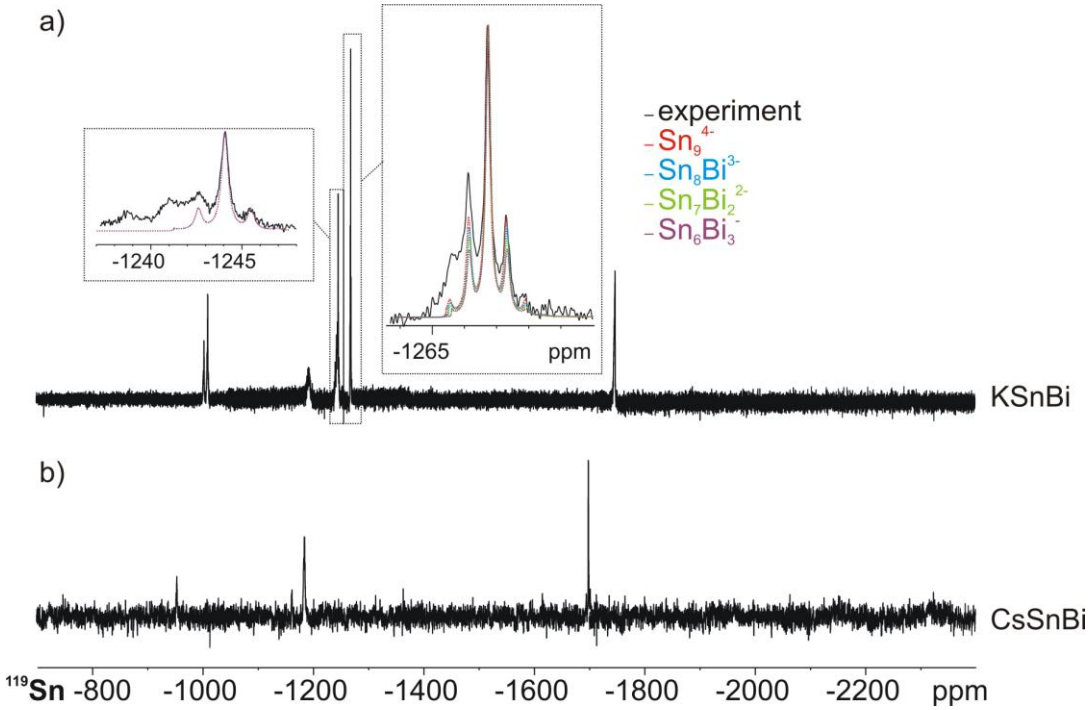

AF Figure 1: Experimental (black) and simulated (colored) ^{119}Sn NMR spectra of the ternary phases KSnBi (a) and CsSnBi (b), recorded at 195 K in liquid ammonia.

According to the literature,[1,2] the most upfield shifted signal at –1746 ppm with $J_{117Sn,119Sn}$ = 1532 Hz can be assigned to $[Sn_2Bi_2]^{2-}$. The three signals at –1267, –1244 and –1192 ppm can be assigned to $[Sn_{9-x}Bi_x]^{(x-4)-}$ with different Sn-Bi compositions. The signal at –1267 ppm fits the simulated spectrum of Sn_9^{4-} very well and agrees with our previous results and the literature of Rudolph *et al.*[3-5] The by 23 ppm more downfield shifted signal at –1244 ppm best fits the simulated spectrum of $[Sn_6Bi_3]^-$. Downfield shift as well as signal attenuation by the incorporation of more electropositive Bi is in agreement with this assignment. For the most downfield shifted signal of this set at –1192 ppm, accordingly, we suggest a nine-atomic cluster, in which even more Sn is substituted by Bi, however, an exact determination of the composition was obscured by low signal intensities. The two signals of the third set appeared at –1011 and –1004 ppm and because of the higher oxidation state of ten-atomic clusters, most likely, represent two different $[Sn_{10-x}Bi_x]^{(x-2)-}$ clusters. A definitive assignment to distinct cluster compositions, again, was obscured by low intensities of ^{117}Sn satellites, which prevents a simulation of the coupling pattern. Nevertheless, this assignment is corroborated by ESI-MS measurements, in which Sn_{10}^{2-} was detected. For CsSnBi four signals at –954, –1162, –1185 and –1699 ppm ($J_{117Sn,119Sn}$ = 1525 Hz) were detected. These signals illustrate the influence of the softer and hence, more strongly coordinated cation Cs, which is in agreement with our previous results and the literature.[3] AF Table 1 gives an overview of the detected signals and their assignment in both samples.

AF Table 1: At 195 K detected compounds and their ^{119}Sn chemical shifts in the co-solvations of the ternary phases KSnBi and CsSnBi with [18]-crown-6 in liquid ammonia.

Species	**δ(KSnBi) [ppm]**	**δ(CsSnBi) [ppm]**
$[Sn_2Bi_2]^{2-}$	–1746	–1699
Sn_9^{4-}	–1267	–1185
$[Sn_6Bi_3]^-$	–1244	–1162
$[Sn_{10-x}Bi_x]^{(x-2)-}$	–1011	–954

1. Wilson, W. L.; Rudolph, R. W.; Lohr, L. L.; Taylor, R. C.; Pyykkö, P.; *Inorg.Chem.* **1986**, *25*, 1535-1541
2. Lips, F., Dehnen, S., *Angew. Chem.* **2009**, *121*, 6557-6560.
3. Wilson, W. L.; Rudolph, R. W.; Lohr, L. L.; Taylor, R. C.; Pyykko, P. *Inorg. Chem.* **1986**, *25*, 1535-1541.
4. Rudolph, R. W.; Wilson, W. L.; Parker, F.; Taylor, R. C.; Young, D. C. *J. Am. Chem. Soc.* **1978**, *100*, 4629-4630.
5. Rudolph, R. W.; Wilson, W. L.; Taylor, R. C. *J. Am. Chem. Soc.* **1981**, *103*, 2480-2481.

6. A New Light and X-ray Stable As_4 Source – The ^{75}As NMR Spectroscopic Evidence for Reversible As_4 Binding

For these studies, I performed the NMR spectroscopic investigations, while the synthesis and the characterization of the solids as well as the sample preparation were performed by Christoph Schwarzmaier.

Maria Neumeier, Christoph Schwarzmaier, Manfred Scheer, Ruth M. Gschwind

to be published

6.1 Abstract

Phosphorous and arsenic, both, possess molecular modifications built up by discrete spherically aromatic E_4 (E = P, As) moieties. These show a global tetrahedral symmetry, with each of the As atoms possessing a trigonal pyramidal surrounding. In these molecules the four atoms are linked by six covalent E–E single bonds. In contrast to P_4, the lacking stability and the time consuming synthesis prevented As_4, the molecular modification of arsenic, from being characterized crystallograghically. In this contribution, we present the preparation of the first homoleptic metal-arsenic complex $[Ag(\eta^2\text{-}As_4)_2]^+(pftb)^-$ **1** from As_4 and weakly coordinated $[Ag(CH_2Cl_2)]^+(pftb)^-$ (pftb = $\{Al[OC(CF_3)_3]_4\}$) in good yields. Furthermore, the suitability of **1** as storage medium for molecular arsenic is studied. Under exclusion of oxygen and moisture Ag^+ coordination is shown to provide significant stabilization for As_4, which results in light and X-ray stability of **1**. Moreover, we provide the challenging ^{75}As NMR spectroscopic evidence for the targeted release of molecular arsenic in solution. Here, a combination of high local symmetry and fast correlation times provided sufficiently small electric field gradients across the As atoms. These conditions reduced quadrupolar relaxation rates and helped to sharpen the ^{75}As signals. With our investigations we extend the observable ^{75}As NMR signals in solution from atoms with local octahedral and tetrahedral to trigonal pyramidal symmetry. Furthermore, with complex **1** we introduce an economic and stable storage medium for molecular yellow arsenic, which is suitable for the in situ generation of As_4 in chemical reactions.

6.2 Introduction

Today phosphorous plays a major role in the production of fertilizers, flame retardants and herbicides. The key intermediate in most of these processes is white phosphorous P_4 ($1.5 \cdot 10^6$ t annual production)[1] that is either oxidized with oxygen or chlorine. Under the exclusion of oxygen, P_4 can be stored at ambient temperatures without remarkable decomposition. In the last decades, the activation of white phosphorous by main group elements[2] and transition metals[3,4] has become an area of ongoing interest in chemistry. Phosphorous' heavier analogue, arsenic, has long been known for its toxicity and today is mainly used as additive in metal alloys and in GaAs semiconductors.[5] Among a variety of modifications, arsenic also possesses a molecular form, As_4, which is known as yellow arsenic.[6] In contrast to P_4, the knowledge about the spherically aromatic As_4[7] is rather limited,

owing to its time consuming synthesis[8] combined with its lack of stability. At ambient conditions, especially when exposed to light or X-ray, As_4 polymerizes to its metallic modification, named grey arsenic.[9] Additionally, even in solution, smallest traces of grey arsenic accelerate the decomposition of As_4. Therefore, attempts to determine the As-As bond distance from a single crystal failed so far. Besides, the instability of the conventionally prepared solutions of yellow arsenic prevented its embedding into an appropriate matrix, in which the latter can be characterized crystallographically. Therefore, a light stable storage medium for yellow arsenic is desirable from which a targeted release of the latter is possible and leads to stable As_4 solutions. Such an in situ generation of As_4 would allow for more sophisticated reactions, which can help to generate suitable materials for the X-ray analysis of molecular arsenic. Therefore, the first homoleptic metal-arsenic complex $[Ag(\eta^2\text{-}As_4)_2]^+(pftb)^-$ **1** was prepared from As_4 and the weakly coordinated silver(I) complex $[Ag(CH_2Cl_2)]^+(pftb)^-$. The latter then was investigated as potential storage medium for molecular arsenic. Therein, the As_4 tetrahedrons are spaced by silver cations, which potentially avoid the light induced polymerization. The stability of **1** was tested by aging the pure complex under an argon atmosphere at –30 °C. Furthermore, the targeted release of **1** by the addition of LiCl was studied. Both, the incorporation and release of As_4 (see Scheme 1) could be monitored by ^{75}As solution NMR. Despite its favorable natural abundance of 100 %, ^{75}As possess a high quadrupolar momentum of 31.4 x 10^{-30} m^2. This leads to very fast spin-lattice relaxation times, which cause severe line broadening. These relaxation rates can be reduced by high local symmetry and fast correlation times, which leads to relatively sharp ^{75}As signals.[10] Thus, until now, the observation of As signals in solution was limited to a few exceptionally symmetrical arsenic compounds with a octahedral (O_h: AsF_6^-, $[As(OTeF_5)_6]^-$) or tetrahedral (T_d: AsR_4^+ (R = H, Me, Et, Pr, Bu), AsO_4^{3-}) coordination of the As atom.[11,12] By using solvents, which provide sufficient small viscosities at room temperature (CD_2Cl_2, toluene), we were able to promote the correlation of the As_4 molecules and, hence, enable the detection of As atoms with local trigonal pyramidal geometry.

6.3 Results and Discussion

First of all, the reaction of yellow Arsenic with the weakly coordinated silver(I) salt $[Ag(CH_2Cl_2)]^+(pftb)^-$ to a potential storage medium for As_4 was studied. Complex formation was investigated by ESI mass spectrometry and the consumption of As_4 was monitored by a

comparison of the ^{75}As NMR spectra of pure As_4 and the reaction product. The latter was then characterized by X-ray diffraction. As_4 was freshly prepared[8] and a ^{75}As spectrum was recorded. Subsequently, As_4 was reacted with $[Ag^+(pftb)^-]$ under rigorous exclusion of moisture and air at room temperature in toluene (see Scheme 1). ESI mass and ^{75}As NMR spectra were recorded from the resulting product. Recrystallization by diffusion of hexane into a saturated solution of the product in dichloromethane led to colorless crystals suitable for X-ray structure analysis.

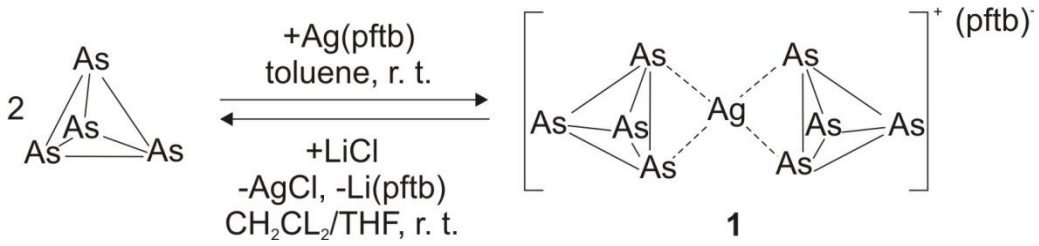

Scheme 1: Reaction of As_4 and $[Ag(CH_2Cl_2)]^+(pftb)^-$ at room temperature in toluene yields 80-90 % of **1**. The targeted release of As_4 is achieved by the addition of LiCl, leading to the precipitation of AgCl and Li(pftb), which shifts the equilibrium towards free As_4. Incorporation and subsequent release yield about 75 % of the initially used As_4 in appreciably stable solutions.

Compound **1** is obtained as a colorless powder, which is sensitive to moisture and air, but remarkably stable, when stored under an argon atmosphere at −30 °C. In the ESI mass spectrum of the product two signals at an m/z ratio of 406.4 and 706.3 were observed. These could be assigned to the two cationic fragments $[Ag(As_4)]^+$ and $[Ag(As_4)_2]^+$, which indicated the formation of **1**. The yields of the reaction were 80-90 %. For ^{75}As NMR analysis, product **1** was dissolved in dichloromethane and the resulting spectrum was compared to an As spectrum obtained from freshly prepared As_4 (see Figure 1). The ^{75}As spectrum of yellow Arsenic (Figure 1a) reveals a single peak at −892 ppm with a half width of 2090 Hz. In contrast, the reaction product does not show any signal from 0 to −1200 ppm (Figure 1b). The chemical shift of As_4 is in good agreement with AsP_3, which represents a mixed tetrahedral cluster with phosphorus, the lower homologue of arsenic. For this compound a ^{75}As MAS signal was reported at −962 ppm.[13] The remarkable line broadening of As_4 is connected to very small spin-lattice relaxation times of ^{75}As, primarily governed by the quadrupolar relaxation mechanism. The latter is particularly effective for large electric field gradients across the observed atom and can be reduced by high local symmetry (vide supra).[10]

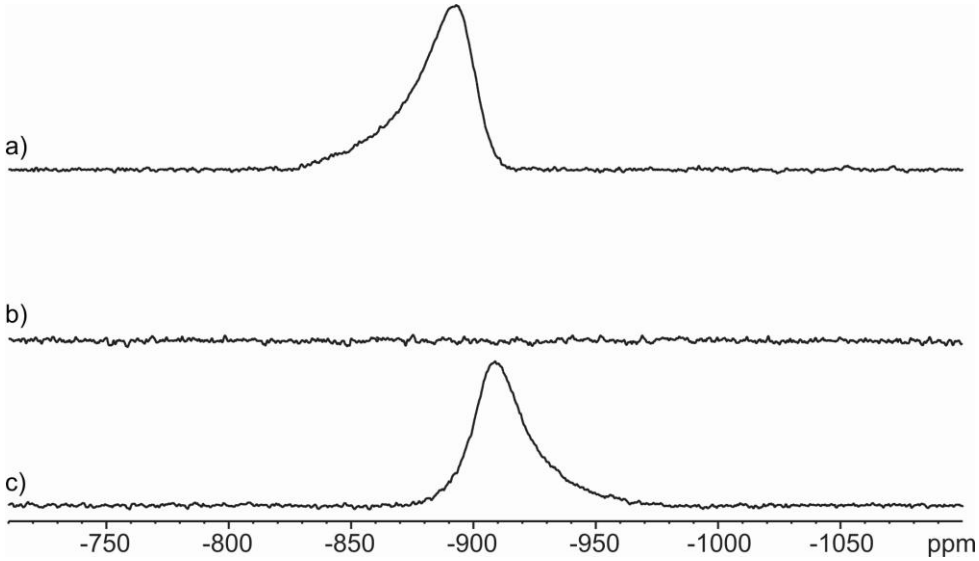

Figure 1: 1D ^{75}As spectra at 300 K of (a) yellow arsenic, conventionally prepared from grey arsenic in toluene/dichloromethane, (b) complex **1** in dichloromethane and (c) As_4 regenerated from **1** by the reaction with LiCl in dichloromethane/tetrahydrofurane. Both, (a) and (c), reveal a signal of As_4, which is severely broadened by quadrupolar relaxation, whereas **1** shows no detectable signal, which is due to reduced local symmetry of As_4 in the silver(I) complex. The 11.6 ppm chemical shift difference of (a) and (c) stems from the presence of toluene, which interacts with the spherical aromatic As_4 in the conventional solution (a).

In yellow arsenic, the As_4 tetrahedrons show a trigonal pyramidal symmetry for each As atom. Obviously, this is enough to make the molecule detectable in toluene/dichloromethane, which exhibits a sufficiently small viscosity to get fast correlation times at 300 K. The lacking product signal of **1** was attributed to the complexation of As_4 by the silver cation. The latter induces a significant polarization effect on the As_4 tetrahedrons and with that reduces the symmetry. Therefore, the quadrupolar relaxation is faster. The latter, in turn, leads to severe line broadening and, hence, the disappearance of the ^{75}As signal. This lowered symmetry is also illustrated by the X-ray analysis of **1** (see Figure 2).

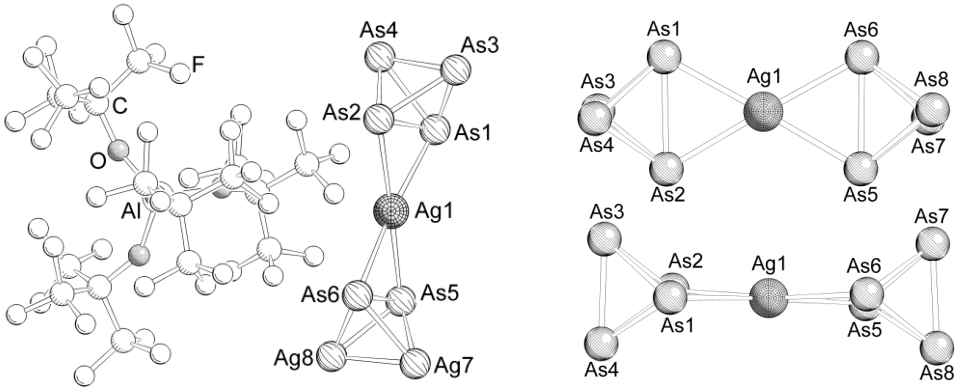

Figure 2: Solid state molecular structure of **1** (left) together with the top and side view of the cationic part of **1** (right) show the side-on coordination of two As_4 tetrahedrons to the silver(I) cation.

The complex shows the side-on coordination of two intact As_4 tetrahedrons to a silver(I) cation in an almost coplanar fashion. The two $AgAs_2$ planes only deviate by 9 ° from the perfect co-planarity. The bond lengths of the coordinating As1-As2 and As5-As6 bonds are 2.585(2) and 2.569(2) Å, respectively, whereas the As3-As4 and As7-As8 bond distances of 2.423(2) and 2.419(2) Å are slightly shorter. The shortest bonds are found between the coordinating and non-coordinating As atoms and lie in the range of 2.379(2) and 2.396(2) Å. Calculation of the As–As–As bond angles gave values between 57.11(5) and 65.59(5) °. The different bond lengths and angles illustrate the distortion of the As_4 tetrahedrons induced by the coordination to the silver(I) cation. In sum, the reaction of As_4 and $[Ag(CH_2Cl_2)]^+(pftb)^-$ gave **1** as an outstanding light stable product in good to excellent yields. The coordination to silver(I) provides significant stabilization, which might be due to a spacing effect of Ag^+. The latter makes the contact of the individual As_4 tetrahedrons unlikely and therefore prevents them from the light induced polymerization. Furthermore, this coordination reduces the local symmetry, which is displayed in both, the X-ray structure and the NMR analysis of **1**.

Having shown the incorporation of As_4 into the first exceptional light stable homoleptic silver(I) complex **1**, we investigated the targeted regeneration of yellow Arsenic, which would qualify **1** as a storage medium for As_4. Furthermore, the properties of the obtained solutions were studied and compared to conventionally prepared As_4 solutions. Therefore, we reacted **1** with LiCl at room temperature (see Scheme 1). The course of the reaction was visible to the naked eye and, additionally, could be followed in the ^{75}As spectra. Upon the addition of LiCl to a solution of **1** the precipitation of insoluble salts started immediately and, simultaneously, the solution turned pale yellow. The ^{75}As NMR spectrum of the reaction product in dichloromethane revealed a 2350 Hz broad signal at –908 ppm (see Figure 1), which signifies an upfield shift of 11.6 ppm and 260 Hz broadening compared to the conventionally prepared As_4 (see Figure 1a). Presumably, the chemical shift offset displays an aromatic solvent induced shift for the spherically aromatic As_4. This effect can be observed for aromatic solutes when displacing an aliphatic solvent by an aromatic one and was explicitly investigated for ^1H spectroscopy. There, the shift can be as large as ±1.5 ppm.[14] Owing to the synthesis of classically prepared and from **1** released As_4, different solvents were used for the NMR investigation of the spherically aromatic yellow arsenic.[7] While the conventionally prepared As_4 was synthesized and analyzed in toluene/CD_2Cl_2, the NMR spectrum of As_4 released from **1** was recorded in CD_2Cl_2/THF leading to the chemical shift offset. Such a signal shift was also reported for white phosphorous, which represents the higher homologue

of yellow arsenic. Depending on the water content of the sample, P_4 shows a 2 to 7 ppm upfield shifted signal in CD_2Cl_2 compared to white phosphorous in benzene.[15] The signal shift of the spherically aromatic As_4 indicates different intermolecular interactions to aliphatic and aromatic solvents. This is also corroborated by the sharpened As_4 signal by adding aromatic additives. The presence of toluene in the conventional yellow arsenic sample can perturb the intermolecular interactions between the tetrahedral molecules, which leads to fast correlation and, therefore, a reduced linewidth. In contrast, in the sample with regenerated As_4 the absence of aromatic additives lead to unperturbed interactions between the As_4 molecules, which can reduce the free correlation and, hence, broaden the NMR signal. Owing to the analogy of arsenic and phosphorous combined with the facilitated detection of free As_4, which is due to its high symmetry, we assume that both detected ^{75}As signals stem from As_4 tetrahedrons. Hence, the targeted release of molecular arsenic from **1**, by the reaction with LiCl was successful. By this method obtained solutions of As_4 contain approximately 75 % of the initially employed arsenic and show a remarkable light stability (> 4 h). Presumably, the co-precipitation of grey arsenic and other impurities during the salt metathesis frees the solution from polymerization seeds, which would otherwise lead to enhanced decomposition of molecular arsenic. The straightforward release procedure can be done within twenty minutes at room temperature and consumes only small amounts of solvent. Compared to solutions obtained via the classical synthesis route,[8] our As_4 solutions are about five times higher concentrated.

6.4 Conclusions

In conclusion, in the reaction of As_4 and $[Ag(CH_2Cl_2)]^+(pftb)^-$ we presented the formation of the first homoleptic arsenic-metal complex **1** in good to excellent yields. For the latter an outstanding light stability, provided by the coordination of As_4 to silver(I) was shown. Moreover, we extended the scope of observable ^{75}As NMR signals from octahedrally and tetrahedrally arranged As atoms to trigonal pyramidal symmetry. With that, we were able to provide the NMR spectroscopic evidence for the possibility of a targeted release of As_4 by the simple addition of LiCl to a solution of **1**. This straightforward regeneration of approximately 75 % of the initially employed As_4, qualifies the complex as an ideal economic storage medium for yellow arsenic. Our As_4 solutions, obtained by the targeted release from **1**, are five times more concentrated and show significantly elevated light stabilities with respect to

the classically prepared yellow arsenic solutions. The possibility of in situ generated As_4 allows more sophisticated reactions with molecular Arsenic, which have been not possible so far. This can help to make As_4 accessible for X-ray analysis by embedding it into a suitable polymeric or spherical matrix. In fact, such reactions were performed successfully while this manuscript was in preparation.

6.5 References

(1) Streudel, R. In *Chemie der Nichtmetalle*; Walter de Gruyter, 1999; p. 424.

(2) Scheer, M.; Balazs, G.; Seitz, A. *Chem. Rev.* **2010**, *210*, 4236-4256.

(3) Cossairt, B. M.; Cummins, C. C.; Head, A. R.; Lichtenberger, D. L.; Berger, R. J. F.; Hayes, S. A.; Mitzel, N. W.; Wu, G. *J. Am. Chem. Soc.* **2010**, *132*, 8459-8465.

(4) Caporali, M.; Gonsalvi, L.; Rossin, A.; Peruzzini, M. *Chem. Rev.* **2010**, *110*, 4178-4235.

(5) Holleman, A. F.; Wiberg, E. Lehrbuch der Anorganischen Chemie **1995**, 797.

(6) Morino, T.; Ito, T.; Ukaji, Y. *Bull. Chem. Soc. Jpn.* **1966**, *39*, 64-71.

(7) Hirsch, A.; Chen, Z.; Jiao, H. *Angew. Chem. Int. Ed.* **2001**, *40*, 2834-2838.

(8) Scherer, O. J.; Sitzmann, H.; Wolmershäuser, G. *J. Organomet. Chem* **1986**, *309*, 77-86.

(9) Bettendorf, A. *Annalen der Chemie und Pharmazie* **1867**, *184*, 110-114.

(10) Abragam, A. The Principles of Nuclear Magnetism **1961**.

(11) Balimann, G.; Pregosin, P. S. *J. Magn. Reson.* **1977**, *26*, 283-289.

(12) Collins, M. J.; Rao, R. K.; Schroblingen, G. J. *J. Magn. Reson.* **1985**, 137-140.

(13) Croissart, B. M. *J. Am. Chem. Soc.* **2010**, *132*, 8459-8465.

(14) Reichardt, C.; Welton, T. *Solvents and Solvent Effects in Organic Chemistry*; 4. ed.; Wiley-VCH, 2011; pp. 359-422.

(15) Kühl, O. *No Title*; Springer-Verlag: Heidelberg, 2008; pp. 7-23.

6.6 Supporting Information

6.6.1. General Considerations

All manipulations were performed under rigorous exclusion of oxygen and moisture in Schlenk-type glassware on a dual manifold Schlenk line or in N_2 filled glove box with a high-capacity recirculator (< 0.1 ppm O_2). THF was dried by distillation from sodium wire/benzophenone, toluene from potassium, dichloromethane from CaH_2. Acetonitrile was stirred for two hours over CaH_2 and distilled by condensation at room temperature. Deuterated solvents were obtained from Deutero GmbH and were degassed, dried and distilled prior to use.

6.6.2. Experimental Details

Incorporation of As_4 into $[Ag(\eta^2\text{-}As_4)_2]^+(pftb)^-$ (1): At room temperature, a freshly prepared solution of As_4 in toluene (250 mL, 3.6 mmol/l, 270 mg, 0.9 mmol) was given to a solution of $[Ag(CH_2Cl_2)]^+(pftb)^-$ (0.350 g, 0.3 mmol) in dichloromethane (10 mL). Under the exclusion of light, the reaction mixture was stirred for 30 min. The following procedures could then be done under the exposure to light. The solvent was removed in vacuum to give **1** together with grey arsenic. The crude product was then purified from yellow and grey Arsenic by dissolution in dichloromethane (20 mL), filtering through a plug of cellite and removing the solvent in vacuum once more. These three steps were repeated until the removal of the solvent induced no more precipitation of grey arsenic. The resulting off-white powder was washed 3 times with hexane (20 mL) and dried in vacuum. Crystals suitable for X-ray structure analysis were grown by the diffusion of hexane (10 mL) into a solution of **1** (452 mg, 0.268 mmol) in CH_2Cl_2 (3 mL) at -30 °C. Yield: 452 mg, 90 %.

Release of As_4 from $[Ag(\eta^2\text{-}As_4)_2]^+(pftb)^-$ (1): Under the exclusion of light, to a solution of **1** (100 mg, 0.0595 mmol) in a solvent of choice (ideally polar solvents like CH_2Cl_2 or THF), a solution of LiCl (2.5 mg, 0.0595 mmol) in THF (at least 1 mL) was added within 5 minutes. The reaction mixture was stirred for 15 min to give a brownish precipitate. The latter was allowed to settle and the pale yellow solution was filtered through a Teflon tube with filter plug. The amount of released As_4 was then determined. The solvent was removed in vacuum and subsequently exposed to light (at least 12 h) to induce polymerization to grey arsenic. The latter was washed several times with THF to remove last traces of Li(pftb) and AgCl and dried in vacuum. Yield: 27 mg, 75 %.

6.6.3. ESI Mass Spectrometry

Mass spectrometry was performed using a ThermoQuest Finnigan TSQ 7000.

6.6.4. NMR Data Collecting and Processing

The NMR spectra were recorded on a Bruker Avance 600 spectrometer equipped with a 5 mm broadband triple resonance Z-gradient probe. The temperatures for all measurements were controlled by a Bruker BVTE 3900 temperature unit. ^{75}As measurements were carried out with a standard Bruker pulse program (zg) using 140k number of scans, 4 dummy scans, TD = 8k and a relaxation delay of 0.3 s. Data were processed with the Bruker software TOPSPIN 2.1 using the processing parameters SI = 16k, WDW = EM and LB = 80 Hz. The chemical shifts are reported in ppm and externally referenced to $KAsF_6$.

6.6.5. Practical Considerations for ^{75}As NMR

Even though ^{75}As is the only natural isotope of arsenic, the NMR detection poses a challenge. It is well known that nuclei with $I > 1/2$ show very small spin-lattice relaxation times which are governed primarily via the quadrupolar relaxation mechanism.[1] This effect leads to extreme line broadening and makes nuclei with a large quadrupolar momentum hard to observe in NMR spectra. The efficiency of this relaxation mechanism is linked to the deviation of the electric field gradient from axial symmetry and the quadrupolar correlation time. That is to say, the greater the deviation and the slower the correlation, the more effective is this relaxation pathway. Therefore, high local symmetry can lead to relatively sharp ^{75}As signals.

SI Figure 1 exemplarily shows the ^{75}As spectrum of the octahedrally arranged As atom in the external standard $KAsF_6$. In yellow arsenic, in turn, the As_4 tetrahedrons show a distinct, but reduced symmetry compared to $KAsF_6$. The local symmetry in As_4 is enough to make the compound detectable in dichloromethane at 300 K, but broadens the signal to 2090 Hz (As_4 in toluene/CD_2Cl_2) and 2350 Hz (As_4 in CD_2Cl_2/tetrahydrofurane), respectively. These solvents exhibit a sufficiently small viscosity at 300 K to get fast correlation times. Furthermore, the aromatic toluene perturbs the intermolecular interactions between the spherical aromatic As_4 tetrahedrons. This enhances molecular correlation and, hence, leads to a 260 Hz sharper signal than without aromatic additive. In contrast, the coordination of As_4 to the silver cation induces significant polarization and with that reduces the symmetry significantly. Therefore, the

quadrupolar relaxation is faster, which leads to extreme line broadening and hence, the disappearance of the signal.

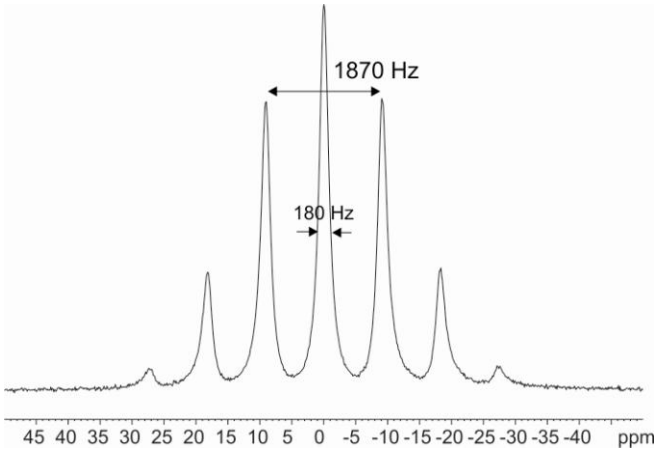

SI Figure 1: 1D ^{75}As spectrum of the external standard $KAsF_6$ at 300 K in acetonitrile. The tetrahedral surrounding of the As atom provides enough symmetry to sharpen the ^{75}As signal to a halfwidth of 180 Hz. With this special symmetry, even the $^1J_{F,As}$ coupling of 1870 Hz is observable.

1. Abragam, "The Principles of Nuclear Magnetism", Oxford University Press, London, 1961.

6.6.6. X-ray Structure Analysis

X-ray crystal structure analysis was performed by using an Oxford Diffraction SuperNova diffractometer with $Cu_{K\alpha}$ radiation (λ = 1.54178 Å) and ATLAS detector or an Oxford Gemini R-Ultra diffractometer with $Cu_{K\alpha}$ radiation (λ = 1.54178 Å) and RUBY detector. Structure was solved and refined by using SIR97,[1] SHELXS97,[2] SHELXL97[2] and WinGX.[3]

1: $C_{16}AgAlAs_8F_{36}O_4$, M = 1674.37 g/mol, crystal dimensions 0.1520x0.0426x0.0280 mm^3, monoclinic space group $P2_1/c$ (No.14), a = 10.3125(5), b = 18.9558(6), c = 20.6898(6) Å; α = 90, β = 99.739(3), γ = 90°, V = 3986.2(3) $Å^3$, Z = 4, T = 123(1), ρ_{calcd} = 2.790 g cm^{-3}, μ = 13.579 mm^{-1}, 40921 reflections collected, 5546 unique reflections (R_{int} = 0.0936), 578 parameters, R_1 = 0.0664 ($I > 2\sigma(I)$), wR_2 = 0.1807 (all data).

1. Altomare, M. C. Burla, M. Camalli, G. L. Cascarano, C. Giacovazzo, A. Guagliardi, A. G. G. Moliterni, G. Polidori, R. Spagna, SIR 97: A new tool for crystal structure determination and refinement. *J. Appl. Cryst.* **1999**, *32*, 115-119.
2. SHELX97 Programs for crystal structure analysis (Release 97-2). (G. M. Sheldrick, Institut für Anorganische Chemie der Universität, Tammanstrasse 4, D-3400 Göttingen, Germany, **1998**).
3. L. J. Farrugia, WinGX suite for small-molecule single-crystal crystallography. *J. Appl. Cryst*. **1999**, *32*, 837-838.

7. Summary

The breath-taking development and the frequent use of organocuprates illustrate their synthetic importance for regio- and diastereoselective carbon-carbon bond formation reactions. Since their discovery by Gilman, organocuprates are the focus of proceeding studies. Empiric optimization of reaction conditions motivated the clarification of the reaction mechanism, forming the basis for further improvements. A lot of expertise was spent on the structure elucidation of organocuprates in the solid state as well as in solution and identified a dimeric assembly as the reactive species. Based on this structure, theoretical studies on the reaction mechanism predicted different π- and σ-intermediates, for which the experimental evidence was provided by NMR spectroscopic investigations. Especially for the square-planar copper(III) intermediate of cross coupling reactions, besides the structural characterization, stabilizing effects of commonly used additives were presented and completed by directed reactions with these intermediate structures. However, to date, structural rearrangements in the copper(III) intermediate as well as the subsequent formation of copper(I) complexes, caused by a changed stoichiometry during the reaction process, were not considered. Therefore, the first part of this thesis focuses on the NMR spectroscopic investigations of these two important points in cross coupling reactions of organocuprates and alkyl halides.

Ligand exchange reactions in the square-planar copper(III) intermediate of a cross coupling reaction have been studied in detail with the help of two dimensional low temperature NMR techniques. In this study, the $^{12}C/^{13}C$ isotopic pattern of this intermediate and the corresponding product indicated ligand exchange reactions. Additional investigations on the mechanism of this scrambling identified a further copper(III) complex, which supports an S_N2-like exchange mechanism instead of a pseudo rotational process. At elevated temperatures similar to synthetic conditions, the product pattern indicated that this ligand exchange is slow compared to reductive elimination, which actually leads to the formation of the desired cross coupling product.

Furthermore, for two different copper salts, subsequently formed copper(I) complexes in cross coupling reactions with alkyl halides, caused by a change in the stoichiometry during the course of the reaction, were studied. In the case of copper iodide, the use of sub-stoichiometric ratios of alkyl lithium for the organocuprate formation lead to a variety of new

organocopper(I) complexes. NMR investigations suggested cuprate analogue structures with less polarized alkyl moieties. These copper rich complexes were also observed in cross coupling reactions, where they can be formed from the emerging alkyl copper compound and the remaining organocuprate. There, the formation of these copper rich complexes reduces the amount of organocuprate available for the desired cross coupling reaction and hence, leads to diminished yields. It was shown that the formation of these unfavorable copper(I) complexes can be avoided by providing a sufficient amount of alkyl lithium compound, which is able to regenerate the reactive organocuprate, but also promotes side-rections. In contrast, in the case of cyanocuprates, besides the heteroleptic cuprate no further copper rich complexes are formed. Hence, the full amount of homoleptic cyanocuprate is available for the cross coupling reaction, which results in better yields than the respective iodocuprate. This discrepancy between iodo- and cyanocuprates might explain the long-standing myths about the special reactivity of cyanocuprates.

Binary alloys, named Zintl phases, are intermetallic structures with heteropolar element-element-bound parts and possess a versatile and fascinating chemistry, ranging from oxidative couplings over the formation of endo- and exohedral and even to intermetalloide clusters. Some of these materials are discussed as attractive cluster-assembled nanomaterials for semiconducting applications. In this context, the electrochemical deposition of a suitable material from solution was demonstrated. However, the knowledge about the solvation of anionic clusters from Zintl phases as well as their stabilities in solution is rather limited, which hampers a targeted material research. Since hetreonuclear NMR spectroscopy in solution presented itself as a powerful method for the structural characterization of Zintl anions of group 15, the second part of this work is about the NMR investigations on the solvation of group 14 polyanions and their stabilities in liquid ammonia.

The first NMR detection of the long-time elusive Si_4^{4-} provided the direct evidence for silicides in solution. Furthermore, for the first time the likewise elusive Sn_4^{4-} was detected in solution. Amazingly high signal intensities and stabilities for both highly charged tetrahedranides were observed by utilizing the stabilizing effect of [2.2.2]-cryptand. Furthermore, the observation of the generation of NH_2^- enabled the first experimental evidence for the long-standing assumption of solvent molecules as oxidizing agent for Zintl anions and in case of silicides, SiH_3^- was detected as degradation product.

Furthermore, the influence of the synthetic route as well as the use of additives during the solvation of polystannides was investigated. With the low temperature synthetic route, in which the polyanions were generated in-situ in solution without additives, the highly charged tetrastannide was obtained. Further investigations addressed the high temperature route, in which the polyanions are precast in the solid state and subsequently dissolved at low temperatures in liquid ammonia. Additive-free solvations indicated a fast oxidation of the highly charged tertrastannide to a less reduced nonastannide. The addition of [2.2.2]-cryptand to the solvation of Rb_4Sn_4 enabled not only the mere detection of Sn_4^{4-}, but also allowed for the observation of the first Sn_5^{2-} signal and at least three separated signals of differently salt and solvent coordinated nine-atomic tin clusters. For one of these Sn_9-clusters, low temperature NMR investigations suggest the freeze of the "diamond-square" process in the conformation of a threefold capped trigonal prism. In further investigations, these polystannides were converted with MesCu. In the absence of [2.2.2]-cryptand a known interstitial complex, in which copper is encapsulated into the nonastannide was observed, whereas in the presence of [2.2.2]-cryptand predominantly a new exo-complex of copper with the tetrastannide was detected. This indicates that, in principle, by the choice of suitable conditions, a distinct polystannide can be selected and addressed in targeted reactions.

Since the generation of the molecular modification As_4 is a rather time consuming process, which has to be done prior to each conversion of As_4, due to its lack of stability, an alternative storage medium was investigated. The first NMR signal of a As_4 cluster provided the experimental evidence of reversible As_4 binding to a silver cation in this storage medium, which is light stable and can be used for the in-situ generation of molecular arsenic in chemical reactions.

8. Zusammenfassung

Die atemberaubend schnelle Entwicklung und der häufige Einsatz von Organocupraten veranschaulichen ihre synthetische Bedeutung für die regio- und diastereoselektive Knüpfung von C-C Bindungen. Seit ihrer Entdeckung durch Gilman befinden sich Organocuprate im Focus zahlreicher Untersuchungen. Empirische Verbesserungen bei der Anwendung von Organocupraten motivierten zur Aufklärung der Reaktionsmechanismen, die als Grundlage für weitere Verbesserungen dienen können. Die Strukturaufklärung im Festkörper und in Lösung, sowie die Identifizierung einer dimeren supramolekularen Struktur als reaktive Spezies bildete dabei einen Meilenstein. Davon ausgehend wurden auf Grundlage theoretischer Rechnungen Reaktionsmechanismen vorgeschlagen, die verschiedene π- und σ-Intermediate enthielten, deren experimenteller Beweis durch NMR spektroskopische Untersuchungen erbracht wurde. Speziell für das quadratisch planare Kupfer(III)-Intermediat der Kreuzkupplungsreaktion, wurden neben der strukturellen Charakterisierung auch stabilisierende Effekte durch klassische Additive, die den Reaktionsmischungen während der Synthese zugesetzt werden, sowie gerichtete Reaktionen mit dem Intermediat untersucht. Bis zum Beginn dieser Arbeit wurden jedoch weder strukturelle Veränderungen im Kupfer(III)-Intermediat noch die Bildung von möglichen weiteren Kupfer(I)-Komplexen untersucht, deren Bildung durch die Veränderung der Stöchiometrie während der Reaktion möglich ist. Mithilfe der NMR-Spektroskopie widmet sich der erste Teil dieser Arbeit der Klärung dieser beiden Fragestellungen in Kreuzkupplungsreaktionen zwischen Organocupraten und Alkylhalogeniden.

In einem quadratisch planaren Kupfer(III)-Intermediat wurden mithilfe der zweidimensionalen Tieftemperatur-NMR-Spektroskopie Ligandaustauschreaktionen während einer Kreuzkupplungsreaktion im Detail untersucht. Die Studie des $^{12}C/^{13}C$-Isotopenmusters des Intermediats und des Produktes ließen auf einen Ligandaustausch schließen. Weiterführende Studien identifizierten einen zusätzlichen Kupfer(III)-Komplex als Intermediat des Austauschprozesses, das einen S_N2 ähnlichen Mechanismus anstelle einer Pseudorotation unterstützt. Bei höheren, den Synthesebedingungen ähnlichen Temperaturen, konnte gezeigt werden, dass dieser Ligandaustausch langsamer ist als die reduktive Eliminierung, die zum gewünschten Kreuzkupplungsprodukt führt.

Des Weiteren wurden für zwei unterschiedliche Kupfersalze, zusätzlich gebildete Kupfer(I)-Komplexe untersucht, die bei Kreuzkupplungen durch Veränderung der Stöchiometrie während der Reaktion entstehen können. Im Fall von Kupferiodid ergab der Einsatz von substöchiometrischen Mengen Alkyllithiumverbindung bei der Synthese des Cuprats eine Vielzahl weiterer Kupfer(I)-Komplexe. Die Charakterisierung dieser Komplexe ergab cupratähnliche Strukturen mit deutlich abgeschwächter Polarisierung der Alkylgruppen. Diese zusätzlichen Kupfer(I)-Komplexe wurden auch in Kreuzkupplungsreaktionen beobachtet, wo sie aus der entstehenden Alkylkupfer-Spezies und dem verbleibenden Organocuprat gebildet werden können. Dabei reduziert die Bildung dieser kupferreichen Komplexe die Menge des für die Reaktion zur Verfügung stehenden Organocuprats und führt dadurch zu schlechteren Ausbeuten. Es konnte gezeigt werden, dass die Bildung dieser unerwünschten Kupfer(I)-Komplexe durch den Einsatz ausreichender Mengen an Alkyllithiumverbindung vermieden werden kann, welche die reaktiven Organocuprate regeneriert, aber auch zu Nebenreaktionen führt. Im Gegensatz dazu wird im Fall der Cyanocuprate außer den heteroleptischen Cupraten keine weiteren kupferreichen Komplexe gebildet. Folglich steht die volle Menge an homoleptischen Cyanocuprat für die Kreuzkupplungsreaktion zur Verfügung und führt daher zu besseren Ausbeuten als das jeweilige Iodocuprat. Dieser Unterschied zwischen Iodo- und Cyanocupraten kann möglicherweise der lange währende Mythos um eine spezielle Cyanocuprat-Reaktivität erklären.

Binäre Legierungen, sogenannte Zintl-Phasen, sind intermetallische Strukturen mit heteropolaren Element-Element Bindungen. Sie besitzen eine vielseitige und faszinierende Chemie, die von der oxidativen Kupplung bis zur Bildung exohedraler und endohedraler und sogar intermetalloider Cluster reicht. Einige dieser Verbindungen werden im Zusammenhang mit der Anwendung als nanostrukturierte Materialien für die Halbleitertechnik diskutiert. In diesem Zusammenhang wurde die elektrochemische Abscheidung bestimmter Materialien aus Lösung bereits gezeigt. Das Wissen über die Prozesse, die beim Herauslösen anionischer Cluster aus Zintl-Phasen, sowie deren Stabilität in Lösung eine Rolle spielen, ist bis dato kaum vorhanden, wodurch eine zielgerichtete Entwicklung neuer Materialien erschwert wird. Nachdem sich die NMR-Spektroskopie auf dem Gebiet der Strukturaufklärung von Zintlanionen der Gruppe 15 bewährt hat, handelt der zweite Teil dieser Arbeit von NMR spektroskopischen Untersuchungen zum Lösungsverhalten von Zintlanionen der 14. Gruppe und deren Stabilität in flüssigem Ammoniak.

Durch die erste NMR Detektion von Si_4^{4-} wurde der direkte Beweis für die Existenz von Siliciden in Lösung erbracht. Außerdem konnte erstmals das hochgeladenen Sn_4^{4-} in Lösung detektiert werden. Durch den stabilisierenden Effekt von [2.2.2]-Kryptand konnten erstaunlich hohe Signalintensitäten und Stabilitäten der beiden hochgeladenen Tetrahedranide erzielt werden. Des Weiteren ermöglichte die Beobachtung der Bildung von NH_2^- den ersten experimentellen Beweis für die lange währende Vermutung, dass Lösungsmittelmoleküle als Oxidationsmittel für Zintl-Anionen dienen können und im Fall der Silicide wurde SiH_3^- als Abbauprodukt detektiert.

Außerdem wurde der der Einfluss der Syntheseroute als auch der Einsatz von Additiven bei der Auflösung von Polystanniden wurde untersucht. Mithilfe der Tieftemperatur-Synthese, bei der die Polyanionen direkt in Lösung erzeugt werden, wurde das hochgeladenen Tetrastannid erhalten. Weitere Untersuchungen widmeten sich der Hochtemperatur-Festkörper-Synthese, bei der die Polyanionen im Festkörper vorgebildet und anschließend bei tiefen Temperaturen in flüssigem Ammoniak gelöst werden. In Lösungsansätzen ohne Additive wurde eine schnelle Oxidation des hochgeladenen Tetrastannids zum Nonastannid beobachtet. Der Zusatz von Cryptand zur Solvolyse von Rb_4Sn_4 ermöglichte nicht nur die Detektion von Sn_4^{4-}, sondern erlaubte auch die erstmalige Beobachtung eines Sn_5^{2-}-Signals und mindestens dreier separierter Signale für verschiedene salz- und lösungsmittel-koordinierte 9-atomige Cluster. Für einen dieser Sn_9-Cluster weisen Untersuchungen mittels Tieftemperatur-NMR auf das Einfrieren des „Diamond-Square-Prozesses“ in der Konformation eines dreifach überkappten trigonalen Prismas hin. In weiterführenden Experimenten wurden Reaktionen dieser Polystannide mit Mesitylkupfer untersucht. Ohne Zusätze wurde ein bereits bekannter interstitieller Komplex gefunden, bei dem ein Kupferatom in ein Nonastannid eingalagert ist. Reaktionen mit [2.2.2]-Cryptand führten hingegen zu einem neuen Exo-Komplex zwischen Kupfer und dem Tetrastannid. Es konnte gezeigt werden, dass prinzipiell durch die Wahl geeigneter Bedingungen verschiedene Polaynionen in Lösung gezielt stabilisiert und zur Reaktion gebracht werden können.

Das in den Untersuchungen der Stannide erlangte Wissen über den stabilisierenden Effekt von Cryptand wurde zur Untersuchung der viel empfindlicheren Silicide in Lösung genutzt. Hierbei wurde das erste NMR Signal eines Silicides detektiert, das sich unter den gewählten Bedingungen als unerwartet stabil zeigte.

Da die Erzeugung von molekularem Arsen bisher nur in einem äußerst aufwendigen Prozess möglich war, der vor jeder Umsetzung aufgrund der mangelnden Stabilität von As_4 wiederholt werden musste, wurde ein alternatives Speichermedium für As_4 untersucht. Dabei erbrachte das erste NMR Signal eines As_4-Clusters den experimentellen Beweis für die reversible As_4-Bindung an ein Silberkation in diesem Speichermedium, das lichtstabil ist und für die in-situ Generierung von molekularem Arsen in chemischen Reaktionen benutzt werden kann.